ISTC 2449p

Final
Project Technical Report
of ISTC 2449p

PLASMA-JET STUDIES FOR PLASMA CHEMICAL FUEL ACTIVATION

(Faculty of Physics of Moscow State University)

(From 30 June 2002 to 30 December 2004)

Dean of Department of Physics
Professor **V.I. Trukhin**

Project Manager
Professor  **I.B. Timofeev**

Phone /Fax: (095) 939-38-85 / 939-17-87 **E-mail: igortim@orc.ru**

Project Duration: from 30 June 2002 to 30 December 2004.

Moscow
January 2005

Partner - EOARD

REPORT DOCUMENTATION PAGE

Form Approved
OMB No. 0704-0188

1. REPORT DATE *(DD-MM-YYYY)*	2. REPORT TYPE	3. DATES COVERED *(From - To)*
18-03-2005	Final Report	01-Jul-02 - 23-Mar-05

4. TITLE AND SUBTITLE
Plasma-Jet Studies for Plasma Chemical Fuel Activation

5a. CONTRACT NUMBER
ISTC Registration No. 2449

5b. GRANT NUMBER

5c. PROGRAM ELEMENT NUMBER

6. AUTHOR(S)
Professor Vladimir Lvovich Bytchkov

5d. PROJECT NUMBER

5e. TASK NUMBER

5f. WORK UNIT NUMBER

7. PERFORMING ORGANIZATION NAME(S) AND ADDRESS(ES)
M.V. Lomonosov Moscow State University
Leninskie Gory
Moscow 119899
Russia

8. PERFORMING ORGANIZATION REPORT NUMBER
N/A

9. SPONSORING / MONITORING AGENCY NAME(S) AND ADDRESS(ES)
EOARD
PSC 802 Box 14
FPO AE 09499-0014

10. SPONSOR/MONITOR'S ACRONYM(S)

11. SPONSOR/MONITOR'S REPORT NUMBER(S)
ISTC 01-7037

12. DISTRIBUTION / AVAILABILITY STATEMENT
Approved for public release; distribution is unlimited.

13. SUPPLEMENTARY NOTES

14. ABSTRACT

This report results from a contract tasking M.V. Lomonosov Moscow State University, as follows: Plasma chemistry mechanisms for accelerating activation of fuels by projected plasma jets will be investigated by the team of Moscow State University (MSU). The approach will exploit excited state transitions and related dissociation processes, instead of the conventional paradigm that uses plasma-dynamic discharge, stimulating fuel ignition with short powerful ultra-violet radiation pulses that creates plasma electrons for the activation. It is envisioned that this new approach will produce substantially more effective ignition than the conventional method at much lower temperatures, at which there is no decomposition of the fuel by radiation. Experimental studies of properties of plasma jets in steady air, theoretical and computational investigations of the activation of air-propane mixture at 300-760 Torr are proposed to test the hypothesis. The effect of plasma activation on the ignition delay time and combustion velocity will also be theoretically investigated.

15. SUBJECT TERMS
EOARD, Physics, Fluid Mechanics

16. SECURITY CLASSIFICATION OF:			17. LIMITATION OF ABSTRACT	18. NUMBER OF PAGES	19a. NAME OF RESPONSIBLE PERSON
					William B. McClure, Col, USAF
a. REPORT	b. ABSTRACT	c. THIS PAGE	UU	108	19b. TELEPHONE NUMBER *(include area code)*
U	U	U			+44 (0)20 7514 4376

Contents

Objectives of the Project

Plasma chemistry mechanisms for accelerating activation of fuels by projected plasma jets are investigated by the team of Moscow State University (MSU). Main attention is paid to excited state transitions and related dissociation processes inside the excited area created by a plasma jet and in its vicinity. This approach is different from the conventional paradigm that uses plasma-dynamic discharge, stimulating fuel ignition with short powerful ultra-violet radiation. It is envisioned that this new approach will produce substantially more effective ignition than the conventional method at much lower temperatures, and without decomposition of the fuel by radiation, which take place in the known method..

For verification of the proposed hypothesis we will undertake plasma jet parameter experimental investigations in the motionless is supposed, theoretical and computation investigations of air-propane mixture at pressures 300-760 with a help of nitrogen plasma jets are to be executed. The effect of plasma activation on the ignition delay time and combustion velocity will be theoretically investigated.

The objective of this project is to establish the feasibility of plasma-jets for plasma chemical stimulation of combustion and aerodynamic augmentation. Particular attention will be focused to the understanding of the plasma chemical mechanisms of the activation of fuels, coupling with the fluid dynamic processes and their implications for aerodynamic and propulsive augmentation.

Specific problems to be solved are:

- Assessments of new scheme for using atoms and active radicals for fuel activation
- New experimental data necessary for oblique plasma jet in flow application for reinforcement of new scheme from Item 1.
- Results of numerical modeling interaction of oblique plasma jet with streams with and without fuel mixing and burning.
- Recommendations definitions of high speed fuel flows ignition and combustion stabilizing conditions optimization on a basis of numerical modeling and experimental data on plasma kinetic processes from Item 1 (in combination with plasma jets oblique-to-the-free stream injection and flow gasdynamics).

List of Symbols

$\vec{B} = \mu_0 \vec{H}$	magnetic field
c_x	sound velocity
$c_p = c_p\ (T, P)$	specific heat
$\vec{D} = \varepsilon_0 \vec{E}$	electric inductance
D_ν	effective diffusion coefficient
δ	thickness of the layer
E	electric field
e_s	electric charge corresponding to the particle of s type
ε_0	dielectric constant
φ	angle between vectors $\vec{g}$ and $\vec{n}$,
$\vec{g}$	vector of the free fall acceleration
$h = h\ (T, P)$	enthalpy
I	electric current
k_B, k	Boltzmann constant
L,	mean free path length of particles, characteristic length of a device
λ_e	electron mean free path
λ	thermal conductivity of a gas
M	Mach number
m_s	mass of the particle of s type
m_g,	mass of a gas atom
m_e,	mass of an electron
n_e	electron concentration
n_a	concentration of atoms
n_i	concentration of ions
$\vec{n}$	unit vector along the axis directed from one particle to another
$n_{s,\tau}^{\ i}$	concentration of particles
N	neutral density, concentration of neutral atoms or atoms of a gas
$\eta = \eta\ (T, P)$	plasma viscosity
P, p	gas pressure
Δp	total pressure differential
$\Psi = \Psi\ (T, P)$	radiation losses, radiation ability
$\rho = \rho\,(T, P)$	plasma density
r	characteristic radial size of an arc
$\dot{S}$	the tensor of deformation velocities
$\boldsymbol{S}_\nu$	spectral radiation energy flux,
SW	shock wave
s	enumerates the sorts of particles
σ	plasma conductivity
σ_{SB}	Stephen-Boltzmann constant
τ	enumerates the sorts of particles
T_e	electron temperature
T, T_g	gas temperature
$T_{s,\tau}^{\ i}$	temperature of particles

$T_{a,i}$	temperature of atoms or ions
U	voltage

Introduction

According to the concept of our proposal plasma can be applied for improvement of combustion processes in air mixtures with organic components (propane), in so doing it excites a gas flowing in a combustor. Plasma generators are applied for plasma creation. Ionization and dissociation of molecules takes place in plasmas. Active particles-active radicals and atoms-products of dissociation of molecules are present in plasmas.

Mixing of plasma particles with fuel gas molecules takes place at interaction of plasma jet with mixture flow takes place in a combustor. These particles posses high reaction-ability and they play important role in chemical reactions quickening oxidation process at presence of oxygen molecules and atoms. At presence of hydrocarbon components in a mixture such processes lead to acceleration of combustion processes.

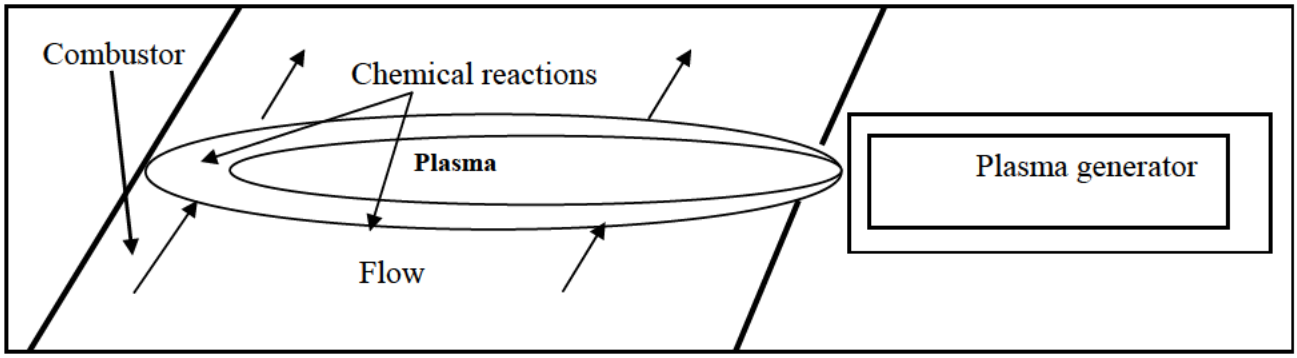

Fig.1.1 Principle scheme of plasma fuel activation with a help of plasma generator.

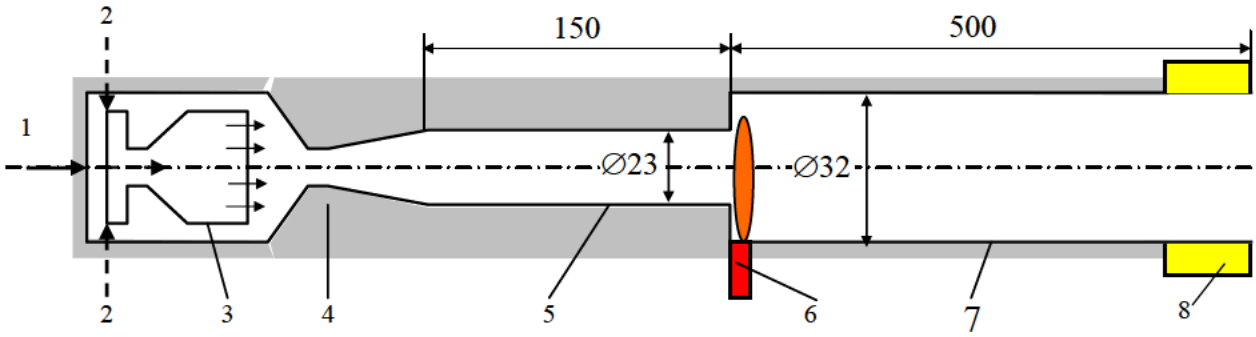

Fig. 1.2 Scheme of test channel
1 – air supply, 2 – fuel supply, 3 – mixer, 4 – supersonic nozzle, 5 – section №1 («insulator»), 6 – plasma generator, 7 – combustor (section №2), 8 – measurement section

In Figure 1.1 one can see a principle scheme of plasma generator application for combustion activation in a gas flow. In Figure 1.2 one can see a supposed experimental scheme in which

proposed concept can be realized. In this figure one can see a test channel for investigations of plasma jet in a supersonic flow, where: 1. is a duct for creation of required flow characteristics; 2. Is storage and supply air high pressure system at $p_{t,\ max} \leq 12$; 3 -storage and supply gaseous fuel (propane) system; 4. plasma generator and system of electrical energy input;5. measurement system of gasdynamic and electrical parameters; 6. system of visual observation and video taping of flow visualization in test channel.

Development and manufacturing of highly effective technological plasma generators for plasma chemical activation of supersonic and subsonic fuel flows and obtaining high enthalpy plasma flows with their help leads to necessity of consideration plasma generator design with vortex flow stabilization and divergent anode duct, see Fig.3. Most important features of such geometry are high consumption characteristics, efficiency of working gas heating and smallness of heat losses into water cooled anode surface [1.1].

Plasma generators of this type differ from others by high enthalpy plasma jet generation capability with high consumption of a working gas at insignificant internal jet length (10-40 mm) and high coefficient of efficiency. Since maximum temperature value in such generators with typical diameter of the inletting anode hole 3-5 mm can exceed 20000 K, and average mass temperature at the outlet reaches 4000-6000 K at a gas consumption 0,5- 5 g/s, then these plasma generators have wide technological applications [1.1-4].

Reliability, comparable simplicity of design of these plasma generators and considerable amount of experimental data on plasma characteristics starting from near cathode region of electric discharge and finishing with region of plasma relaxation at a distance up to 50 from the anode down a flow. This became convincing bases for choice of mainly this scheme of plasma generator's design. High efficiency of electric field energy in the arc to thermal energy of a flow is insured by vortex jet stabilization at tangential delivery of plasmaforming gas (nitrogen, argon). Convective and conductive loses to water cooling wall of diverging duct are considerably decreased at such means of the discharge organization. So main loses are connected with radiation energy losses and their role increases with rising of plasma temperature.

Most convenient plasma forming gases from the point of view of repeated use of plasma generators are nitrogen and argon. They insignificantly destroy electrodes in comparison with air.

Calculations of thermal plasma composition of air and nitrogen of ours our and [1.1-7], see Fig.1.4-5 allow to conclude that main prospective temperature range at plasma generator's outlet is T= 4000-10000 K from the point of view active radical generation. Calculations show that atom concentration is of the order of magnitude of molecules or higher in this temperature range, so one have expect here the most efficiency of realization of the proposed concept.

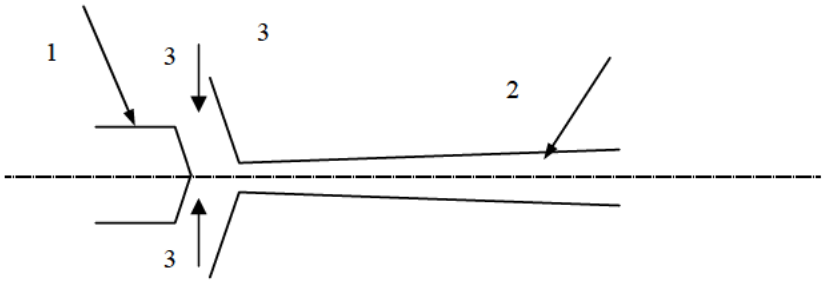

Availal Fig.1.3. Geometry of electrode units of plasma generator: 1 - cathode, 2 – water cooled anode with diverging duct, 3 – plasma forming gas (N_2, Ar). enerator in range P=10 - 15 кВт.

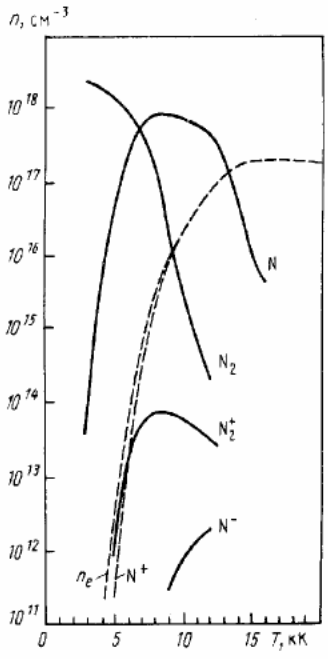

Fig.1.4 Component composition of equilibrium nitrogen plasma at constant pressure P=10^5 Pa

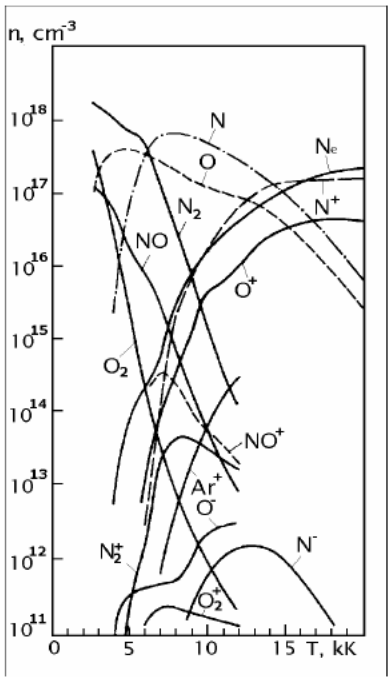

Fig.1.5 Component composition of equilibrium air plasma at constant pressure P=10^5 Pa

Chapter 1.1. Main arc plasma equations applied in calculations

At considerably high pressure (about of the atmospheric one and higher) electric-arc is close to the thermal equilibrium one [1.4,1.7]. The evaluation of the deviation of electron temperature T_e from the temperature of heavy particles T_g can be made by known relation [1.7-8]

$$1-\frac{T_g}{T_e}\approx\frac{3\pi}{32}\frac{m_g}{m_e}\left(\frac{\lambda_e e E}{\frac{3}{2}k T_e}\right)^2, \qquad (1.1)$$

where m_g, m_e, are masses of a gas atom and electron, e is electron charge, λ_e is electron mean free path, E – electric field, k – the Boltzmann constant. It can be transformed to more obvious form, if we consider that the Joule heat from the arc is transported mainly by the thermal conductivity,

$T\sim\sigma E^2 r^2/\lambda$,

and take into the account the equation for the current

$I\approx\sigma E\pi r^2$,

where σ is plasma conductivity, λ - thermal conductivity of a gas, r is characteristic radial size of an arc

$$1-\frac{T_g}{T_e}\approx\frac{3\pi}{32}\frac{m_g}{m_e}\left(\frac{\lambda_e e\cdot\lambda}{\frac{3}{2}k I}\right)^2. \qquad (1.2)$$

For typical values of nitrogen at the temperature T_g ~2000- 4000 K, λ -0.1 W/(m·K), λ_e ~10^{-6} m already at I ~ 10 A we have $1-\frac{T_g}{T_e}\sim 10^{-4}$, or plasma state within the arc is close to thermal equilibrium.

Because of this result one-temperature model of plasma in arc-discharges is usually developed and we also will use it in our approach. For this situation at the first step of analysis we will represent the equation system.

Gasdynamic part of equation system for electric-arc discharge plasma includes the continuity equation

$$\frac{\partial\rho}{\partial t}+div(\rho\cdot\vec{V})=0; \qquad (1.3)$$

the momentum equation is

$$\rho\frac{\partial\vec{V}}{\partial t}+\rho(\vec{V}\cdot grad)\vec{V}=(\rho-\rho_\infty)\vec{g}+\vec{E}div\vec{D}+\vec{j}\times\vec{B}-grad(P+(2/3)\eta\, div\vec{V})+2div(\eta\dot{S}); \qquad (1.4)$$

the energy equation is

$$\rho\frac{\partial}{\partial t}\left(h+\frac{V^2}{2}\right)-\frac{\partial P}{\partial t}+\rho\vec{V}\,grad\left(h+\frac{V^2}{2}\right)=\vec{j}\,\vec{E}-\Psi+$$
$$+div\left(2\,\eta\vec{V}\dot{S}-(2/3)\eta\vec{V}\,div\vec{V}+\frac{\lambda}{c_p}grad\,h\right) \quad ; \qquad (1.5)$$

the Maxwell's equations are

$$rot\,\vec{E}+\frac{\partial\vec{B}}{\partial t}=0\,, \qquad (1.6)$$

$$rot\,\vec{H}=\vec{j}+\frac{\partial\vec{D}}{\partial t}\,, \qquad (1.7)$$

$$div\,\vec{B}=0\,, \qquad (1.8)$$

and Ohm's law

$$\vec{E}+\vec{V}\times\vec{B}=\frac{\vec{j}}{\sigma}+\frac{1}{e\,n_e}\left[\vec{j}\times\vec{B}-grad\,P_e\right]. \qquad (1.9)$$

System (1.3)-(1.9) is supplemented with the equations

$$\rho=\rho(T,P)\;;\;\sigma=\sigma(T,P)\;;\;\lambda=\lambda(T,P)\;;\;\eta=\eta\,(T,P)\;; \qquad (1.10)$$

$$c_p=c_p\,(T,P)\;;\qquad h=h\,(T,P)\;;\;\Psi=\Psi\,(T,P)\;; \qquad (1.11)$$

$$\vec{B}=\mu_0\,\vec{H}\;;\qquad \vec{D}=\varepsilon_0\,\vec{E}\,. \qquad (1.12)$$

The following notations in (1.3)-(1.12) were used: $\vec{g}$ is a vector of the free fall acceleration; $\dot{S}$ is the tensor of deformation velocities with the components

$S_{ik}=(\partial V_i/\partial x_k+\partial V_k/\partial x_i)/2$,

where V_i, V_k are the components of the vector $\vec{V}$; x_i, x_k are coordinates, $k, i=1, 2, 3$; ρ_∞ is density of the ambient medium, P_e is partial density of electrons, Ψ is radiation energy flux.

Let us simplify the system of equations (1.3) – (1.12). Estimates show that in equations we can neglect by the Archimedes and the Coulomb forces. Indeed the Archimedes number

$Ar=\left|\rho-\rho_\infty\right|g\,L/(\rho V^2)$

(L is characteristic length). For typical conditions of arcs, $\rho\sim 5\cdot 10^{-3}$ kg/m^3, $\rho_\infty\sim 1.5$ kg/m^3, $V\sim 10^2$ m/s, $L\sim 10^{-2}$ m we have $Ar\sim 10^{-2}$.

In the Ohm's law it is usually enough to account the first terms in the left and right hand sides of the equation. Indeed, the estimates of the typical conditions at P=1 atm, I = 200 A, ($\sigma\sim 10^4$ sm/m, $V\sim 10^2$ m/s ,$\delta\sim 10^{-3}$ m , $n_e\sim 10^{23}$ m^{-3}, $L\sim 10^{-2}$ m) show that the ratios of density of the inductive electric current, density of Hall's current and density of the current caused by the gradient

of the electron's pressure to the density of the current in the arc have the following orders of magnitude

$$\frac{\sigma V B}{j} \sim \mu_0 \sigma V L \sim 10^{-2} \ ;$$

$$\frac{\sigma j B}{j e n_e} \sim \frac{\mu_0 \sigma I}{2 \pi e n_e \delta} \sim 10^{-2} ;$$

$$\frac{\sigma \, grad \, P_e}{j e n_e} \sim \pi \sigma k T \delta / (I e) \sim 10^{-2} .$$

In such cases the represented terms can be omitted because of their small value and the Ohm's law will be used in its simplest form

$$\vec{j} = \sigma \vec{E} . \qquad (1.13)$$

Using (1.7)-(1.13) we can determine the ratio of the electrostatic force to the electromagnetic one

$$\frac{\left|\vec{E}\right| div \, \vec{D}}{\left|\vec{j}\right| \cdot \left|\vec{B}\right|} \approx \frac{\varepsilon_0}{\mu_0 \sigma^2 \delta^2} \sim 10^{-7} ,$$

where 2δ is the thickness of the conducting region of the arc, ,$\delta \sim 10^{-3}$ m.

Further simplification of the system (1.3)-(1.12) are connected with the symmetry condition $\partial / \partial \varphi = 0$

and the condition of absence of external magnetic field.

Boundary conditions for the considered system of equations are the following.

Existence of the attachment of the flow on the walls

$$\vec{V} = 0 , \qquad (1.14)$$

mall thermal flow to walls

$$\frac{\partial T}{\partial n} = 0 , \qquad (1.15)$$

where n is the normal to the wall's surface.

Tangential component of electric field satisfies the following conditions on the metallic walls

$$E_\tau = 0 . \qquad (1.16)$$

On the dielectric surfaace and between electrodes

$$H_\varphi = \frac{I}{2 \pi r} , \qquad (1.17)$$

Where *I* the current,

$$H_\varphi = 0 \qquad (1.18)$$

on the outlet.

On the symmetry axis we have

$$V_r = 0, H_\varphi = 0, \frac{\partial P}{\partial r} = 0, \quad \frac{\partial T}{\partial n} = 0. \qquad (1.19)$$

This equation system and corresponding boundary conditions are used in our conditions.

In calculations for the Project we use reliable thermal physical data and their interpolations. Data for density $\rho(p, T)$, specific heat $c_p = c_p(T, P)$ and enthalpy $h(p, T)$ for nitrogen and air are represented in [1.3-5, 1.11-17]. Data about viscosity $\eta(p, T)$, electric conductivity $\sigma = \sigma(T, P)$ and thermal conductivity $\lambda(p, T)$ are presented in [1.3-5]. Data on radiation Ψ_0 are presented in [1.3] their detailed analysis one can find in [1.3, 1.4,1.17].

Analysis of experimental and theoretical data for nitrogen showed that at p/p_n = 0.3 – 3, where p_n is normal atmospheric pressure one at calculations can use the following approximations

$\rho(p, T) = \rho(p_n, T) \cdot p/p_n$,

$\Psi_0(p, T) = \Psi_0(p_n, T) \cdot [\rho(p, T)/\rho(p_n, T)]^2$,

$h(p, T) = h(p_n, T)$, $\eta(p, T) = \eta(p_n, T)$,

$\lambda p, T) = \lambda(p_n, T)$,

The mass flow rate is given at the inflow to the plasma generator, ρv_z, $v_\varphi = v_z$, the pressure is extrapolated inside the plasma generator to the inflow boundary, $\frac{\partial p}{\partial z} = 0$, the density and the temperature are determined from the condition of the isentropic gas transition from the normal state to the state with the determined pressure, $e^S \approx p/\rho^\gamma$ (S- is the entropy, γ - is the adiabatic exponent), the velocity of the inflow is determined by the given mass flow rate.

Necessary data for calculations of interaction of plasma jets with air and nitrogen are presented in the following references.

Sources for thermal physics data

Gas	**ρ**	**η**	**ψ**	***h***	**λ**	**c_p**	**σ**
N_2	**[1.11]**	**[1.12]**	**[1.13]**	**[1.11]**	**[1.12]**	**[1.11]**	**[1.12]**
Air	**[1.13-16]**	**[1.4]**	**[1.16]**	**[1.14-16]**	**[1.4]**	**[1.14-16]**	**[1.4]**

Chapter 1.2. Free-Lagrange Method for Computing of Two - Dimensional Magneto-Gas-Dynamic Flows

In present investigations we use the Implicit Free-Lagrange method for carrying out of our Computations. Let us briefly stop on it.

The IFLA (Implicit Free-Lagrange) method was developed for computing two-dimensional non-stationary MGD flows (see, e.g. [1.9-10]). This is a method based on an implicit completely conservative operator-difference MGD on an irregular triangular Lagrangian grid of variable structure. The grid structure must be changed because a Lagrangian grid associated with a moving medium may be distorted in the process of computation. The appearance of triangular cells that strongly deviate from a regular triangle disrupts the approximation of differential operators by their grid analogs and ultimately leads to breakdown of the grid. Automatic grid adjustment in computing time, which involves arbitrary changes of grid structure preserving the triangularity property, makes it possible to maintain a nearly perfect grid. Grid-structure adjustment in the IFLA method is possible also because the difference operators are written on an arbitrary irregular triangular grid.

The non-stationary IFLA method is a sequence of time steps. The n-th step input is an irregular triangular grid ω_n with the values of magneto-gas-dynamic functions at the instant t_n defined in its cells and nodes. Each time step is executed in two stages. The first stage analyzes the quality of the triangular grid, and if necessary makes a local adjustment of grid structure on the basis of the metric principle. The function values are recalculated for the new grid (ω_n)', so that the recalculation for the centers of the new cells preserves the conservation laws and the gradient values of these functions at the nodes. The latter condition is highly significant for computation of complex magneto-gas-dynamic flows. The second stage of the time step evaluates the magneto-gas-dynamic functions on the grid ω_{n+1} at the instant t_{n+1} using an implicit operator-difference scheme. The implicit Completely Conservative operator-Difference Scheme (CCDS) of two-dimensional MGD used in our method is constructed and analyzed by operator approach [1.18] of the theory of difference schemes, which has been developed and consistently implemented in all stages of our work.

IFLA method was thoroughly tested in solution of many problems and proved to be successful at solution of important problems of gas dynamics, plasma physics and astrophysics [1.9-10]. In particular it gave reliable results at solution of a problem of nitrogen plasma jet interaction with oncoming flow [1.19].

References to Chapter 1.

1.1.Isakaev E.Kh., Grigoriants R.R., Spektop N.O., Tyuftiaev A.S. Teplofizika Vysokikh Temperatur, 1994,V.32, №4, P.627.

1.2. Isakaev E, A.Yablonsky, A.Kogan, V.Katarzhis, V.Kutnov, P.Ivanov. The Repair of Railway Frogs Using Plasma Sprayed Coating, Annals of New York Academy of Sciences, Heat and Mass Transfer under Plasma Conditions, ed. P.Fauchais, J.Van der Mullen and J.Heberlein, vol.891, 1999, p.231-235.

1.3. Zel'dovich Ya.B., Rayzer Yu.P. Physics of Shock Waves and High Temperature Hydrodynamic Phenomena. Moscow: Nauka. 1966.

1.4. Engel'sht V.S., Gurovich V.Ts., Desyatkov G.A., Zhaynakov A.Zh., Ivlyutin A.I., Kozlov P.V., Levitan Yu.S., Lelyovkin V.M., Nevelev D.V., Semyonov V.F., Slobodyanyuk V.S., Spektorov V.L. Theory of Electric Arc Column. Novosibirsk: Nauka. 1990.

1.5. Kalitkin N.I., Kuz'mina L.V., Rogov V.S. Tables of thermaldynamic functions and transport coefficients of plasma. Institute of applied mathematics AS USSR. Moscow. 1972.

1.6. Protasov Yu.S., Chuvashev S.N. Physical Electronics of Gas Discharge Devices. V.1. Plasma Electronics. Moscow: Vysshaya Shkola. 1993.

1.7. Zhukov M.F., Koroteev A.S., Uryukov B.A. Applied dynamics of thermal plasmas. Novosibirsk. Nauka. 1975.

1.8. Finkelburg W., Maecker H. Electrische Bögen und thermisches Plasma. Handbuch der Physik, Bd. XXII, S. 254 – 444, 1956.

1.9. N.V.Ardelyan,and K.V. Kosmachevskii. Implicit Free-Lagrange Method for Computing Two-Dimensional Magnetogas - Dynamic Flows. Computational and Mathematical Modelling. Vol. 6, N 4, pp. 209-224, 1995.

1.10. N.V.Ardelyan,and K.V. Kosmachevskii. A Conservative Stable Free- Lagrange Method for the Solution of 2D Magnetohydrodynamic Flows. Max-Planc-Institut Fur Astrophysik. MPA 716, 1993.

1.11. Drellischak K.S. Partition Functions and Thermodynamic Properties of High Temperature Gases. AEDC. TDR-64-22. 1964. V. 10. S.1.

1.12. Capitelli M., Devoto R.S. Transport Coefficients of High Temperature Nitrogen. Phys.Fluids, 1973, V. 16, No.11, p.1835.

1.13. Neuberger A. Composition, Conductance and Summary Radiation of Nitrogen Plasma. AIAA Journal. V.13. N.1.1975.

1.14. Predvoditelev A.S., Stupochenko E.V., Ionov V.P. et al. Thermodynamic functions of air for temperatures from 1000 to 12 000 K and pressures from 0.001 to 1000 atm. Moscow. AS USSR publishers. 1960.

1.15. Tables of thermodynamic functions of air for temperatures from 12 000 to 20 000 K and pressures from 0.001 to 1000 atm. Ed. Predvoditelev A.S., Moscow. AS USSR publishers. 1959.

1.16. Burhorn F., Wienke R. Plasmazummensetzung, Plasmadichte, Entalpie und spezifische Wärme von Stickstoff monoxyd und Luft bei 1, 3, 10 und 30 atm in Temperaturbereich zwischen 1000 und 30 000 K. Z. Phys. Chem. 1960. Bd.215. N.516. S. 269-284.

1.17. Avilova I.V., Biberman L.M., Vorobyov V.S., Zamalin V.M., Kobzev G.A., Lagarkov A.N., Mnatsakanyan A.H., Norman G.E. Optical Properties of Hot Air. Moscow: Nauka. 1970.

1.18. Samarskii A.A. Theory of difference schemes. Moscow. Nauka. 1977.

1.19. Ardelyan N., Bychkov V., Kosmachevskii K., Chuvashev S., Malmuth N. Modeling of Plasmas in Electron Beams and Plasma Jets . AIAA 2001-3101 Proc. 32-nd AIAA Plasmadynamics and Lasers Conference and 4 th Weakly Ionized gases Workshop 11-14 June 2001, Anaheim, CA.

Chapter 2. Impact of plasma from cylindrical plasma generator on counter and cross flows

2.1. Approach to solution of a problem of impact of plasma from cylindrical plasma generator on flow.

Before clarifying which parameters of plasma generator with the divergent nozzle are preferable we made modeling of impact of plasma from cylindrical plasma generator on counter and cross flows for known experimental parameters. This allowed to test the opportunity of application of developed numerical method to problems of plasma interaction with counter and cross flows.

We also considered the interaction of flat jet with the supersonic cross flow as in [2.1]. In Fig.2.1 one can see the principle scheme of such interaction of the jet with the crossflow. The crossflow consisting of a flammable mixture interacts with plasma jet at some angle to a flow ($\theta = 0$ -180°).

As in our simulation in Ref. 1, the gasdynamic equations are coupled with the 2-D Maxwell equations and the plasma dynamics equations, accounting for ohmic heating and radiative plasma cooling. All conditions that are modeled correspond to the experiments in Refs. 2,3. Specific parameters are discharge current I= 45 A, Nitrogen mass flow m_f = 0.7 g/s, power input P=7.5 kW and a freestream Mach number, M=2. Appropriate thermodynamic, optical and transport properties of the nitrogen plasma are used in the Computations. A Lagrange method based on a completely conservative implicit difference scheme with an adaptive triangular unstructured grid described in Chapter 1 is applied. This was effective in modeling the coupling of the internal and external flows inside and outside the counterflow jet and its nozzle [2.1]. It effectively simulated special flow features that complicated the modeling. Some of these were 1) greatly disparate length scales that were of the order of 1 mm inside the plasma generator and 100 mm in the external flow stream-tube capture cross section, 2) mixed subsonic and supersonic flow regions, 3) large gradients of plasma conductance (over 3 decimal orders of magnitude for 1 mm), and 4) other large gradients requiring fine grids to resolve.

In what follows, this approach is applied in this investigation of interaction of plasma jets with crossflows.

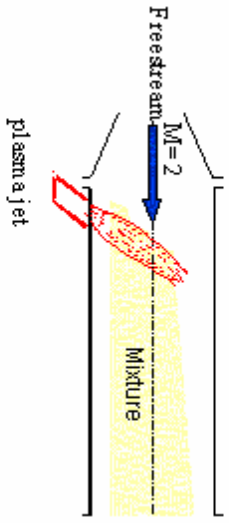

Fig.2. 1 Plasma jet from a slot created by a row of plasma generators.

2. 2. Plasma generators injecting plasma jet to a crossflow

Approach

The model is based on the following system of radiating plasma electrodynamics and gasdynamic equations in more details it is represented in Chapter 1.

$\partial\rho/\partial t + \mathrm{div}(\rho\mathbf{v}) = 0,$ (2.1)

$\rho\, d\mathbf{v}/dt = -\,\mathbf{grad}\, p,$

$\rho\, d\varepsilon/dt = -\, p\, \mathrm{div}\, \mathbf{v} + j^2/\sigma - q,$

$\mathbf{rot}\, \mathbf{E} = -\,\partial\mathbf{B}/\partial t,$

$\mathbf{rot}\, \mathbf{B} = \mu_0\mathbf{j},$

$\mathrm{div}\, \mathbf{B} = 0,$

$\mathbf{j} = \sigma\, \mathbf{E},$

where ρ, p, v, ε are respectively the plasma (gas) density, pressure, velocity, and internal energy; σ is the electric conductance of the gas and plasma, q is the specific power of plasma thermal radiation, **E** is the electric field intensity, **B** is the magnetic field induction, **j** is the electric current density, and $\mu_0 = 4\pi\cdot 10^{-7}$ H/m. An unsteady formulation was applied in cylindrical coordinates. Accordingly, $\mathbf{v} = (v_r, v_\varphi, v_z)$, $\mathbf{B} = (0, B_\varphi, 0)$, $\mathbf{j} = (j_r, 0, j_z)$, $\mathbf{E} = (E_r, 0, E_z)$, $\partial/\partial\varphi = 0$; the subscripts r, φ, z correspond to the radial r, azimuth φ, and axial coordinate z. The plasma equation of state can be expressed as

$p = \alpha\, \rho k_B T/m_{mol},\ \varepsilon = p/[\rho(\gamma - 1)],$ (2.2)

where γ is the adiabatic exponent, k_B is the Boltzmann constant, T is the plasma temperature, m_{mol} is the initial gas molecular mass, and the factor α accounts for the free species number changes resulting from chemical reactions (primarily dissociation and ionization).

The functions $\gamma = \gamma(p,T)$, $\alpha = \alpha(p,T)$, $\sigma = \sigma(p,T)$ and $q = q(p,T)$ for nitrogen plasmas were computed estimated initially from data in Refs. 4-6. Calculations first assumed $\alpha = 1.1$ and $\gamma = 1.4$, but changed with subsequent parametric variations of the temperature, T.

The computational region (see Fig. T.2) includes both the regions inside and outside the plasma generator. No-slip boundary conditions on the walls were assumed for both plasma and gas and $\partial/\partial r = 0$ was applied on the axis of symmetry.

The gas input azimuthal and radial velocities $v_{\varphi 0}$, v_{r0} were determined from the gas density ρ_0 of the given gas flow rate m' and areas of the inflow tangent orifices F_τ, (see Fig. 2), and of the circular input slot F_s: $v_{\varphi 0}, = m'/(\rho_0 F_\tau)$, $v_{r0} = m'/(\rho_0 F_s)$.

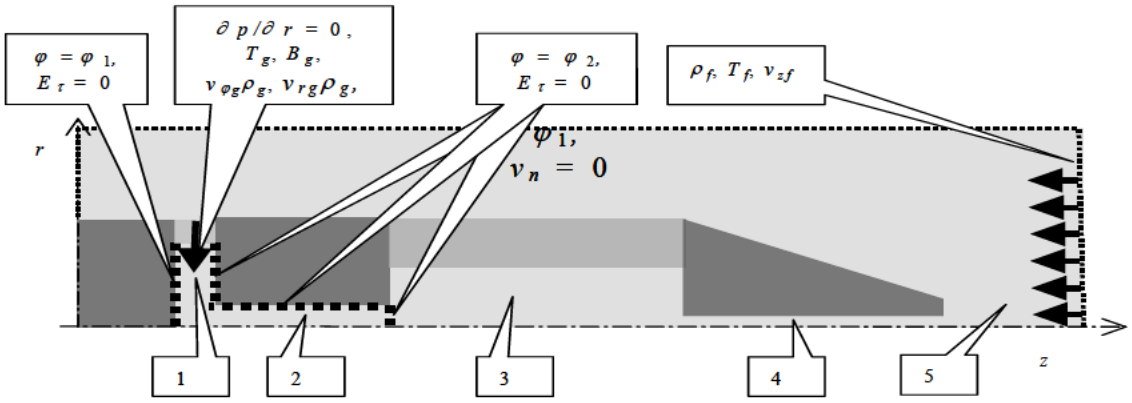

Fig. 2.2 Flow regions: 1 – gas injection slot, 2 – arc, 3 – plasma generator's chamber, 4 – outlet nozzle, 5 – external region.

The input gas temperature T_0 = 167° K. Conditions $p = p_f$, $v_z = -v_{zf}$, $T = T_f$ on the right-hand boundary defined the supersonic ambient flow. Conditions on the left-hand boundary and on the peripheral boundary provided approach to the ambient freestream values.

The entire left-hand wall inside the plasma generator had an electric potential φ_1; in the slot where the gas is injected, the condition on the magnetic field was defined from the total discharge current I. Accordingly, $B_0 = \mu_0 I/(2\pi r_0)$, where r_0 is the distance between the axis and the wall of the jet channel. All the remaining walls were at the electric potential φ_2. To expedite the computations, a small background conductance $\sigma^* < 10^{-3}\,\sigma_{max}$ was assumed to exist in the cold gas; here, σ_{max} is the highest value of plasma conductance in the electric current channel. The computed distribution of electric current in the rest of the channel proved to be practically independent of the fluctuations of the plasma conditions. This is caused by the weak dependence of the nitrogen plasma conductance on plasma pressure and temperature in the parametric region of interest. Accordingly, it was possible to "freeze" this distribution and to avoid its expensive recalculation during the computations. All the data correspond to the conditions in Refs 4,6. There, the number of gas inflow orifices was four and their diameters were 1 mm.

As shown in Ref. 2, the distribution of temperature, pressure and density varies over the nozzle's exit. This showed the main difference between our computations and those of Refs. 4 and 6, where these distributions were assumed constant functions. The distinction between these calculations and Refs. 2.3 and 2.5 is connected with internal heat transfer processes from the source of energy release inside the plasma generator.

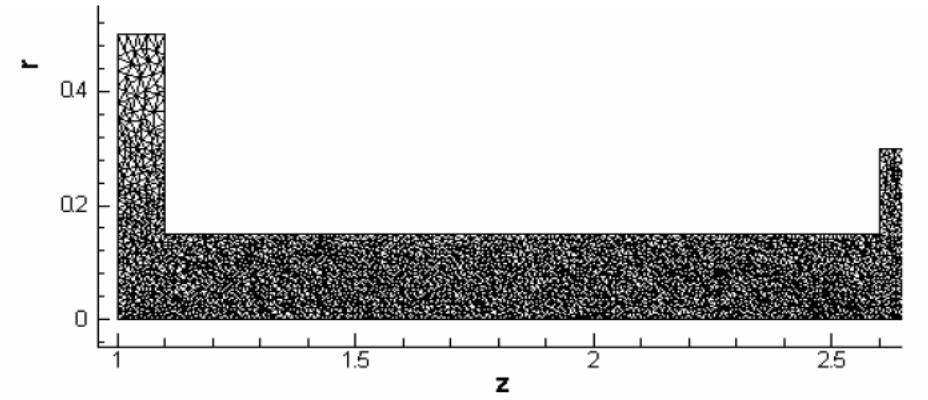

Fig. 2.3. Computational grid inside the plasma generator.

In Fig.2.3-7 are represented distributions of parameters inside and outside of the plasma generator, when injection of plasma takes place at the angle θ=180°. In Fig.2.3-4 one can see the computational grid inside and outside of the plasma generator.

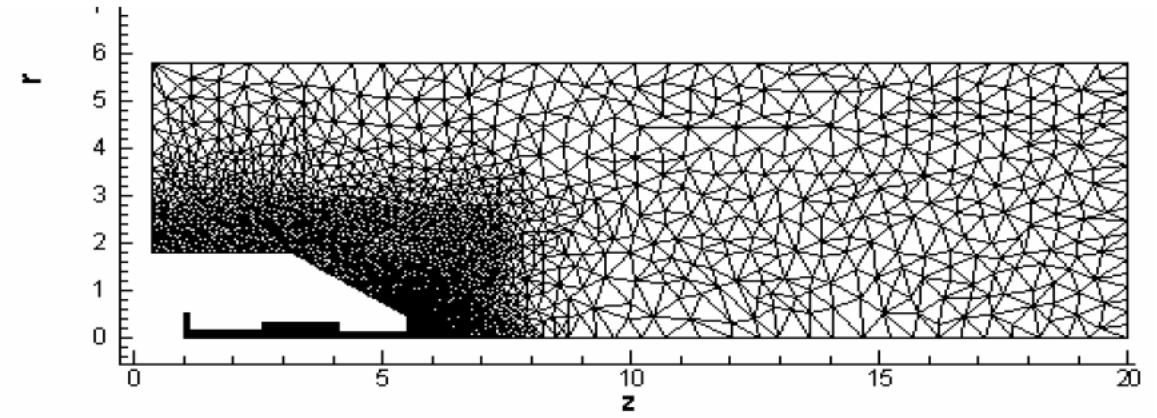

Fig. 2.4. Computational grid outside the plasma generator.

In Fig.2.5 one can see computation results results of pressure distribution inside and outside the plasma generator (in units 10^5 Pa) for time moments t=2.93 ms (a), 4.87 ms (b) и 1.57 ms (c).

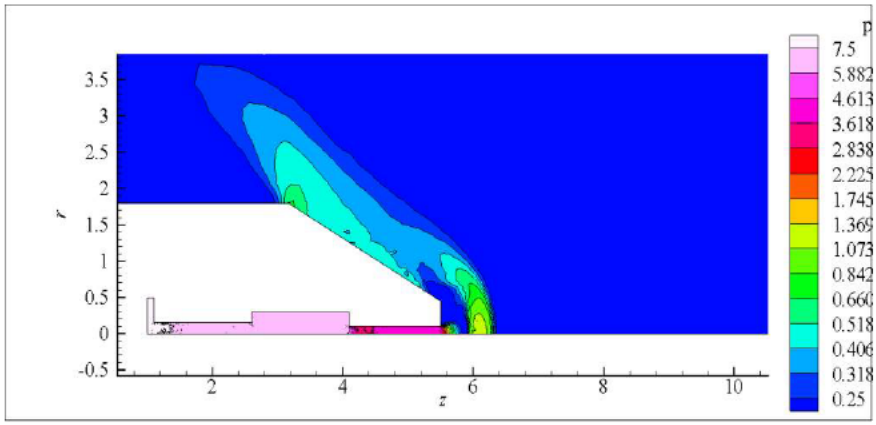

Fig. 2.5a

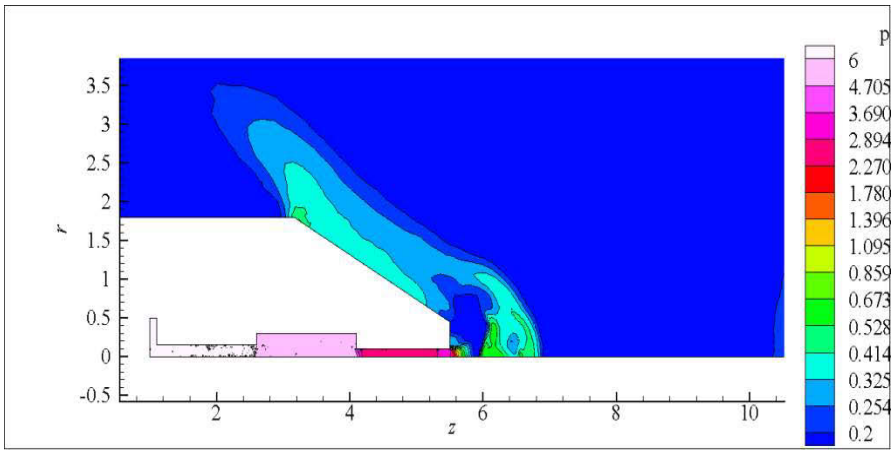

Fig. 2.5b

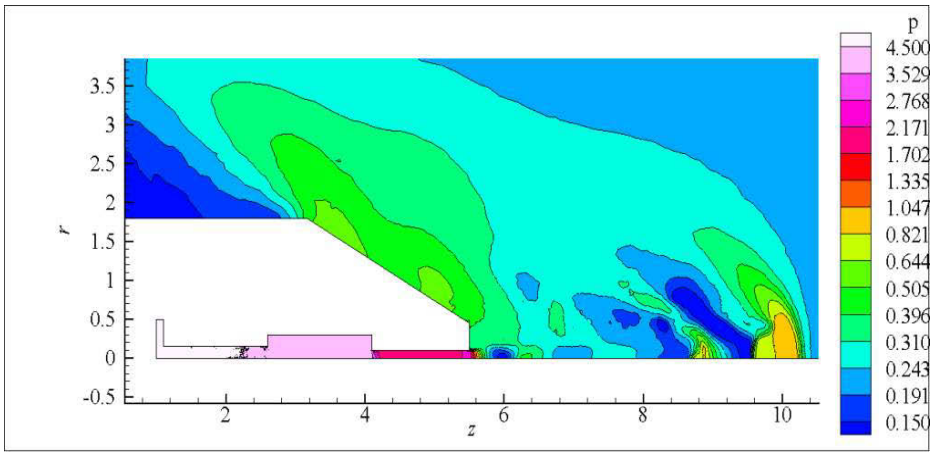

Fig. 2.5c

Fig.2.5. Pressure distributions (in 10^5 Pa) outside and inside of the plasma generator for time moments t=2.93 ms (a), 4.87 ms (b) и 1.57 ms (c)

In the Fig.2.6 one can see distributions of temperature (in units T/T_0) outside and inside of the plasma generator for the same time moments.

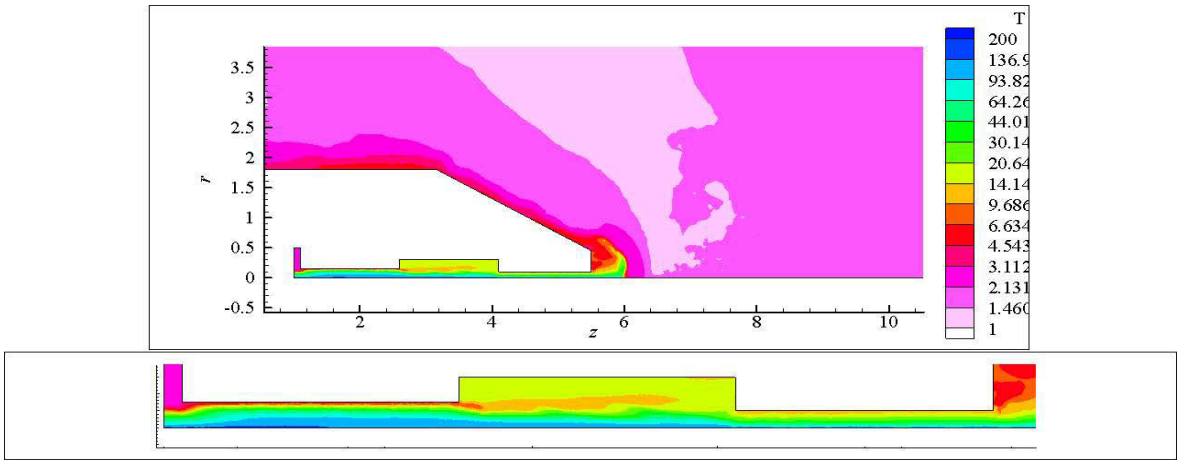

Fig.2.6 a

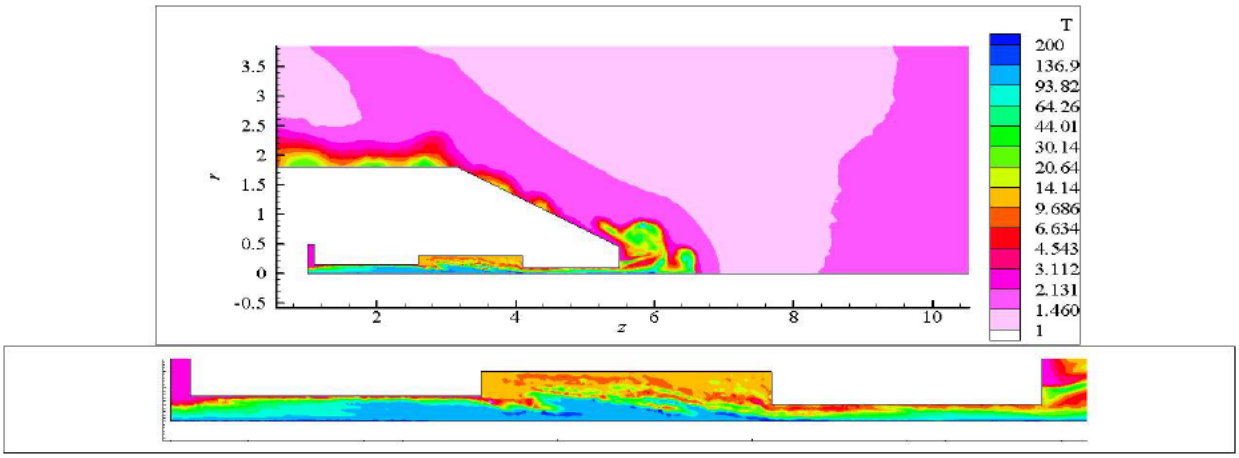

Fig.2.6 b

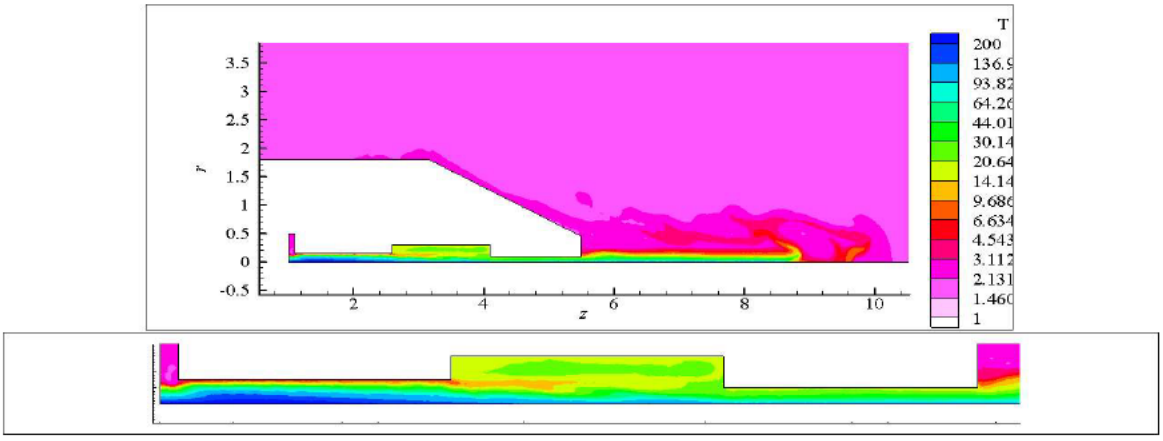

Fig.2.6 c

Fig.2.6. Temperature distributions (in T/T_0) outside and inside of the plasma generator for time moments t=2.93 ms (a), 4.87 ms (b) и 1.57 ms (c)

In Fig.2.7. one can see distributions of the absolute value of velocity outside and inside of the plasma generator for the same time moments (in units10^2 m/s).

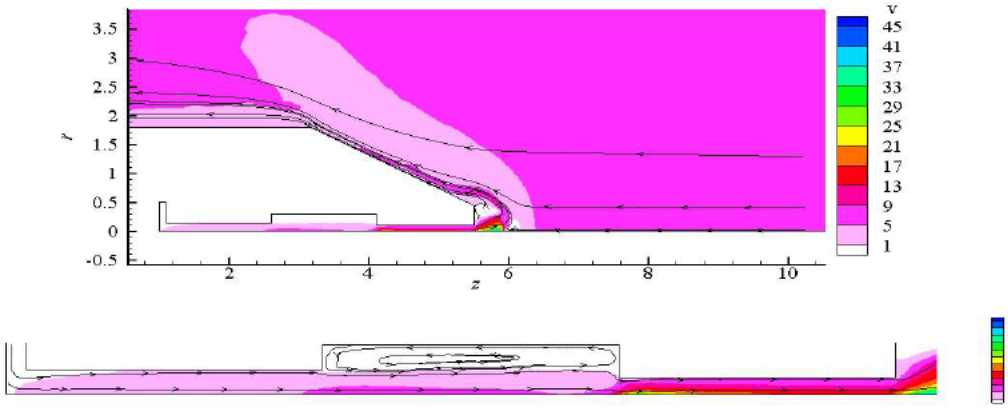

Fig. 2.7 a

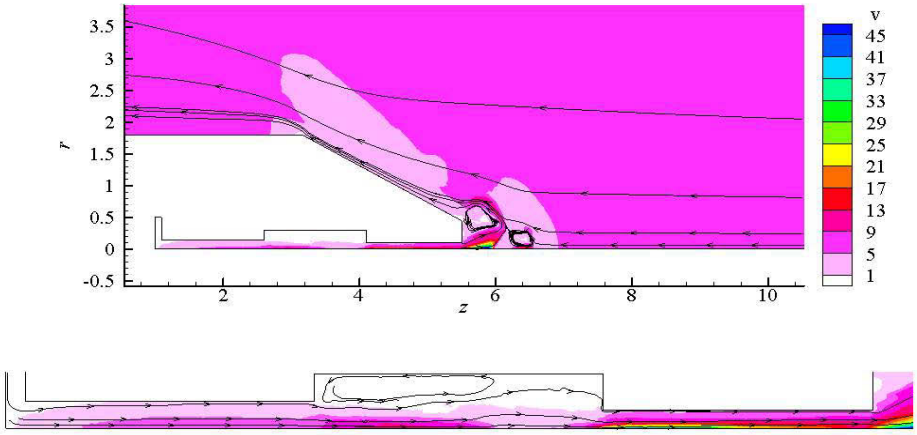

Fig. 2.7 b

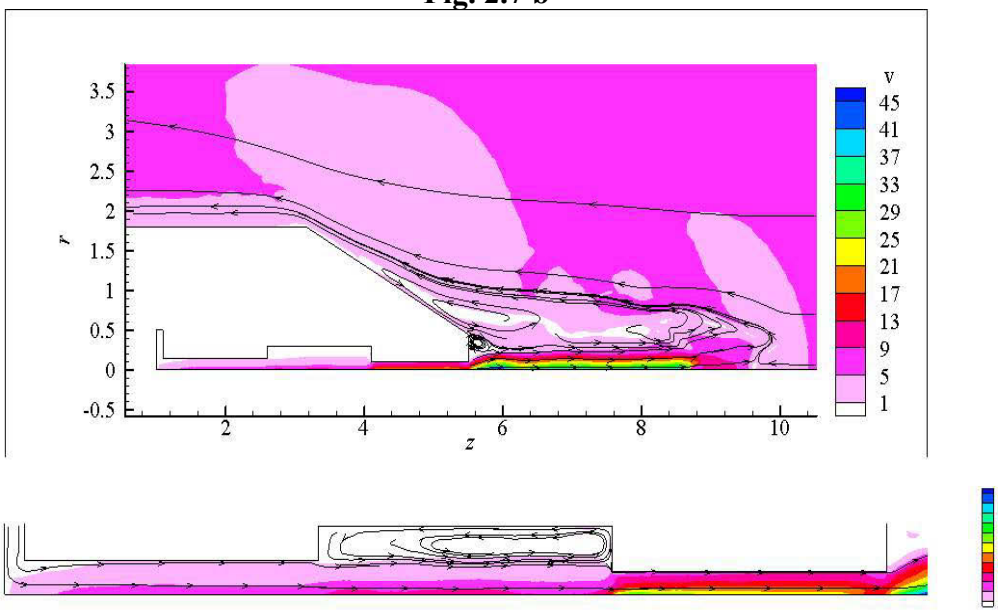

Fig. 2.7c

Fig.2.6. Absolute value of velocity distributions (in 10^2m/s) outside and inside of the plasma generator for time moments *t*=2.93 ms (a), 4.87 ms (b) *и* 1.57 ms (c)

Conducted computations allow to determine distributions of main parameters at the plasma generator exit (cut) necessary for modeling of interaction of plasma jet with a flow in case of the plasma jet incidence to the flow θ = 0 -180°.

Fig.2.5-7 show that the plasma jet significantly effects the flow. Formation of local circular regions with higher temperature and lower pressure take place in the flow. Favorable conditions for ignition of a fuel mixture are created here. However this geometry of interaction is the model one (the plasma is directed along the wall of a combustor) because the interaction of the plasma with the

wall of the combustor would sooner destroy the latter due to high temperature, so it can be considered as the necessary step for calculation of plasma flow interaction at other angles.

One can see from the figures that creation of vortices and stagnation zones takes place in the cavity of the «barrel» type inside the plasma generator, it according to [2.6] can lower the temperature at the exit from the plasma generator, and respectively to decrease efficiency of the plasma jet interaction with the flow. So in computations for the aims of the Project we have conducted analyses of the conical channel of plasma generator design (see below).

To investigate the influence of the radial distribution of the flow variables over the nozzle exit, we made two series of computations. The first used constant flow conditions at the nozzle's exit and the second allowed for variations. For this study, the plasma generator's radius r=10^{-3} m, pressure p=0.235 atm, temperature T=167° K, density ρ=0.5 kg/m^3, Mach number, M=2 was assumed. In addition the jet is directed against the flow (θ=180º) (counterflow case). The characteristic plasma flow time in the calculations is about 10^{-4} s. To resolve the large gradients within the nozzle and near the plasma generator, the total number of calculated points was about 20,000[7].

Calculations for plasma jets injected at angles θ = 135° and 90° with respect to the free stream crossflow have been performed. As contrasted to the internal nozzle flow, the total number of grid points for the external flow field was only about 8,000. However, to resolve the strong gradients, the grid variability parameter was 100. The jet initial profile was considered to be "top hat" (constant over the jet exit region and zero off it), modeling a row of equally spaced plasma generators shown in Fig. 2.1. This formulation is intended to clarify characteristics of the jet interaction with the crossflow, spatial distribution of the flow variables, distribution and special features of the jet influence on the oncoming flow including formation of shocks, dependence on outflow angles, *etc*. To expedite our initial modeling approach, we ignore viscosity and heat conduction effects that are generated on length scales of the order of 0.01 mm. These are infinitesimal on our computational domain. We neglect the global effect of these processes in this analysis as well as combustion and turbulence phenomena.

The free Lagrange method based on a completely conservative implicit difference scheme as well as adaptive, automatically unstructured triangular girding was applied in the numerics. The characteristic size of the cells near the exit nozzle (where the plasma jet is situated) was about 0.1 mm. This was found to be appropriate to simulate large and medium-size vortices and corresponding heat, momentum, and mass transfer processes

2.3. Plasma properties

In order to obtain initial results on plasma composition we started from Refs. 7 and 8 for nitrogen equilibrium thermal plasmas. These showed that N_2 molecules, N atoms and N^+ atomic ions play key roles in the temperature range of interest, which is 5000-10000ºK. These species participated in the following dissociation and ionization reactions:

$N + N \leftrightarrow N_2$,

Concentrations of N^+ atomic ions at these temperatures are much greater than those of molecular N_2^+ ions that appear in the reaction

$e + N_2^+ \rightarrow N_2$.

The corresponding equations for these reactions are the standard ones Ref.9:

$$N^2 / N_2 = F1(T), \qquad (2.3)$$

$$(N^+)^2 / N = F2(T), \qquad (2.4)$$

and also the equation of mass balance

$$\rho / m_N = N + 2N_2,$$

where ρ is nitrogen density, m_N-weight of the nitrogen atoms. Thus,

$$F1 = 3.34 \cdot 10^{23} \cdot T^{0.5} \cdot (1 - \exp(-3400/T)) \cdot \exp(-113265/T), \text{cm}^{-3}$$

$$F2 = 1.22 \cdot 10^5 \cdot T^{1.5} \cdot \exp(-168677/T), \text{cm}^{-3}.$$

These equations were used for our plasma modeling.

2.4. Discussion of plasma jet results

Figure 2.8 shows our experimentally obtained flow patterns for a hydrocarbon plasma jet interacting with an air crossflow for θ=90°. The velocity and temperature of the plasma jet were $V_j \approx 850$ m/s, T≈6000ºK respectively. The Mach number and temperature of the crossflow were M=2, T=167ºK. These characteristics are close to those of experiments [2.3, 2.5] whose conditions we used in our computations. Figure 2.8 shows that the plasma jet is strongly deflected by the crossflow. Moreover, two regions are formed that have distinctly different temperatures. One (red-moderately hot) part is

long and the other (blue and white-very hot) part is thin. This structure is consistent with our computations that are shown in Figs. T9 to be discussed in what follows.

Fig. 2. 8. Time-averaged photo exposure from our experiment of plasma jet interaction with the crossflow at θ= 90°. Velocity of the plasma jet $V_j \approx 850$ m/s, T≈6000 K. Mach number of the crossflow M=2, T=167º K.

Figure 2.9 corresponds to a cross section of the jet flow injected at $\theta = 135°$ into nitrogen. In Fig. 2.10, isotachs are shown for $\theta = 90°$ injection into nitrogen. Characteristics of the crossflow are the same as previously considered.

It is apparent that for the conditions investigated in this paper, the computations for injection angles of 135° and 90° give similar results. This suggests that at least for our parameter space the effect of injection angle may be weak. This observation may apply to combustion processes in more general parametric ranges. If this conjecture is correct, it can be exploited to reduce the number of computations in which reactive species are assessed. The results obtained for these cases are in qualitative agreement with the experimental picture of the flow in Fig. 2.8. In contrast, results for uniform conditions at the nozzle exit differ considerably from experimental and non-uniform ones.

The computations show that during time intervals of the order of $(5\text{-}10)\times10^{-4}$ s, the jet expands and accelerates from the nozzle face. During this period, the Mach number reaches M~3 even in the hot part of jet, where T~4000º K. In addition, the jet screens the flow and a bow shock is formed ahead of it. The oncoming flow is deflected by the shock to flow along the jet. These processes result in velocity differences between the jet and surrounding flow as much as 3000 m/s.

Mixing of the fluid from the jet occurs with the region it shadows behind itself as well as that ahead of itself. Low values of pressure, temperature and density in the cavity behind the jet. Some vortical structures are observed on the mixing layers, possibly due to computational viscosity in this nominally inviscid formulation. These are consistent with those observed in the experiments discussed in Refs. 2.10, 2.12 and 2.13. A cavity is formed behind the jet and its size increases with time. In a real fluid, this cavity would represent a separated flow region in which the vorticity is driven by the jet shear layer entrainment. References 2.10, 2.12 and 2.13 show coherent large scale vortical structures from such shear layers. Expansion of the cavity is accompanied by creation of a bow shock.

The temperature plots in Fig.2.9d show patches of heated gas. They resemble experimentally observed elongated structures on the surface of a hydrogen jet injected into a supersonic crossflow

discussed in Ref. 2.12. More detailed calculation of the shear layer between jet and oncoming flow shows Rayleigh-Taylor instabilities Ref.2.11. The size of area where T>900º K is much larger than that of the dissociated gas as shown in Figs. 2.9-11. Mixing associated with this instability could facilitate combustion processes inside a combustor.

The density variations in Fig. 2.9c show that the jet bow shock travels with a velocity V~ 1300 m/s at the time $t=0.5 \cdot 10^{-4}$ s. This is associated with a shock Mach number M~3.

Figure 2.11 shows equilibrium concentration contours of atoms N and ions N^+ obtained by formulas (2.3)-(2.4). It is evident that the concentrations of atoms are high. They are the same order as those of the molecules for which $N \sim 10^{18}$ cm^{-3} in the jet. Concentrations of ions are high $N^+ \sim 10^{17}$ cm^{-3}. The region that they occupy is much smaller than that of the atoms. It also appears that the zone of atom production is much smaller than that of the gas heated region. For air however, it will be much larger, since the dissociation energy of oxygen molecules is about one half of that of the nitrogen molecules. This can enhance combustion and propulsion efficiency.

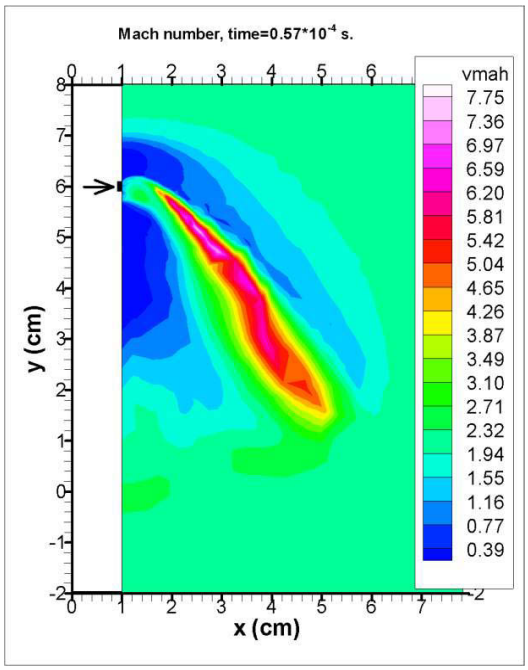

Fig. 2.9a Isomachs (θ=135°)

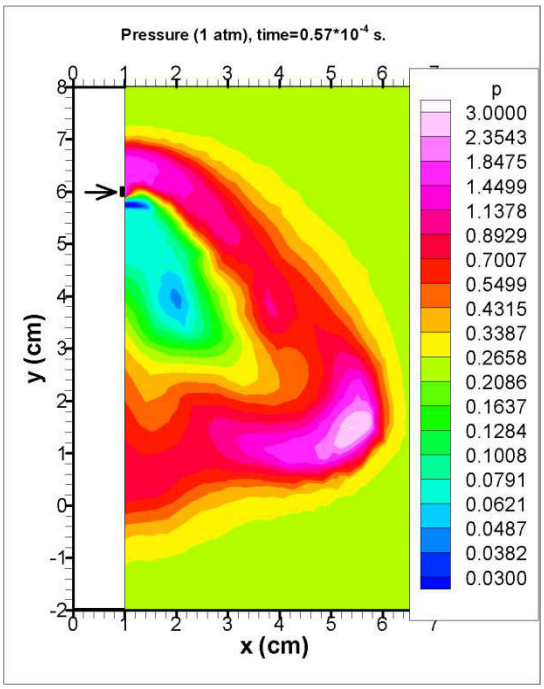

Fig. 2.9b Isobars (θ=45°)

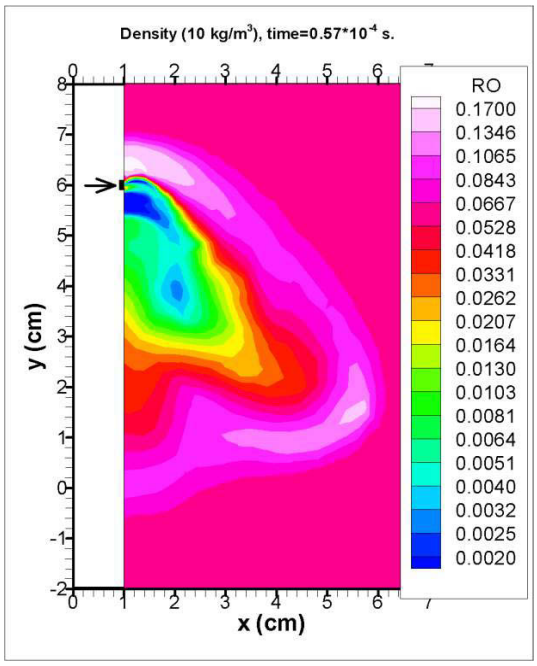

Fig. 2.9c Density contours (θ=135°)

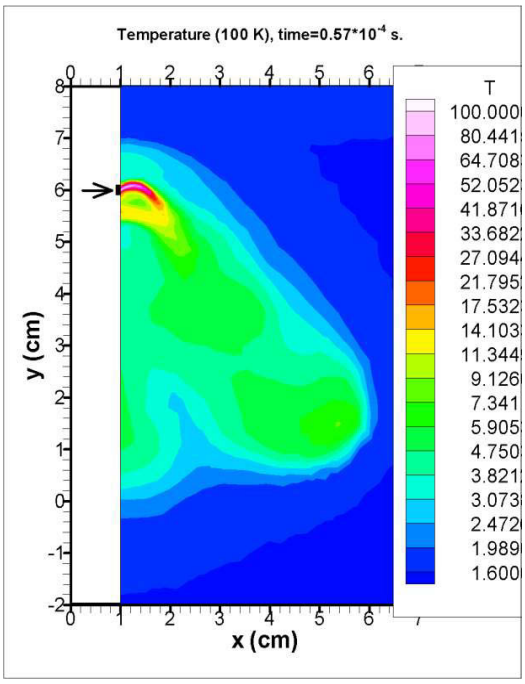

Fig. 2.9d Isotherms (θ=45°)

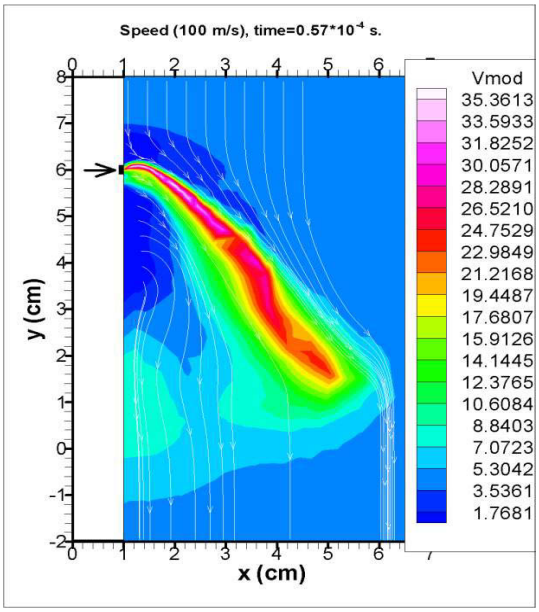

Fig. 2. 9e Isomachs (θ=135°)

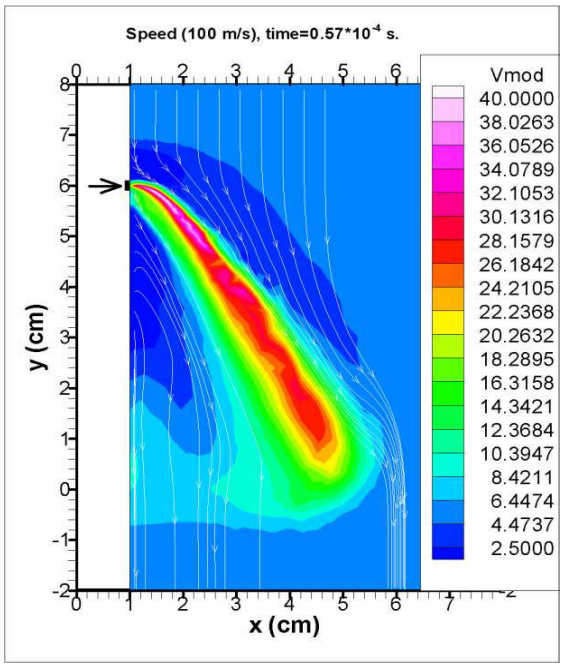

Fig.2.10 Plasma jet interaction with the crossflow at θ=90°: T=3000 K, M=1, P=3 atm. The crossflow parameters: M=2, P=0.25 atm, temperature T =167 K. Flow speed contours.

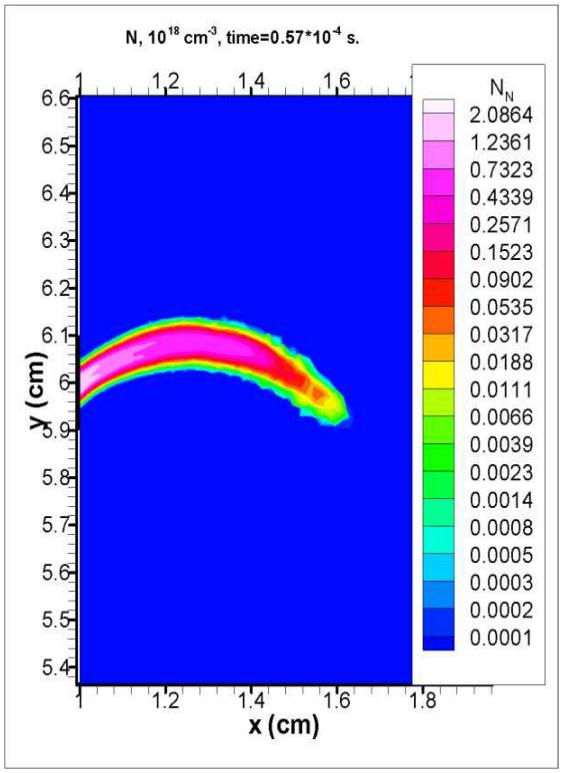

Fig. 2.11a Spatial distribution of atoms in nitrogen (N, 10^{18} cm^{-3}) (θ=135°) excited by nitrogen plasma jet.

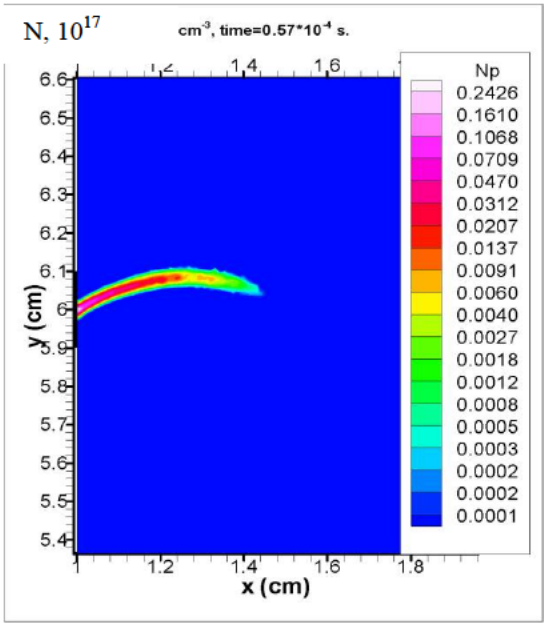

Fig. 2.12.b Spatial distribution of atomic ions in nitrogen (N^+, 10^{17} cm^{-3}) (θ=135°) excited by nitrogen plasma jet.

2.7.Conclusions to Chapter 2.

This chapter presents a theoretical-computational analysis of plasma jet interaction with a crossflow. It emphasizes special features of the coupling of the plasma chemistry and gasdynamics of importance to ignition and combustion in hypersonic propulsion systems. This analysis is a first step to assess the effectiveness of plasma-jet injection for augmentation of ignition-combustion processes.

Equations for plasma jets in a crossflow including transport, chemical and ionization processes were applied. The equations derived were numerically treated by an implicit free-Lagrange method using and adaptive unstructured grid.

Our computations show a complex and non-uniform structure of the flow outside the plasma generator. High atom concentrations inside the plasma jet are apparent. This fact differentiates plasma jets from hot gas jets and can lead to combustion and propulsion enhancement over that possible with the latter. Our results are in qualitative agreement with our own experiments and those of others. It is hoped that these results will stimulate new studies that clarify the relative roles of plasma and gasdynamic processes in these flows.

References to Chapter2.

2.1 Ardelyan N., Bychkov V., Chuvashev S., Kosmachevskii K. and Malmuth N. AIAA paper -2001-3101, *Proceedings 32nd AIAA Plasmadynamics and Lasers Conference and Fourth Weakly Ionized Gases Workshop*, 11-14 June 2001, Anaheim, CA.

2.2 Malmuth N.D., Fomin V.M., Maslov A.A., Fomichev V.P. AIAA paper 99-4883, *Proceedings Ninth AIAA International Space Planes & Hypersonic System & Technologies Conference* 1-4 November 1999 Norfolk, Virginia.

2.3 Fomin, V.M., Maslov, A.A., Malmuth, N.D., Fomichev, V.P., Shashkin, A.P., et.al. *AIAA Journal* **40** No.6, June 2002.

2.4 Ardelyan N.V., Kosmachevskii K.V., Chuvashev S.N., Radiating Plasma Dynamics, Moscow, Energoatomizdat, 1991, P. 191-249.

2.5 Fomin F.M., Maslov A.A., Malmuth N.D., et.al. 2-nd workshop on magneto-plasma-aerodynamics in aerospace applications. Moscow 5 april-7 April 2000. P.112-120.

2.6 Theory of thermal electric-arc plasmas. Ed. Prof. M.F. Zhukov, Prof. A.S. Koroteev. Novosibirsk. Nauka. 1987.

2.7 Capitelli M., Devoto R.S. Phys. Fluids. 1973. V.16. N 11. P.1835-1841.

2.8 Noyberger A. Raketnaya tehnika i kosmo-navtika (Rocket and Space Technique), 1975. V.13. N 1. P.3-5.

2.9 Smirnov B.M. Physics of weakly ionized plasmas. Moscow. Nauka. 1978.

2.10 Ben-Yakar A., Hanson R.K. Supersonic Combustion of Cross-flow Jets and the influence of cavity flame-holders. AIAA 99-04-84 paper. Reno. 1999.

2.11 Theory of turbulent jets. Ed. G.N. Abramovich. Moscow. Nauka. 1984.

2.12 Haven, B., Kurosaka, M., Kidney and Anti-Kidney Vortices in Crossflow Jets, *J. Fl. Mech*., Vol. 352**,** 1997, p. 27.

2.13 Haven, B., Yamagata, D., and Kurosaka, M., Anti-kidney Pair of Vortices in Shaped Holes and Their Influence on Film Cooling Effectiveness, ASME Paper 97-GT-45, 1997.

Chapter 3. Computations of gasdynamic parameters of plasma generator with divergent channel

3.1. Formulation of a problem.

Starting from the interest of analysis of application possibility of plasma generator with divergent channel for influencing on supersonic gas gaseous mixure flows we carried out computations for the plasma generator represented in experimental section of the Report (see below).

From a gasdynamic point of view such a plasma generator is a generator with a conical nozzle [3.1-2]. The detailed gasdynamic analysis of conical nozzle is presented in [3.3], according to it a flow in such a nozzle represents a complicated structure. In vicinity of a conjunction point between the radius and conical parts of a nozzle can take place a flow stagnation at some conditions. A compression wave origins a shock wave. It reflects many times from a symmetry axis and of the nozzle wall. Its intensity increases at approaching to the axis of symmetry, and farther down the flow it decreases because of an influence of rarefaction. In majority of cases an intensity of a wave is not great. Existence of a shock leads to non-homogeneity in distribution of a flow parameters over cross sections of a flow.

Parameters of the plasma generator under the designing are the follows: Minimal nozzle diameter 3 mm. Full angle 12°, half angle 6°. Nozzle length along the axis 30 mm. Cathode diameter 4.5 mm. Half angle of the conical cathode 75°. The distance from the cathode to the nozzle 1.7 mm. An area of the pass in channels equals to an area in the critics of the nozzle. Nominal power 10 kW, gases nitrogen or argon, energy input is distributed at a distance of 5 mm in front of the cathode.

In Fig 3.1 one can see the computation grid for such a plasma generator used in our calculations.

The calculation data is the follows. Minimal nozzle diameter 3 mm. Full angle 12°, half angle 6°. Nozzle length along the axis 30 mm. Cathode diameter 4.5 mm. Half angle of the conical cathode 75°. The distance from the cathode to the nozzle 1.7 mm. An area of the pass in channels equals to an area in the critics of the nozzle. Nominal power 10 kW, gases nitrogen or argon, energy input is distributed at a distance of 5 mm in front of the cathode.

The calculated plasma generator with nitrogen as plasma forming gas variant has the following parameters: gas consumption - 0.7 g/s. Electric power of the source 9 kW. Ratio of translational and rotational (at inlet) velocities equals to tg(6°). Plasma generator injects into a

normal medium at pressure 1 atm and temperature 300 K. At the starting moment in the cross section of the inlet conditions are normal: P=1 atm and T=300 K.

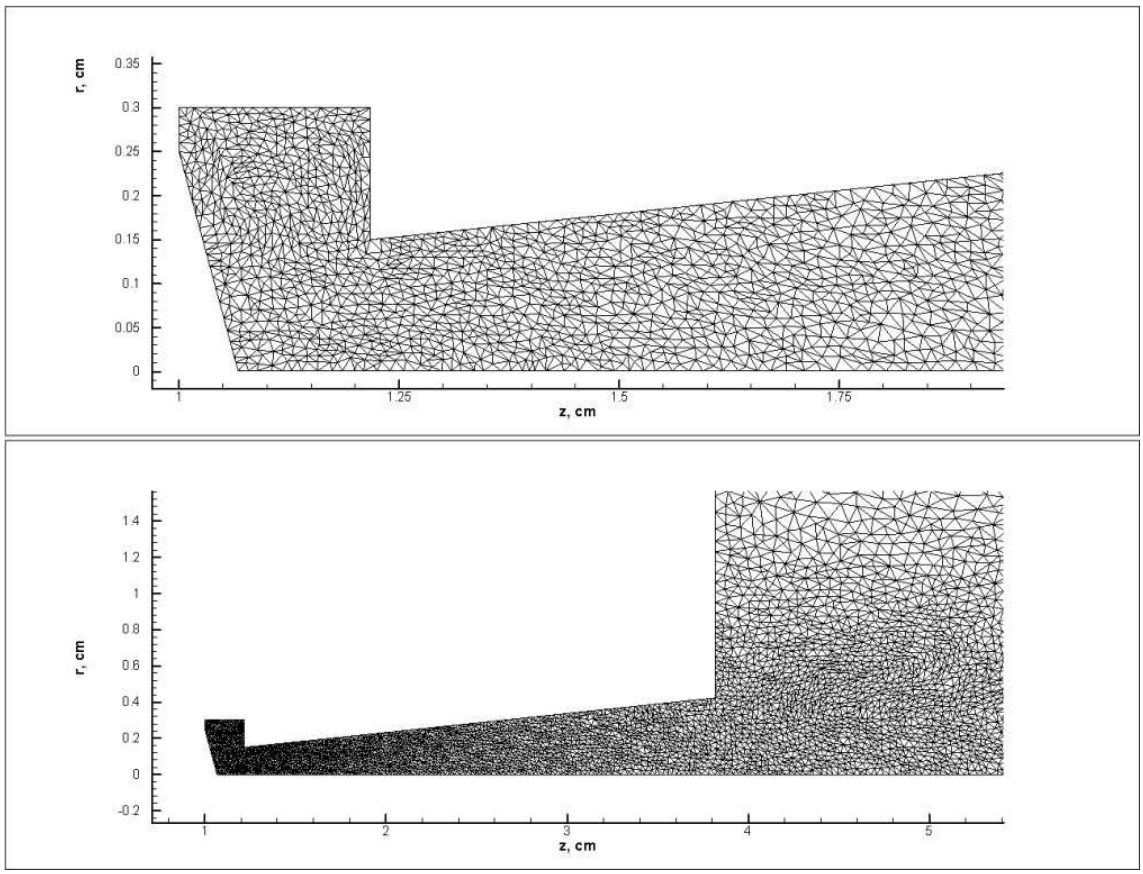

Fig.3.1. Computational grid of internal and external regions of the plasma generator being under the design.

3.2 Initial calculations. Initially calculations have been conducted only for inflowing of a gas in the plasma generator in an absence of energy input to a discharge, conditions of so called "cold" plasma generator. In Fig.1-4 are presented the data on pressure (p is in atm), temperature (T in 100 K), Mach number (vmah= $|v|/|a\ (local)|$) and z component of a velocity (vz in 100 m/s) distributions in a «cold» plasma generator. Indicated time corresponds to stationary parameters to which the flow has approached.

Calculations show that some increase of pressure in the plasma generator conical part takes place near walls, where the gas heating takes place. Formation of the vortex area takes place near the channel center in the vicinity of plasma generator outlet. Distributions of vz velocity component and of Mach number outside the plasma generator show appearance of complex vortex structures at the exit from the plasma generator.

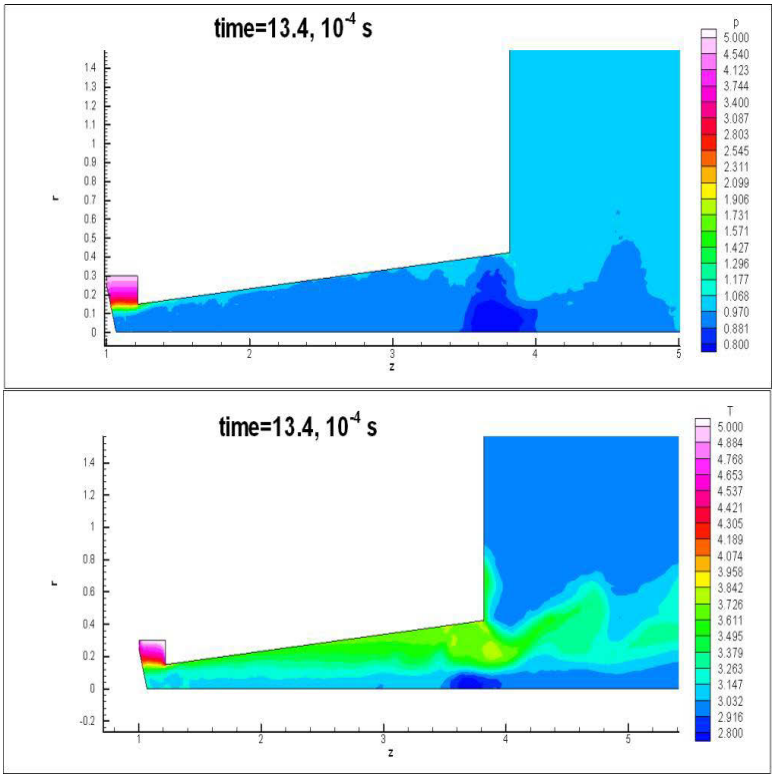

Fig. 3.2, 3. Distributions of pressure and temperature in a «cold» plasma generator.
Pressure (p in atm), temperature (T in 100 K), z, r – in cm.

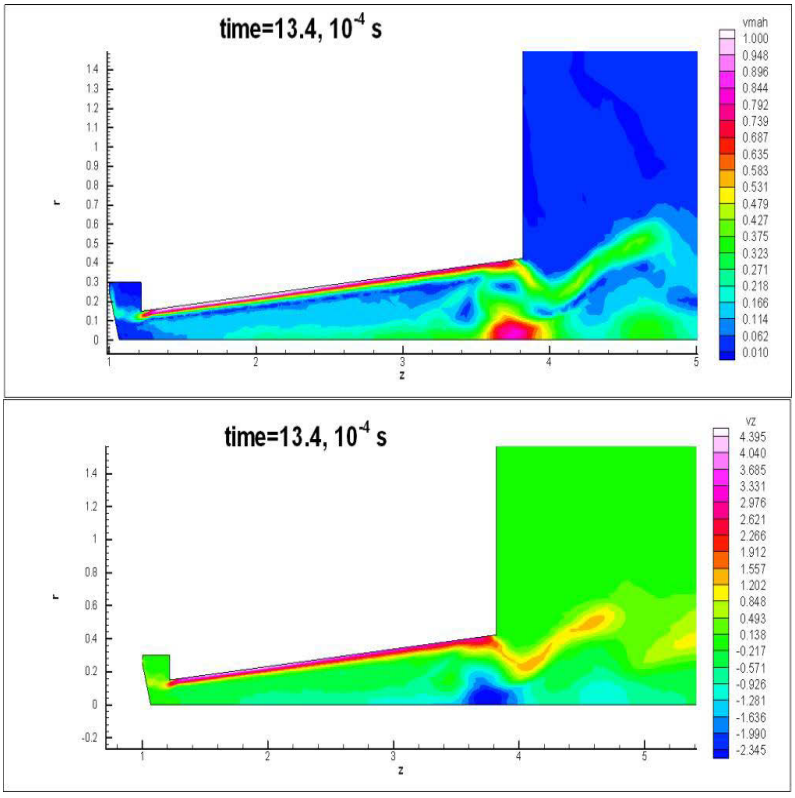

Fig. 3. 4,5. Distributions of Mach number module and of z component of a velocity in a "cold" plasma generator.
vz in 100 m/s , M=vmach= $|v|/|a\ (local)|$, z, r – cm.

3.3 Comparison with available experiments.

In calculations we located the zone of energy input in the area near the electrode (at a distance ~L/3, where L is a length of the plasma generator) it produced the energy input with the power equal to those of the plasma generator as it was done for acceleration of calculations in.

In Fig. 3.6.a-d results of plasma generator work dynamics in time are presented, so called "hot" plasma generator. They show that the stationary state of the plasma generator is realized not immediately but in the result of several intermediate states leading to reconstruction of a flow. After that the state with high temperature in the center of a channel is reached.

Obtained results are in qualitative agreement with experimental ones obtained for analogous plasma generator [3.4-5] with the conical diverging plasma nozzle and parameters (diameter 5-6 mm of the anode, diverging angle 6°, consumption 1.5 g/s and power 50-100 kW), which by minimum power is by ~ 5 times greater than our plasma generator and by nitrogen consumption is greater by ~ 2 times.

The temperature in T [3.5] in initial section ~ L /3 changed over radius from 0.3 to31 kK, and in our computations from 0.3 to ~45 kK and had close distribution over radius to those of [3.5] (see Fig. 3.6c. Higher values in our computations in comparison with [3.5] could be conditions by neglect of thermal conductivity processes in computations, their account should lead to redistribution of temperature with decreasing of its value in a center of a channel. Values of mean mass density of the same order of magnitude (5-6 g/cm^3), we also observed analogous radial distribution of gas density.

Electron concentration was about $N_e \approx 8 \cdot 10^{17}$ cm^{-3}. Electron concentration in [3.5] was proposed a mechanism of additional photoionization due to VUV radiation of the plasma for a description of such a high values of electron concentrations. High values of electron concentrations in our computations are conditioned by the high gas temperature.

Clarification of real reasons of this difference requires additional experimental and theoretical investigations with the definite conditions in the arc produced by our plasma generator.

Computation results on the atom concentrations give large values of the order $N \approx 5\text{-}7 \cdot 10^{16}$ cm^{-3}, this shows the prospects of this plasma generator application for the problems of a fuel ignition.

Conducted analysis and comparison with experiment show principally correct modeling of processes in the plasma generator of the given type.

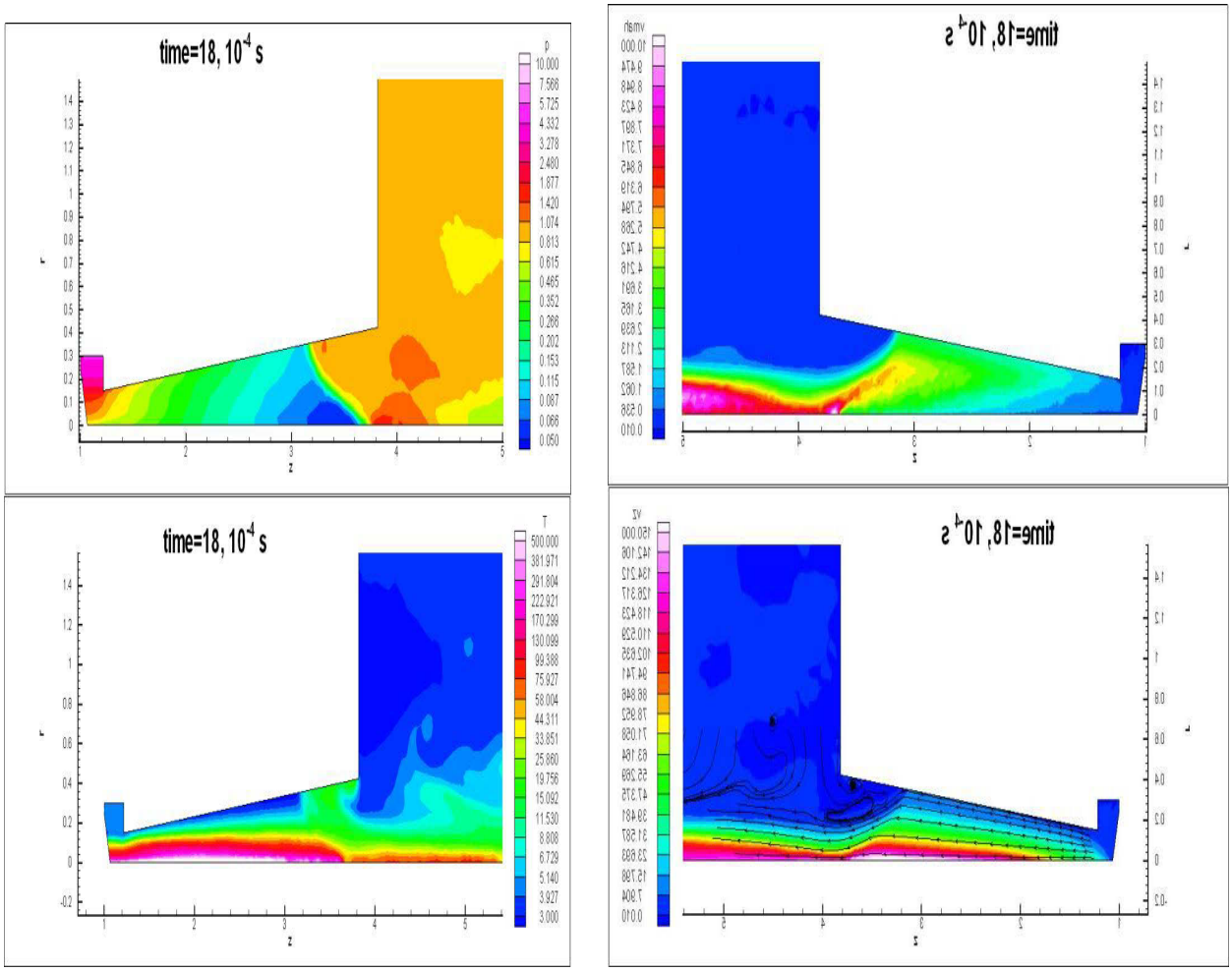

Fig. 3.6 a Pressure, temperature, vz and vmach distributions in a "hot" plasma generator at $18 \cdot 10^{-4}$ s.

Pressure (p , atm); temperature(T ,100 K); vz , 100 m/s , vmach= ⏐v⏐/⏐a (local)⏐z, r –cm.

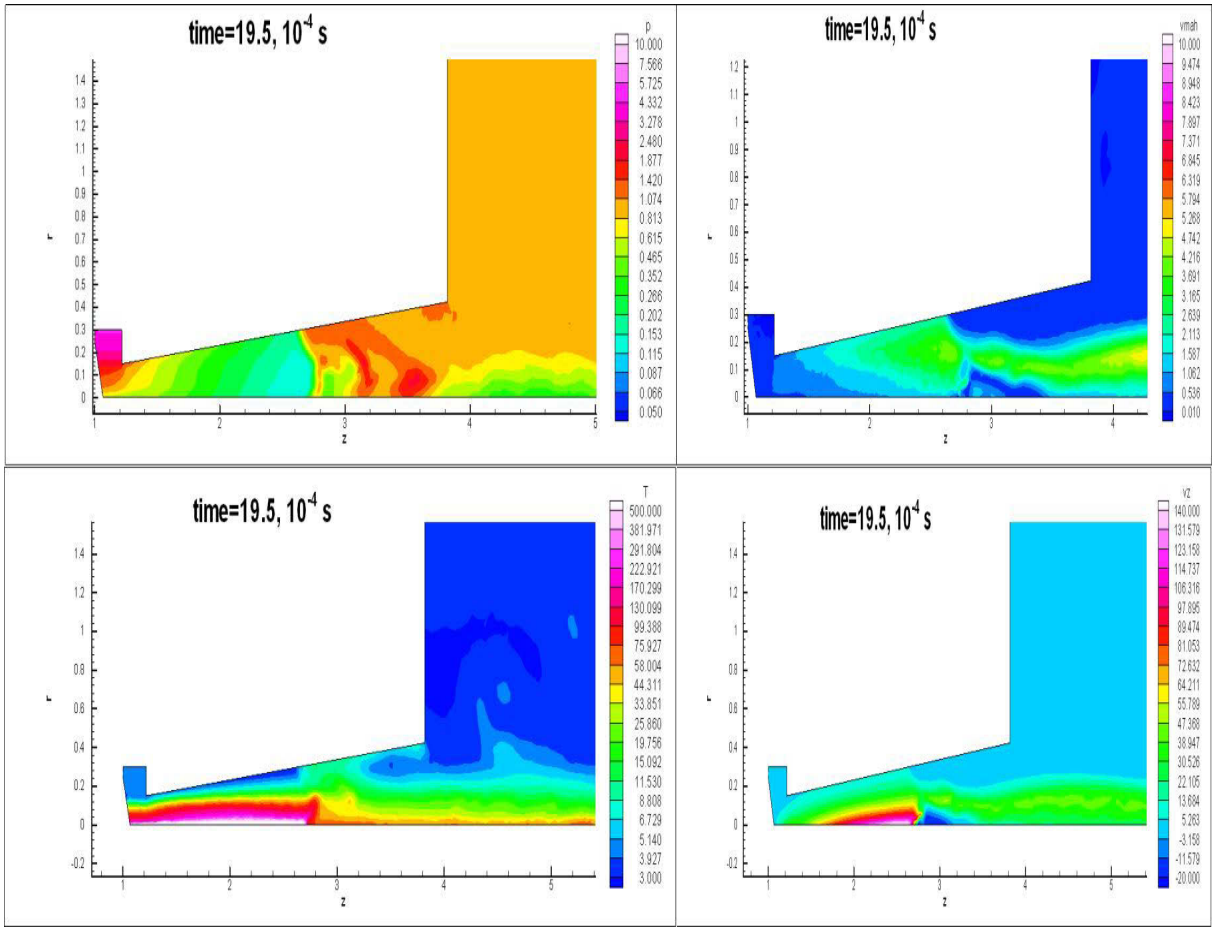

Fig. 3.6b Pressure, temperature, vz and vmach distributions in a "hot" plasma generator at $19.5 \cdot 10^{-4}$ s. Pressure (p , atm); temperature(T ,100 K); vz , 100 m/s , vmach= $|v|/|a\ (local)|$ z, r – cm.

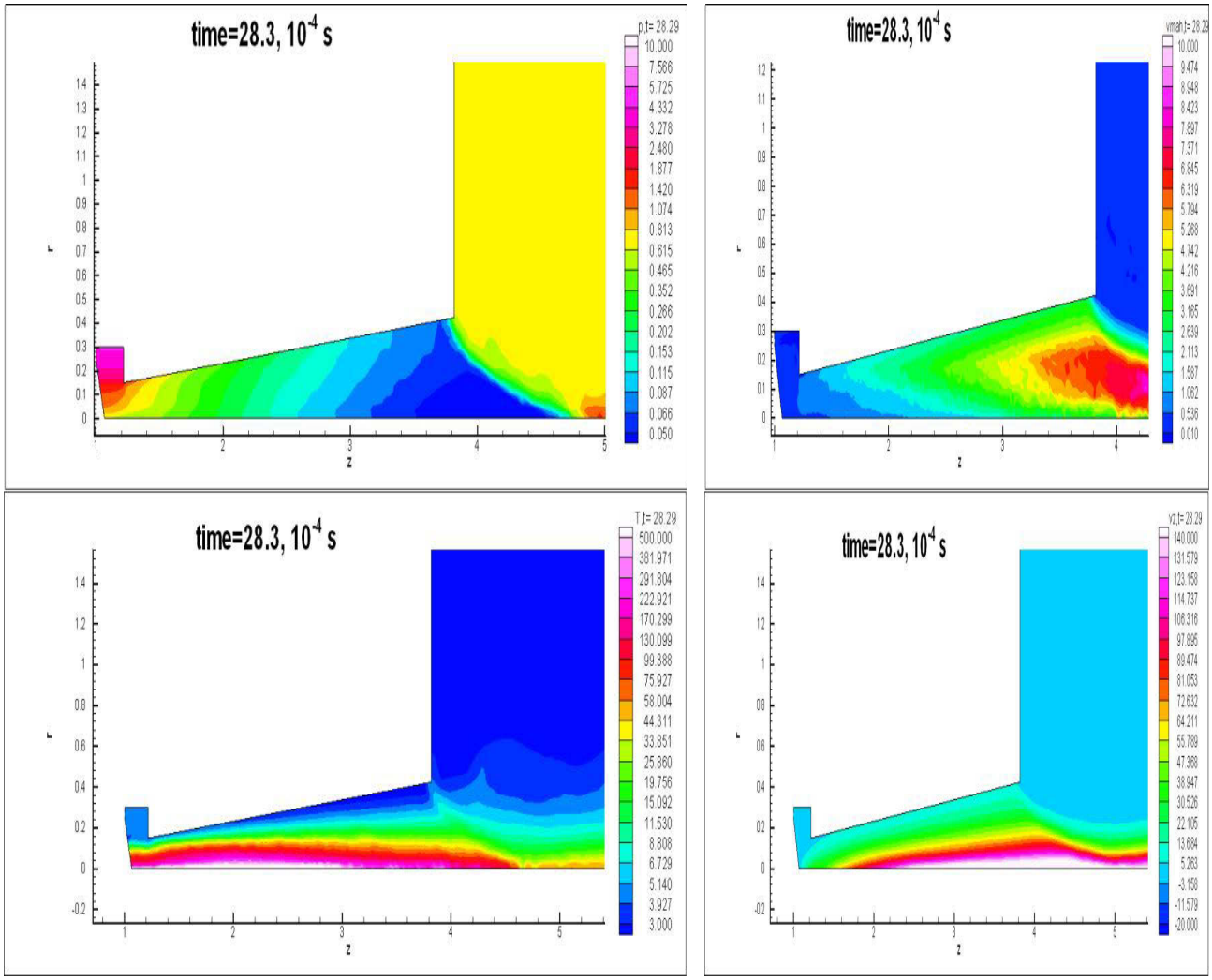

Fig. 3.6c. Pressure, temperature, vz and vmach distributions in a "hot" plasma generator at $28.3 \cdot 10^{-4}$ s. Pressure (p , atm); temperature(T ,100 K); vz , 100 m/s , vmach= $|v|/|a\ (local)|$ z, r – cm.

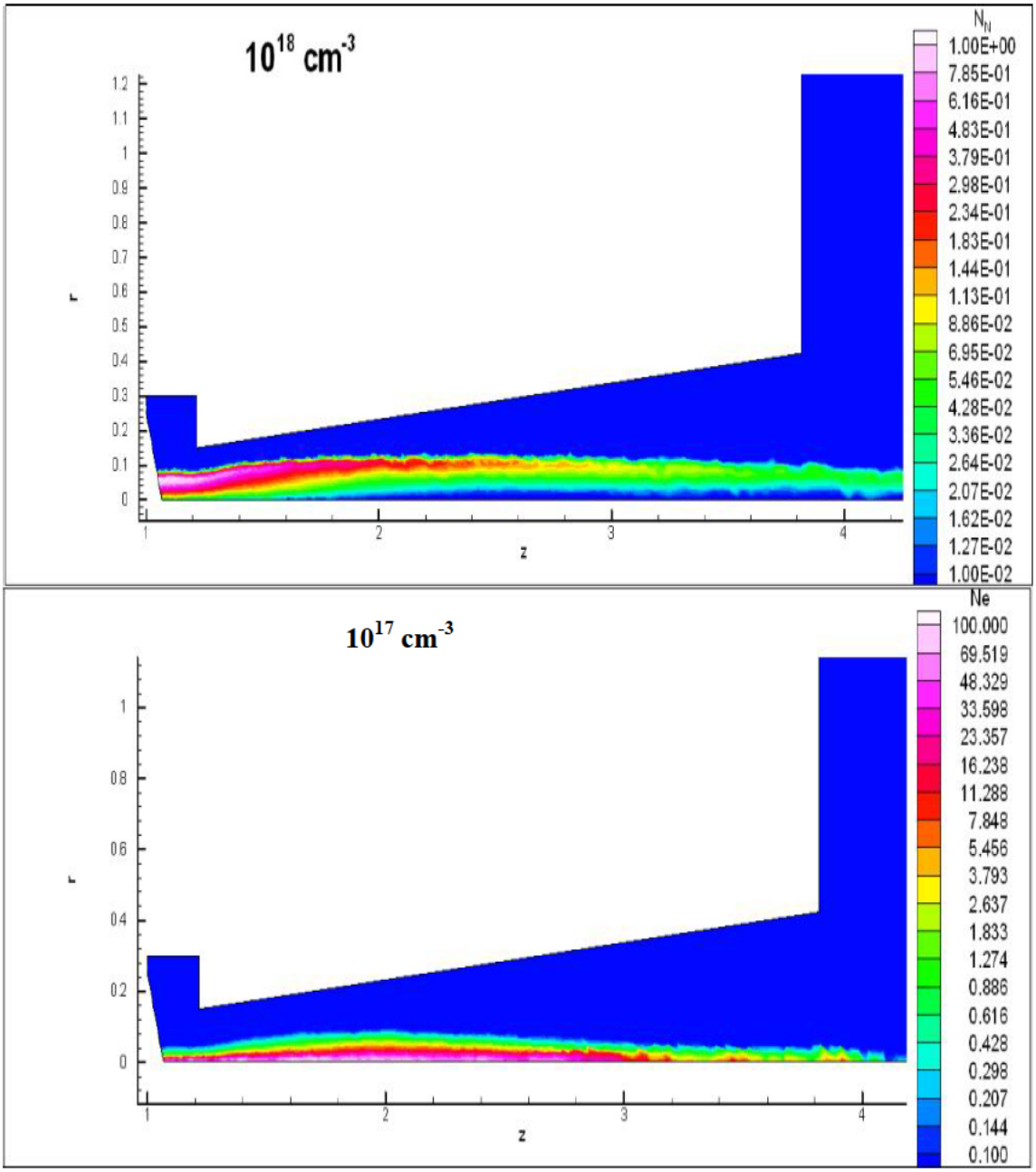

Eig. 3.6d distributions of electron Ne and atom N concentrations in a "hot" plasma generator at 28.3·10^{-4} s. Ne is in 10^{12} cm^{-3} , **N** is in 10^{18} cm^{-3}, z, r –cm.

3.4. Investigations of interaction of a jet with the oncoming flow

During the next stage of investigations we plan to study the action of the nitrogen jet from the conical nozzle plasma generator on the oncoming airflow. As showed our previous calculations it is necessary to know the distribution of its main parameters at its outflowing at θ =180° into a gas. So we have undertaken such computations of interaction of the plasma generator jet with nitrogen flow at θ=180°.

We have undertaken our computations for counter flow with a Mach number M=2. In Fig. 3.7 a-f one can see computation data of interaction of a such plasma jet with nitrogen flow not long before its coming to a quasi-stationary state.

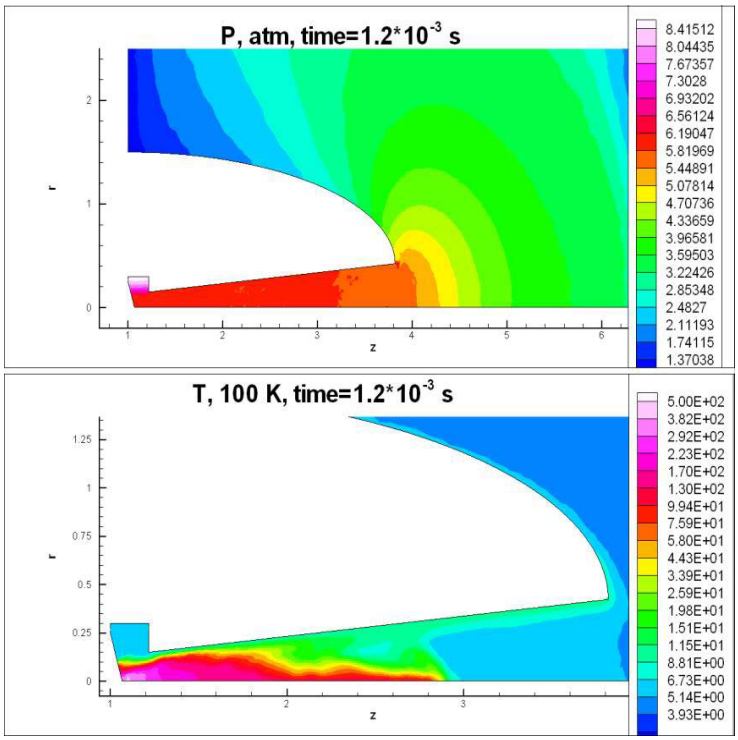

Fig. 3.7 a,b Pressure and temperature distributions in a plasma generator jet interacting with the oncoming flow at the incidence angle θ=180°. Nitrogen, M=2, P_∞= 1 atm, T_∞= 300 K, z, r –cm.

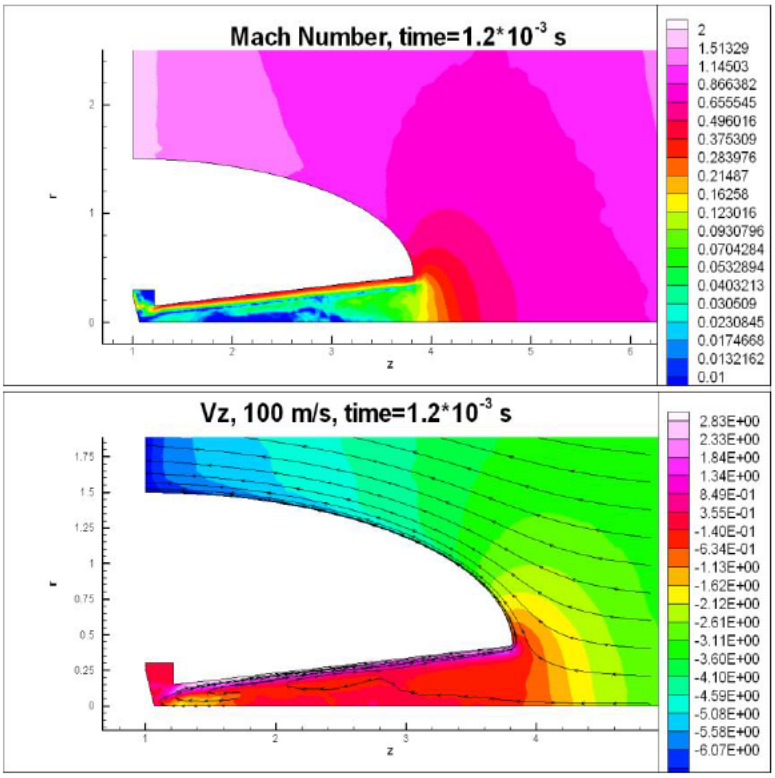

Fig. 3.7 c,d Distributions of a Mach number and Vz velocity in a plasma generator jet interacting with the oncoming flow at the incidence angle θ=180°. Nitrogen, M=2, P_∞= 1 atm, T_∞= 300 K, z, r –cm.

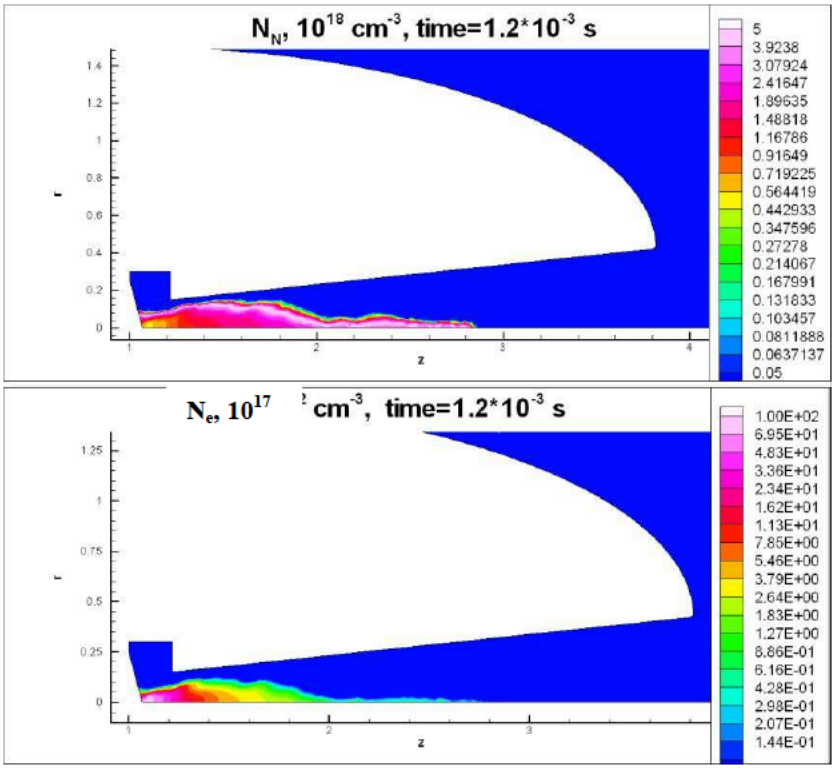

Fig. 3.7 e,f Distributions of electron Ne and atom N concentrations in a plasma generator jet interacting with the oncoming flow at the incidence angle θ=180°. Nitrogen, M=2, P_∞= 1 atm, T_∞= 300 K, z, r –cm.

Computations have been carried out in a following way. Start of computations with a source of a disturbance (counterflow) took place at time moment 2.08 s where gasdynamic data obtained on plasma jet injection to a motionless gas (see above) have been used. The counterflow to the stream was given at z>10 cm. This lead to a decay of the discontinuity. A shock goes forward with increased pressure (more than 3) and Mach number (less than 0.5). A back wave in a decay of the discontinuity is also a shock one. It moves slowly along a flow. On a left outletting boundary we have zero boundary condition of the outletting velocity, so on this boundary a shock also has appeared. In the next moment we changed the boundary condition on the outletting boundary. We put there the outletting velocity generating the rarefaction wave up the flow, it was accepted to be equal to a velocity of the oncoming flow in order to eliminate the shocks of density increase in the oncoming flow.

In connection with these results we now have a computational information about the plasma generators operation in the subsonic flow of the increased pressure. Its peculiarities are: the oncoming flow locks the plasma generator, a gas goes out only in a thin layer along a surface of a nozzle. The pressure in the plasma generator is increased, the radiation increases also (proportionally to square of the pressure) and the summed effect of the gas heating-expansion becomes smaller.

Now we conduct continuous computations of penetration of a jet through the oncoming flow until it comes to a stationary state. Obtained corresponding values will be used in solution of a problem of air stream activation.

Our computations have shown that the distribution of flow parameters at the outlet of the plasma generator has highly non homogeneous character. For smoothing of these distributions we have to account effects of thermal conductivity and viscosity in the plasma generator channe data on which is represented in [3.6-7].

3.5. Viscosity, thermal conductivity and different angles of swirling inside the plasma generator influence on plasma parameter distributions

In this part of the report we present computation results of the plasma jet injection towards the flow. The purpose of computations was to clarify the viscosity and thermal conductivity influence and the different angles of swirling inside the plasma generator on the plasma parameter distributions over the out letting nozzle cross section. These parameter distributions [3.2] later are applied for modeling of plasma jet interaction with a cross flow at the angle (180°>θ>0°).

The computation jet variants corresponded to the jet injection to the oncoming supersonic flow with the parameters: the incident flow velocity is M=2, the pressure 0.2 atm. and the temperature is 250° K.

As earlier the mass flow rate was given at the inflow to the plasma generator, the pressure is extrapolated inside the plasma generator to the inflow boundary, density and the temperature are determined from the condition of the isentropic gas transition from the normal state to the state with the determined pressure , the velocity of the inflow is determined by the given mass flow rate.

The figures in all the computation variants are represented for the time moment when the plasma jet head reached approximately 15 cm.

Computation variants are the following:

B 1. The plasmaforming gas mass flow rate is 5 g/s, the swirling angle is 45°, the energy input is ≈15 kW, viscosity and thermal conductivity effects have been disregarded.

B 2. The plasmaforming gas mass flow rate is 2 g/s, the swirling angle is 45°, the energy input is ≈15 kW, viscosity and thermal conductivity effects have been disregarded.

B3. The plasmaforming gas mass flow rate is 2 g/s, the swirling angle is 45°, the energy input is ≈15 kW, viscosity and thermal conductivity effects have been accounted.

B4. The plasmaforming gas mass flow rate is 2 g/s, the swirling angle is 0° (there is no swirling), the energy input is ≈15 kW, viscosity and thermal conductivity effects have been accounted.

B1 variant In Fig.3.B1a-c one can see distributions of the pressure, temperature and the velocity absolute value (the module of the velocity) in the conical plasma generator at the inputted power W~15 kW (injection to the counterflow). The plasmaforming gas mass flow rate is 5 g/s, the swirling angle is 45°, viscosity and thermal conductivity effects have been disregarded.

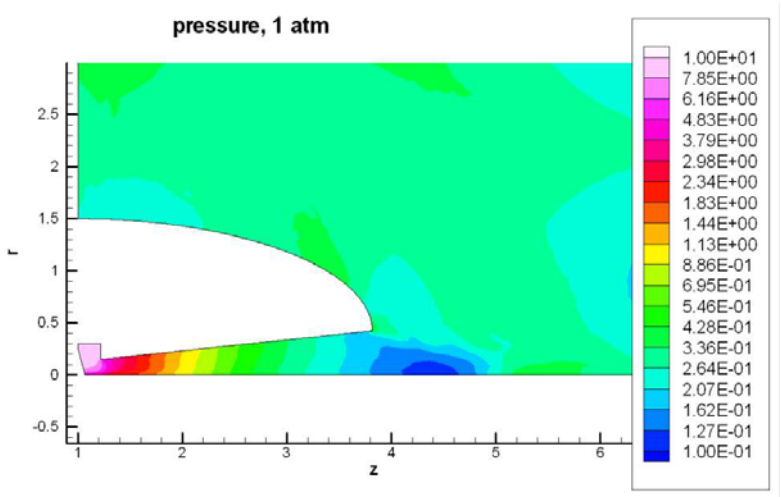

Fig.3.B1a. Pressure distribution in the conical plasma generator at the inputted power of W~15 kW (injection to the counterflow). The plasma forming gas mass flow rate is 5 g/s, the swirling angle is 45°, viscosity and thermal conductivity effects are disregarded.

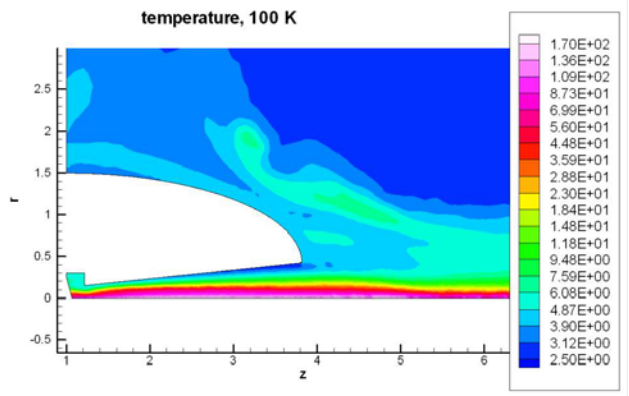

Fig. 3.B1b. Temperature distribution in the conical plasma generator at the inputted power of W~15 kW (injection to the counterflow). The plasma forming gas mass flow rate is 5 g/s, the swirling angle is 45°, viscosity and thermal conductivity effects are disregarded.

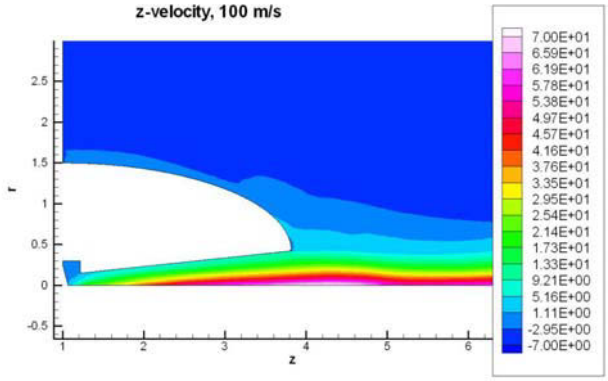

Fig.3.B1c. The velocity module distribution in the conical plasma generator at the inputted power of W~15 kW (injection to the counterflow). The plasma forming gas mass flow rate is 5 g/s, the swirling angle is 45°, viscosity and thermal conductivity effects are disregarded.

B2 variant. In Fig.3.B2 a-c one can see distributions of the pressure, temperature and the velocity absolute value (the module of the velocity) in the conical plasma generator at the inputted power W~15 kW (injection to the counterflow). The plasma forming gas mass flow rate

is 2 g/s, the swirling angle is 45°, viscosity and thermal conductivity effects have been disregarded..

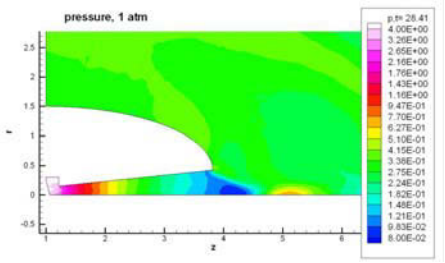

Fig.3.B2a. Pressure distribution in the conical plasma generator at the inputted power of W~15 kW (injection to the counterflow). The plasma forming gas mass flow rate is 2 g/s, the swirling angle is 45°, viscosity and thermal conductivity effects are disregarded.

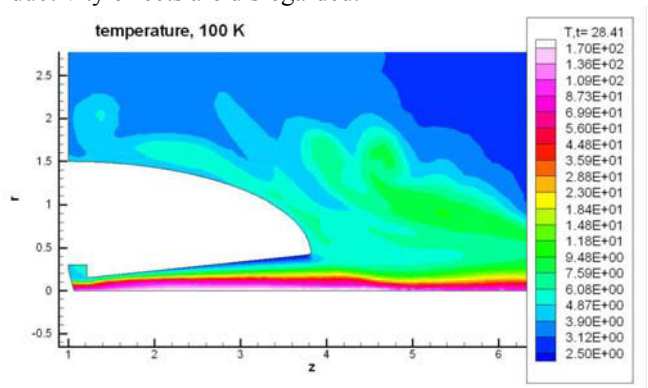

Fig.3.B2b. temperature distribution in the conical plasma generator at the inputted power of W~15 kW (injection to the counterflow). The plasma forming gas mass flow rate is 2 g/s, the swirling angle is 45°, viscosity and thermal conductivity effects are disregarded.

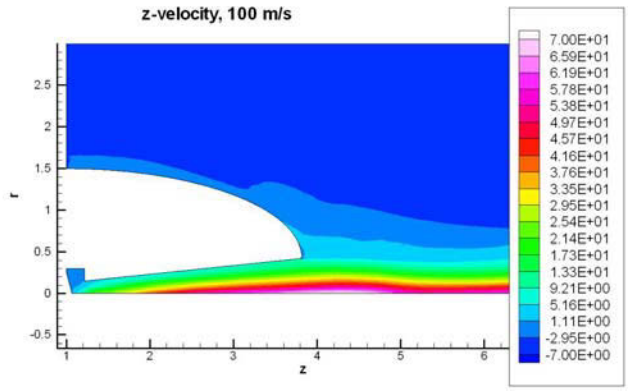

Fig.3.B2c. Distribution of the velocity module in the conical plasma generator at the inputted power of W~15 kW (injection to the counterflow). The plasma forming gas mass flow rate is 2 g/s, the swirling angle is 45°, viscosity and thermal conductivity effects are disregarded.

B3 variant. In Fig.3.B3 a-c one can see distributions of the pressure, temperature and the velocity absolute value (the module of the velocity) in the conical plasma generator at the inputted power W~15 kW (injection to the counterflow). The plasma forming gas mass flow rate is 2 g/s, the swirling angle is 45°, viscosity and thermal conductivity effects have been accounted.

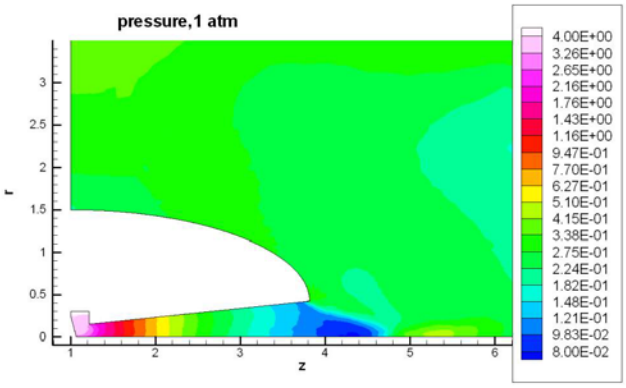

Fig.3.B3a. Pressure distribution in the conical plasma generator at the inputted power of W~15 kW (injection to the counterflow). The plasma forming gas mass flow rate is 2 g/s, the swirling angle is 45°, viscosity and thermal conductivity effects are accounted.

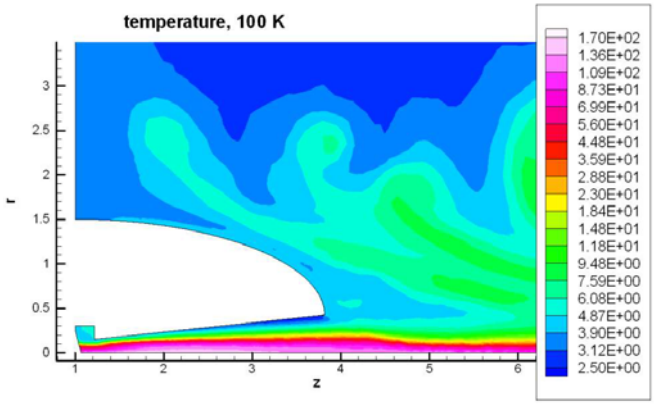

Fig.3.B3b. Temperature distribution in the conical plasma generator at the inputted power of W~15 kW (injection to the counterflow). The plasma forming gas mass flow rate is 2 g/s, the swirling angle is 45°, viscosity and thermal conductivity effects are accounted.

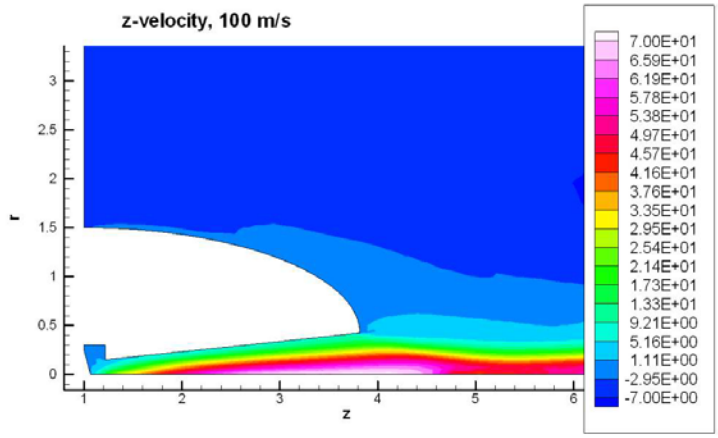

Fig.3.B3c. Distribution of the velocity module in the conical plasma generator at the inputted power of W~15 kW (injection to the counterflow). The plasma forming gas mass flow rate is 2 g/s, the swirling angle is 45°, viscosity and thermal conductivity effects are accounted.

B4 variant. In Fig.3.B4 a-c one can see distributions of the pressure, temperature and the velocity absolute value (the module of the velocity) in the conical plasma generator at the inputted power W~15 kW (injection to the counterflow). The plasma forming gas mass flow rate is 2 g/s, the swirling angle is 0° (no swirling), viscosity and thermal conductivity effects have been accounted.

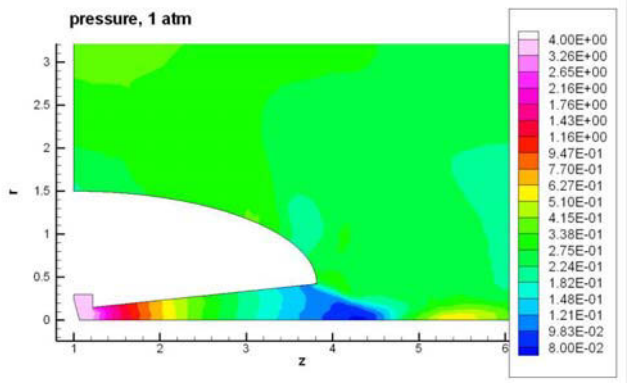

Fig.3.B4a. Pressure distribution in the conical plasma generator at the inputted power of W~15 kW (injection to the counterflow). The plasma forming gas mass flow rate is 2 g/s, the swirling angle is 0°, viscosity and thermal conductivity effects are accounted.

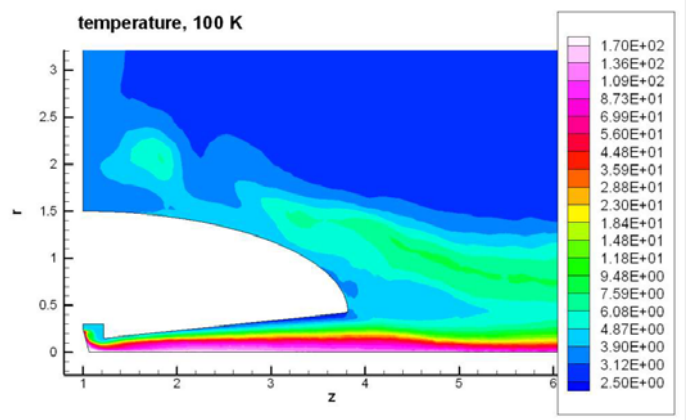

Fig.3.B4b. Temperature distribution in the conical plasma generator at the inputted power of W~15 kW (injection to the counterflow). The plasma forming gas mass flow rate is 2 g/s, the swirling angle is 0°, viscosity and thermal conductivity effects are accounted.

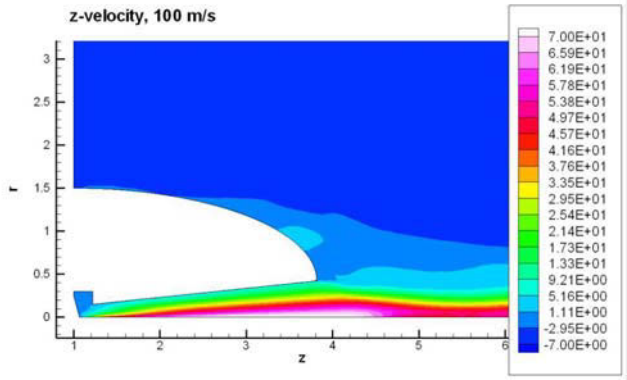

Fig.3.B3c. Distribution of the velocity module in the conical plasma generator at the inputted power of W~15 kW (injection to the counterflow). The plasma forming gas mass flow rate is 2 g/s, the swirling angle is 0°, viscosity and thermal conductivity effects are accounted.

The comparison of B1 and B2 computation results shows that the increasing of the mass flow rate of the plasma forming gas at other same parameters leads to the enlarging and mainly to the elongation of the hot area outside the plasma generator.

The comparison of B2 and B3 computation results shows that accounting of thermal conductivity and viscosity substantially influences distributions of temperature and the absolute velocity value and to increasing (widening in the transversal direction by~1.5-2 times) of the region with high values of parameters. This substantially changes the temperature distribution in the counterflow outside the plasma generator.

The comparison of B3 and B4 computation results shows that variation of the swirling angle weakly influences the parameter distribution inside and outside the plasma generator. This says that the swirling is necessary only for the stabilizing of the jet inside the plasma generator and to prevent melting of its surface due to the development of different instabilities developed at plasma local thermal non-uniformity what is correlated with the results of [3.8]. This result allows us to use parameter distribution computation results obtained with accounting of swirling and without of it at the investigation of the plasma jet interaction with the cross supersonic flow. The last conclusion requires additional experimental validation.

3.6. Interaction of flat plasma jet containing of a row of plasma generators with conical nozzle.

In frames of works on the project we carried out calculations of flat plasma jet containing of a row of plasma generators with conical nozzle and creating a slot (see Chapter 2)

Calculations of the plasma jet from the conical plasma generator (with the diverging channel) and the supersonic crossflow interaction at angles 90° and 135° have been made for determining of optimal conditions for the fuel activation. These computations are of the principle interest from the point of view of the conical plasma generator application for problems of the fuel ignition and combustion. In this case we have the comparison opportunity with our computation results for the plasma generator with the cylindrical channel with a cavity for plasma mixing , see Chapter 2.

The flow parameters were the same as in Chapter 2 and section 3.4: the crossflow velocity was M=2, the pressure was 0.2 atm, the temperature was 250 K.

As earlier the mass flow rate was given at the inflow to the plasma generator, the pressure is extrapolated inside the plasma generator to the inflow boundary, density and the temperature are determined from the condition of the isentropic gas transition from the normal state to the state with the determined pressure, the velocity of the inflow is determined by the given mass flow rate.

In the present calculations we use the data of B4 (section 3.4) computations on the jet radial parameters at the outlet from the nozzle when the gas mass flow rate was 2 g/s, the swirling angle was 0°, and the viscosity and thermal conductivity effects were accounted.

However, the viscosity and thermal conductivity effects at computations of the jet interaction with the crossflow outside the plasma generator proves to be small at typical times of the hydrodynamic interaction at typical gas temperatures outside the plasma generator.

In Fig.3.5.1. a-d one can see the pressure, temperature, Mach number and the velocity absolute value (the module of the velocity) distributions at the plasma jet interaction with the

crossflow at 90° angle, at the inputted power W~15 kW. The mass flow rate of the plasma forming gas is 2 g/s, the swirling angle is 0°.

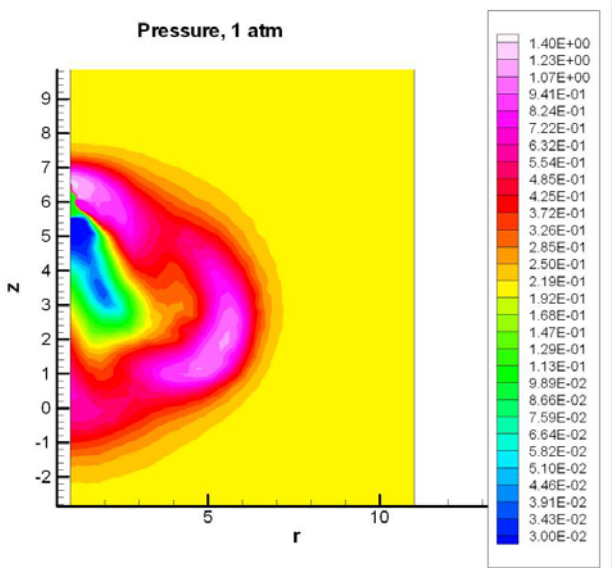

Fig.3.5.1.a Pressure distribution at the plasma jet interaction with the crossflow at 90° angle, at the inputted power of W~15 kW.

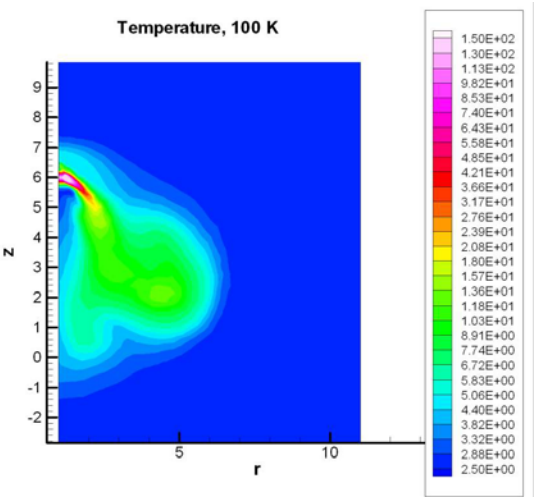

Fig.3.5.1.b Temperature distribution at the plasma jet interaction with the crossflow at 90° angle, at the inputted power of W~15 kW.

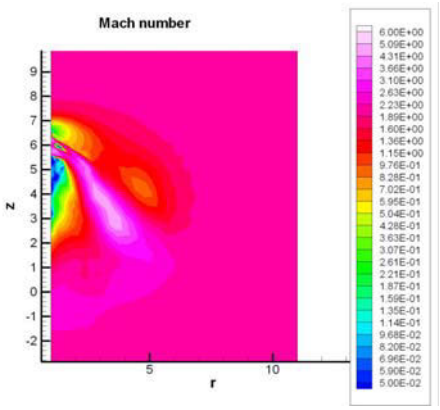

Fig.3.5.1.c Mach number distribution at the plasma jet interaction with the crossflow at 90° angle, at the inputted power of W~15 kW.

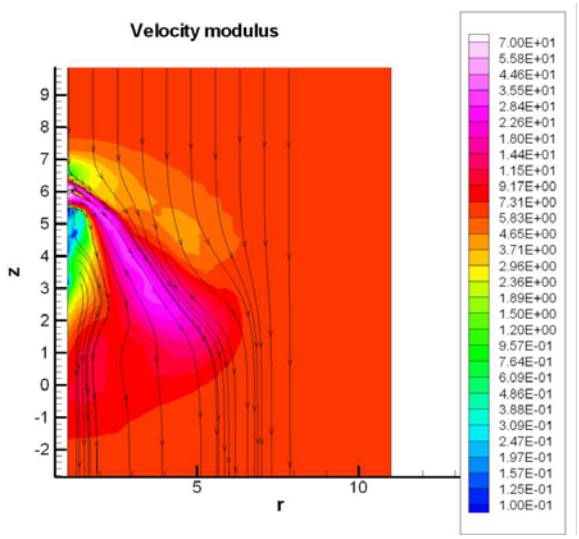

Fig.3.5.1.d The module of the velocity distribution at the plasma jet interaction with the crossflow at 90° angle, at the inputted power of W~15 kW.

In Fig.3.5.2. a-d one can see the pressure, temperature, Mach number and the velocity absolute value (the module of the velocity) distributions at the plasma jet interaction with the crossflow at 135° angle, at the inputted power W~15 kW. The mass flow rate of the plasma forming gas is 2 g/s, the swirling angle in the plasma generator is 0°.

The appearance of the interaction between the jet and the flow at the angle 90° is practically the same as in the case of the plasma generator with the cylindrical channel (with the cavity) analyzed by us in Chapter 2. The external supersonic crossflow drifts and turns the jet down the flow. In the case of Chapter 2 the character of the interaction at 90° and 135° with crossflow was analogous.

However, the comparison of interaction of the jet and the crossflow in case of the conical plasma generator at the angles 90° and 135° reveals the substantial differences.

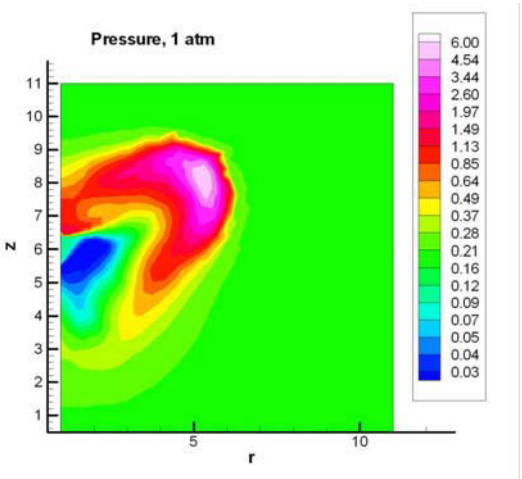

Fig.3.5.2.a Pressure distribution at the plasma jet interaction with the crossflow at 135° angle, at the inputted power of W~15 kW.

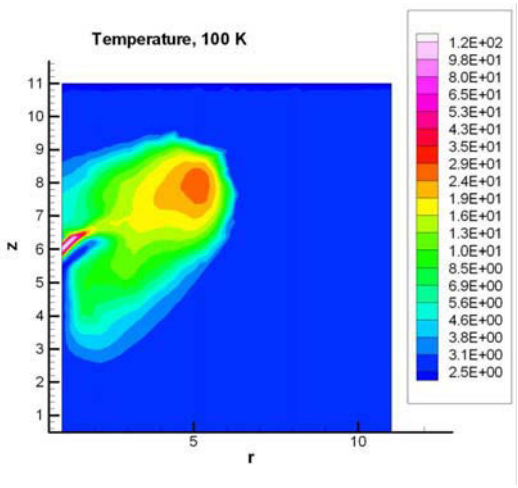

Fig.3.5.2.b Temperature distribution at the plasma jet interaction with the crossflow at 135° angle, at the inputted power of W~15 kW.

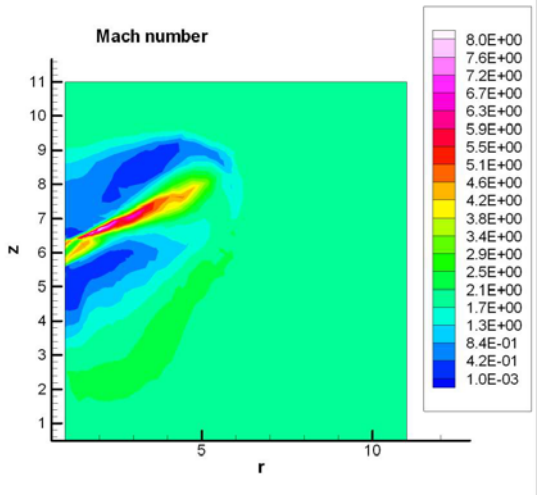

Fig.3.5.2.c Mach number distribution at the plasma jet interaction with the crossflow at 135° angle, at the inputted power of W~15 kW.

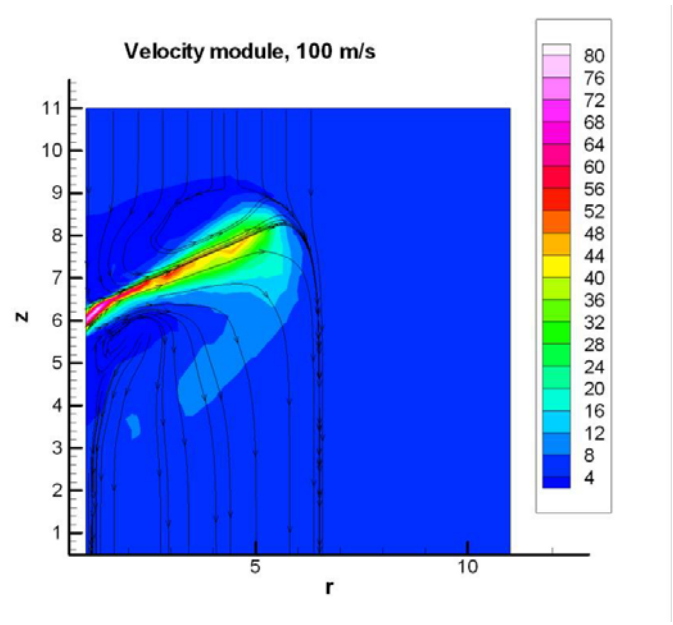

Fig.3.5.2.d The module of the velocity distribution at the plasma jet interaction with the crossflow at 135° angle, at the inputted power of W~15 kW.

Fig. 3.5.2.a demonstrates that deep penetration of the jet towards the flow takes place. Fig. 3.5.2.b demonstrates that the gas temperature distribution at the plasma jet interaction with the crossflow at 135° angle is extremely non-uniform. The hot region is brought forth towards the flow. So the region of the plasma-flow increases in comparison with the case of 90°. Its temperature is 3000 K. It is quite enough for the ignition of the hydrocarbon fuels. This effect can be extremely useful in problems of the fuel ignition and combustion. Fig. 3.5.2.d demonstrates that the incident gas flows around the plasma area. At that the interaction time increases in comparison with the case of 90°, and it is in its turn is useful at initiating of chemical reactions.

Undertook computations have shown the prospects of the conical plasma generator with the diverging plasma channel application for the problems of the fuel activation and ignition in the supersonic flow.

3.7. Conclusions to Chapter 3

Numerical modeling of interaction of plasma generator with divergent nozzle with motionless gas and the counterflow was made. Comparison of computation results with known experiments showed satisfactory agreement. It allows to use developed approach for чmodeling of interaction with cross flows of gases and flammable mixture.

The comparison of computation results shows that:

increasing of the mass flow rate of the plasma forming gas at other same parameters leads to the enlarging and mainly to the elongation of the hot area outside the plasma generator;

accounting of thermal conductivity and viscosity substantially influences distributions of temperature and the absolute velocity value and to increasing (widening in the transversal direction by~1.5-2 times) of the region with high values of parameters, this substantially changes the temperature distribution in the counterflow outside the plasma generator;

variation of the swirling angle weakly influences the parameter distribution inside and outside the plasma generator. This says that the swirling is necessary only for the stabilizing of the jet inside the plasma generator and to prevent melting of its surface due to the development of different instabilities developed at plasma local thermal non-uniformity what is correlated with the results of [3.8]. This result allows us to use parameter distribution computation results obtained with accounting of swirling and without of it at the investigation of the plasma jet interaction with the cross supersonic flow. The last conclusion requires additional experimental validation.

We carried out calculations of flat plasma jet containing of a row of plasma generators with conical nozzle and creating a slot (see Chapter 2) interaction with the cross supersonic flow

at angles 90° and 135° for possible experimental conditions for determination of optimal conditions for fuel activation.

Comparison with results for plasma generator with cylindrical channel shows longer range and larger area of plasma jet interaction with the cross and counter flow in the case of plasma generator with conical nozzle. Most interesting results were obtained at plasma jet interaction with the cross flow at the angle of 135° . The gas temperature distribution at the plasma jet interaction with the crossflow is extremely non-uniform in this case. The hot region is brought forth towards the flow. So the region of the plasma-flow increases in comparison with the case of 90°. Its temperature is 3000 K. It is quite enough for the ignition of the hydrocarbon fuels. This effect can be extremely useful in problems of the fuel ignition and combustion.

Literature to Chapter 3.

3.1. Ardelyan N., Bytchkov V., Kosmachevskii K., Chuvashev S., Malmuth N. D., Modeling of a plasma generator by electron-beam and plasma jets for aerodynamic applications. AIAA 2001-3101. 32-nd AIAA Plasmadynamics and Lasers Conference and 4-th Weakly Ionized Gases Workshop. 11-14 June 2001. Anaheim. CA.

3.2. Ardelyan N., Bytchkov V., Kosmachevskii K., Solodovnikov N., Timofeev, and Malmuth N. D., Modeling of a plasma jet interaction with cross flows for propulsion enhancement. AIAA 2003-1191. 41-st AIAA Aerospace Sciences Meeting and Exhibit. 6-9 January 2003. Reno. Nevada.

3.3. Pirumov U. G., Roslyakov G.S. Gasdynamics of nozzles. Nauka. Moscow. 1990.

3.4. Belevtsev A.A., Isakaev E.Kh., Markin A.V., and Chinnov V.F. Spectroscopic Analysis of Spatial Distribution of the Electron Temperature and Concentration in High-enthalpy flows of Argon and Nitrogen Plasma. High Temperature. 2002. V.40, No 1, P. 26-33.

3.5. Chinnov V.F. On a role of VUV radiation in near anode area of high current plasma generators with diverging anode channel. Teplofizika Vysokikh Temperatur. 2002. V.40, No 4, P. 533-543.

3.6. Engel'sht V.S., Gurovich V.Ts., Desyatkov G.A., Zhaynakov A.Zh., Ivlyutin A.I., Kozlov P.V., Levitan Yu.S., Lelyovkin V.M., Nevelev D.V., Semyonov V.F., Slobodyanyuk V.S., Spektorov V.L. Theory of Electric Arc Column. Novosibirsk: Nauka. 1990.

3.7. Boullos M.I., Fauchais P., Pfender E. Thermal plasmas: fundamentals and applications. V.1. Plenum Press. New-York. 1994.

3.8. Koroteev A.S., Mironov V.M., Svirchuk Yu.S. Plasma generators. Mashinostroenie. Moscow. 1993.

Chapter 4. Interaction of nitrogen plasma jet with propane air mixture

4.1. Calculations of plasma parameters for possible experimental conditions when nitrogen plasma jet is injected from plasma generator to motionless propane air mixture.

This part of work is necessary for possible experimental modeling and choice of optimal hydrodynamic conditions. In this investigation part we posed the problem of ignition of stoichiometric propane-air mixture by the nitrogen plasma jet with the parameters: plasma forming mass flow rate 2 g/s, temperature of the gas 1000 K, power putted to plasma is 5 kW at the gas pressure 0.2 atm.

The solution of this problem was necessary before modeling of plasma jet-incident flow and of plasma jet-crossflow interactions for choice of initial conditions of plasma jet injection to propane-air mixture at some angle to a flow.

Modeling of chemical kinetics of the stoichimetric propane-air mix combustion.

For analysis of ignition and combustion properties of the hydrocarbons in air it is necessary to make choice of main chemical reaction leading to them. A number of works on the propane combustion is rather large and it includes different approaches to the combustion modeling [4.1 - 7] and different sets of chemical reactions taking part in these processes. However in solution of problems connected with modeling of complex gasdynamic flows together with combustion processes it is necessary reduce as possible the number of chemical reagents leaving the main features of the processes. In this direction we know a number of references [4.8-11] devoted to development and application of the simplified schemes for description of complex gasdynamic processes with combustion. Using results of works [4.9-10] in our investigations of gas discharges in the propane-air mix [4.12-13] we obtained times of the mix ignition consistent with our experiments. This determined the choice of the reference [4.9] as starting one for ignition and combustion of stoichiometric propane-air mix by the plasma jet. We do not know now any work devoted to ignition of flammable mixes by plasma jets. So there was no opportunity to compare our results.

The following one step system of chemical reactions describes well variation of pressure and component composition at the combustion of the propane-air stoichiometric propane air mix [4.9]

$$\frac{d\,n1}{dt} = -k1 \qquad (4.1.1)$$

$$\frac{d\,n2}{dt} = -k2 \qquad (4.1.2)$$

$$\frac{d\,u}{dt} = k3 \qquad (4.1.3)$$

n1 and n2 correspond to weight concentrations of propane and oxygen, u is the volume energy density released at combustion. Coefficients in the equations above have the following form :

$$c1 = A \cdot exp(-E/T)$$

$$k1 = (m1)^{1-\alpha} \cdot (m2)^{-\beta} \cdot c1 \cdot (n1)^{\alpha} \cdot (n2)^{\beta}$$

$$k2 = 5.0 \cdot (m1)^{-\alpha} \cdot (m2)^{1-\beta} \cdot c1 \cdot (n1)^{\alpha} \cdot (n2)^{\beta} \qquad (4.1.4)$$

$$k3 = (m1)^{-\alpha} \cdot (m2)^{-\beta} \cdot c1 \cdot (n1)^{\alpha} \cdot (n2)^{\beta} \cdot \Delta H$$

$A=10^{12}$; E=15 100 K[4.9];

T is in K, m1, m2 are the molar masses of the propane and oxygen respectively (at normal conditions they are m1=44, m2=32), α=0.1; β=1.65 [4.9]; the dimensions: [ni]=[g/cm^3], and [u] =[J/cm^3], so the right hand sides of equations (4.1.1)-(4.1.2) are expressed in g/(cm^3 s), and the right hand sides of the equation (4.1.3) is expressed in J/(cm^3 s). The propane –air mix has the following component composition N_2: O_2: C_3H_8=0.7465: 0.2105: 0.043, it was determined by the standard equation [4.14-15]

$$C_3H_8 + 5O_2 + 5 \cdot 3.762 N_2 \rightarrow 3CO_2 + 4H_2O + 5 \cdot 3.762 N_2$$

The formation of substances enthalpy ΔH was calculated by us on a basis of the standard equation [4.14-15]:

$$\Delta H(T) = h_{C_3H_8}(T) + 5h_{O_2}(T) - 3h_{CO_2}(T) - 4h_{H_8O}(T)$$

with a help of data represented in [4.16], and it proved to be $\Delta H = (2.08 \pm 0.04) \cdot 10^6$ [J/mol] in the range 200-4000 K, which corresponds to the temperature range necessary at ignition and combustion of propane –air mixes

4.1.2 Modeling of the plasma gas dynamics of the propane –air mix combustion.

At theoretical and numerical modeling we used the model based on the following equation system of radiative plasma electrodynamics represented in Chapter 1.

In the present case stoichiometric propane-air mix parameters, enthalpy of substances formation and chemical reactions of propane and oxygen were given outside the plasma generator and plasma jet, and inside them the problem was solved as it was in Chapters 2-3.

For computations we used Lagrange method on a completely conservative implicit difference scheme with an adaptive triangular unstructured grid. This was effective in modeling the coupling of the internal and external flows inside and outside the counterflow jet and its nozzle , see Chapter 2-3. The total number of knots was 15000-150000. The grid concentrated in the region of the combustion by the adaptive method.

Chapter 4.1.3 Results of plasma jet from the plasma generator injection to motionless stoichiometric mixture.

Obtained data at the gas pressure 0.2 atm , power putted in the gas 5 kW, initial mixture temperature T=1000 K and plasma forming gas mass flow rate 2 g/s are represented in Fig. 4.1.3.1-4.1.3.5.

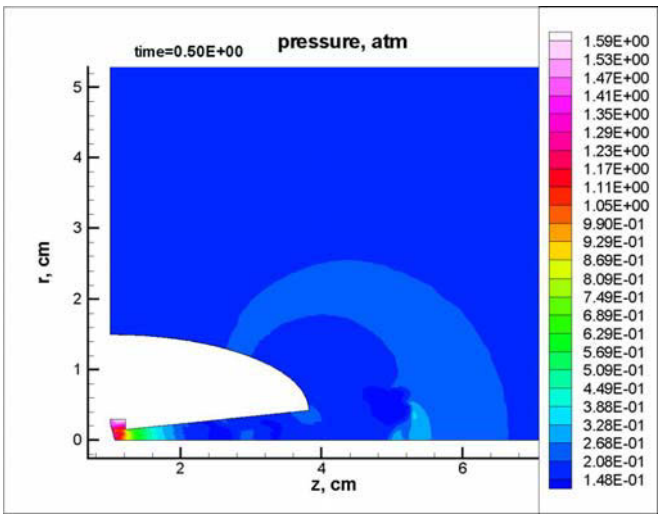

Fig. 4.1.3.1 Pressure distribution at plasma jet injection to stoichiometric propane air mixture at time moment 0.5 ·10^{-4} s. Pressure 0.2 atm , Power 5 kW, initial temperature T=1000 K.

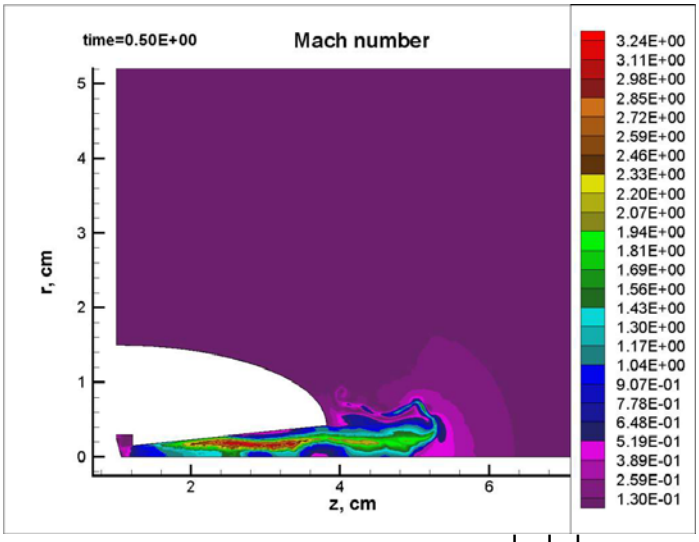

Fig. 4.1.3.2 Mach number (mach= |v|/|a (local)|**) distribution at plasma jet injection to stoichiometric propane air mixture at time moment 0.5 ·10^{-4} s.** Pressure 0.2 atm , Power 5 kW, initial temperature T=1000 K.

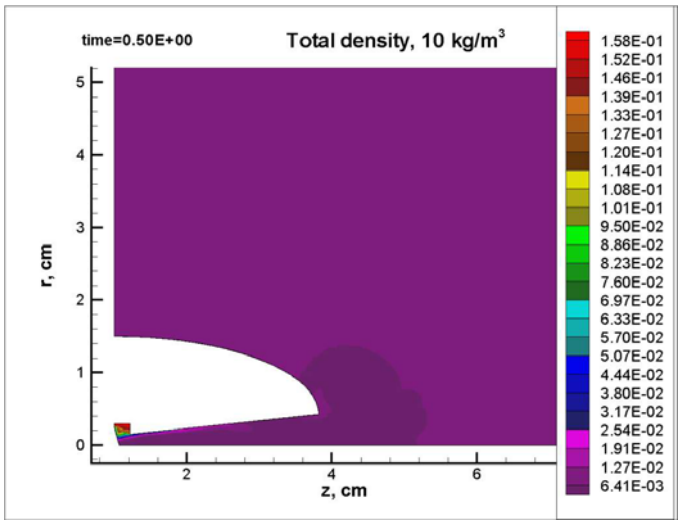

Fig. 4.1.3.3 Density distribution at plasma jet injection to stoichiometric propane air mixture at time moment 0.5 ·10^{-4} s. Pressure 0.2 atm , Power 5 kW, initial temperature T=1000 K.

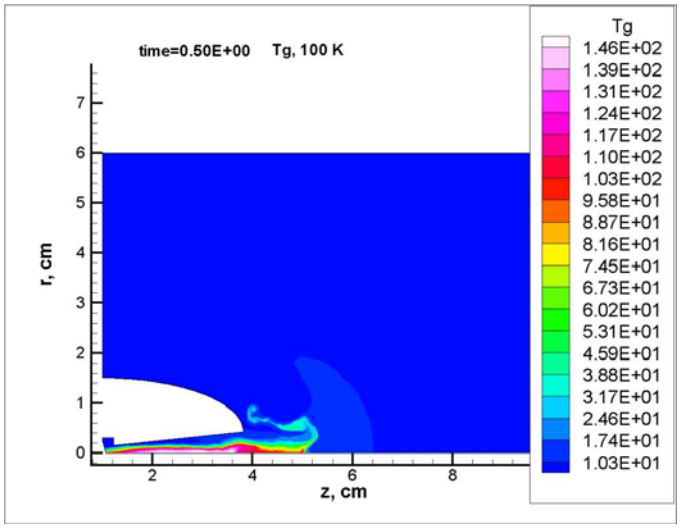

Fig. 4.1.3.4 Temperature distribution at plasma jet injection to stoichiometric propane air mixture at time moment 0.5 ·10^{-4} s. Pressure 0.2 atm , Power 5 kW, initial temperature T=1000 K.

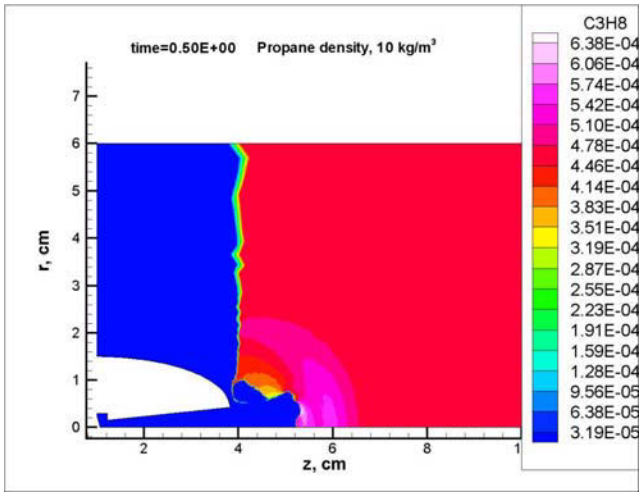

Fig. 4.1.3.5 Propane density distribution at plasma jet injection to stoichiometric propane air mixture at time moment 0.5 ·10^{-4} s. Pressure 0.2 atm , Power 5 kW, initial temperature T=1000 K.

The given power of 5 kW putted in the gas was chosen basing on results of Chapter 3, as the power at which the ignition of the flammable mixture can take place.

Analysis of results represented in Fig. 4.1.3.1-4.1.3.5. shows that the presence of ignition source over the jet surface leads to the reconstruction of gasdynamic flows. In particular pressure and mixture density around the jet are reconstructed. The ignition takes place only in thin layer near the side jet surface. At this power and at the considered computation times there is not the complete combustion of the fuel.

However, our calculations show that the jet at the given parameters can be applied for the ignition of the flammable mixture.

4.2.1 Calculation of flow parameters when the injection of cylindrical plasma jet takes place to the incident supersonic flow of stoichiometric propane-air mixture.

This part of work was necessary from the point of view of modeling and choice of optimal hydrodynamic conditions.

In this part of investigations we posed the problem of the stoichiometric mixture propane-air ignition oncoming with Mach number M=2 on the plasma jet with parameters: plasma forming gas mass flow rate 2 g/s, gas temperature of the oncoming flow 1000 K at pressure 0.2 atm. Jet parameters corresponded to those investigated by us in Chapters 2-3, when we considered the jet interaction with the incident air. The plasma generator power was 15 kW since in previous calculations we clarified that the plasma penetration of the incident flow takes place at the power putted in the gas of ≥ 13 kW.

The solution of this problem was necessary before modeling of plasma jet-incident flow and of plasma jet-crossflow interactions for choice of initial conditions of plasma jet injection to propane-air mixture at some angle to a flow.

The general system of equations added with the balance equations of oxygen and propane in represented above. The calculations were made with the adaptive grid in the combustion region, the flow at T=1000 K comes on the get, the pressure is 0.2 atm. The plasma generator power is 15 kW, the plasma forming gas mass flow rate is 2 g/s.

In Fig. 4.2.1-4.2.4 one can see results of calculations for main gasdynamic parameters realizing at the plasma jet interaction with the incident flow of the flammable (stoichiometric propane-air) mixture.

The calculations show that the incident flow stops and turns back the plasma jet. The shock wave appears at that, pressure and temperature rise in the area of the interaction, and the combustion wave is realized. It propagates in all directions from the jet. At its reflection from the limiting wall of the volume there appears a typical Mach foot. At that the temperature in the air of gas dynamic interaction rises up to 4000 K, caused by the propane combustion.

In Fig.4.2.5 one can see results of propane density calculations that is realized at the plasma jet interaction with the incident hot flow. One can see that there is a rise of propane density in the front, it leads to acceleration of the combustion process.

Analysis of calculated data shows that at the interaction of the jet with propane-air mix there takes place the ignition of the mix and the detonation realization during the time of ~0.6 10^{-4} s. This reveals the availability of pulse periodic plasma jets for realization of the detonation ignition of the flammable mixtures.

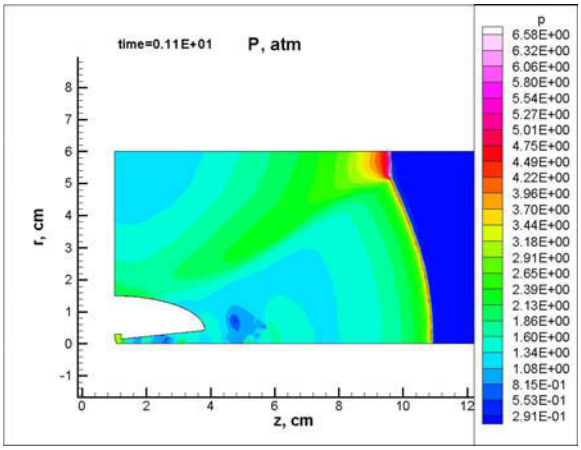

Fig.4.2. 1. Plasma jet injection to stoichiometric propane-air mixture: pressure distribution. Initial pressure in the incident flow is 0.2 atm, initial gas temperature is 1000 K, plasma generator power is 15 kW. Computation time is 1.1 10^{-4} s.

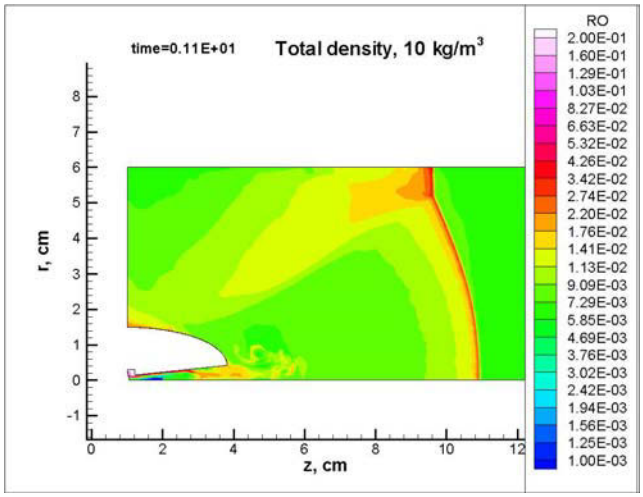

Fig.4.2. 2. Plasma jet injection to stoichiometric propane-air mixture: total density distribution. Initial pressure in the incident flow is 0.2 atm, initial gas temperature is 1000 K, plasma generator power is 15 kW. Computation time is 1.1 10^{-4} s.

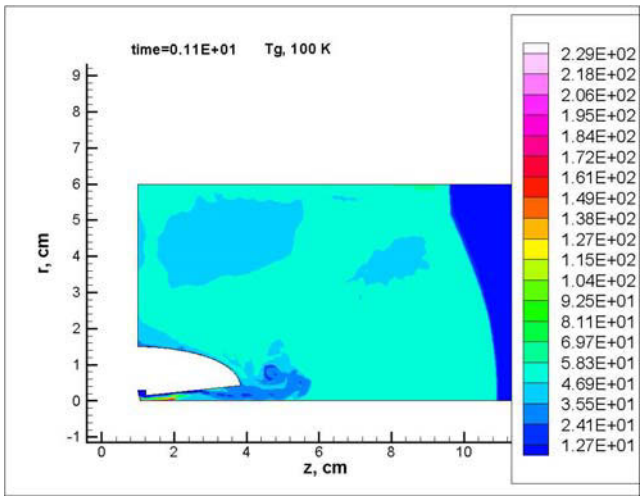

Fig.4.2.3. Plasma jet injection to stoichiometric propane-air mixture: temperature distribution. Initial pressure in the incident flow is 0.2 atm, initial gas temperature is 1000 K, plasma generator power is 15 kW. Computation time is $1.1\ 10^{-4}$ s.

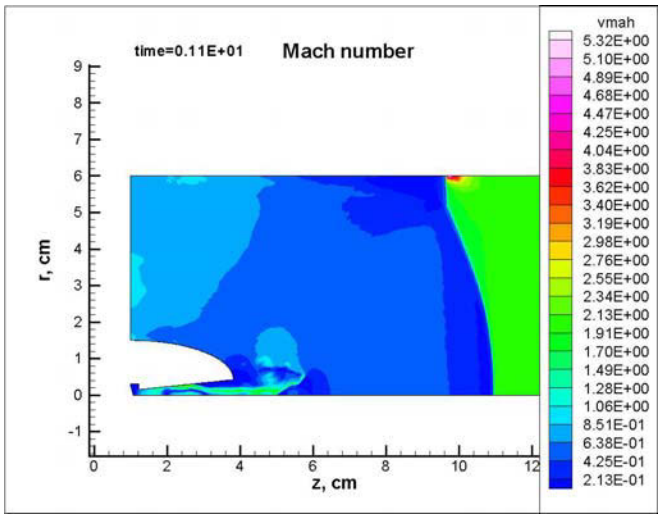

Fig.4.2. 4. Plasma jet injection to stoichiometric propane-air mixture: Mach number distribution. Initial pressure in the incident flow is 0.2 atm, initial gas temperature is 1000 K, plasma generator power is 15 kW. Computation time is $1.1\ 10^{-4}$ s.

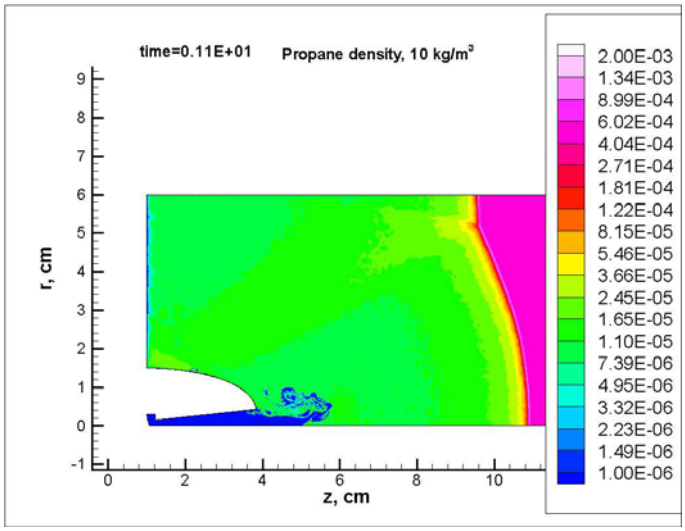

Fig.4.2.5. Plasma jet injection to stoichiometric propane-air mixture: temperature distribution. Initial pressure in the incident flow is 0.2 atm, initial gas temperature is 1000 K, plasma generator power is 15 kW. Computation time is $1.1\ 10^{-4}$ s.

4.3.Parameters of flow at the injection of the flat nitrogen plasma jet from the plasma generator to crossflow.

In Fig. 4.3.1. we remind the displacement of the jet (a row of plasma generators) and the flow at which we consider their interaction.

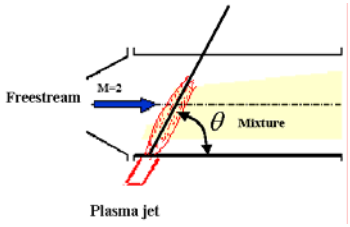

Fig. 4.3.1. Flat plasma jet created by a row of plasma generators

The present computations on the adaptive grid have the principle character for clarification of the interaction features between the plasma jet and the cross flow. The have been carried out to realize high resolution and high accuracy in the region of interaction. Previous calculations in Capter 2-3, were carried out with grid, which was rather detailed only near the boundary of the plasma blow in the crossflow. The grid was rough far from this boundary and did not allow to accurately determine the jet and flow parameters in the region of their interaction.

Method of the jet boundary calculation

The calculation is made by Free Lagrange method on the triangular mesh: the calculated points are moving together with the medium. The changing of the mesh structure and mesh adaptation are made at each step. The adaptation is undertaken so that there were sufficient calculated points in the jet and in the flow excited by it for good reproduction of the flow structure.

The blowing of the jet in the numerical method is realized by the following way. The gas velocity is given in the boundary points (lying on the boundary) of the numerical domain from which the blowing takes place. The thermodynamic parameters of the jet are given in the near boundary cells. These points are moving with the given velocity into the numerical domain at each time step. In the beginning of the next step these points return to the initial position at the boundary from which the blowing takes place. Such a procedure of the blowing realizing in the Lagrange coordinates approximates well the boundary conditions of the blowing. The distances between the boundary and near boundary points increase in the result of this procedure. When these distances exceed the typical quantity of the calculation mesh step then the new nodes are added between the boundary and near boundary nodes.

In order to back trace the jet boundary a new computation variable – an indication is introduced, it is specified in all calculated nodes. The indication is equal to zero in all the points of the incident flow. The indication is equal to unity in the points lying on the boundary from which the blowing takes place. At addition of a new node to the mesh edge the indication in a new point is determined by the indications at the edge ends by linear interpolation. So the indication is larger then zero at the addition of new nodes at the blowing boundary. With time the indication of adding nodes after multiple additions of new nodes will be close to unity at the boundary of blowing. And the indication will be more than zero and close to unity in the calculated points corresponding to the blowing jet. In figures the boundary of the jet is depicted by the indication level line corresponding to its definite value, which is close to unity. In our case this value is equal to 0.8. Values of the indication function lies in the range between 0 and 1, our calculations show that all the indication level lines (between 0 and 1) lie in narrow region approximately determining the boundary between the blowing jet and the incident flow.

Results on the flat jet, (interaction with a supersonic flow).

Gas flow parameters: gas temperature is T=250 K, pressure is 0.2 atm., Mach number is 2.

Plasma jet parameters: nitrogen jet comes out of the plasma generator, electric source power P= 10 kW, gas flow rate 2 g/s, plasma is directed at the angle of 135° to the cross flow.

In Fig. 4.3.2- 4.3.7one can see results of calculations with indication of the boundary between the jet and the flow for the time moment $t = 3 \cdot 10^{-5}$ сек.

Calculations show that the jet creates a shock wave in the gas of the crossflow. In particular the temperature in the gas of the cross flow exceeds 1500° K in the head part. It is probable that the heating in the shear boundary layer is sufficient for the fuel ignition. Examination of this idea requires additional calculations with modeling of processes in the shear boundary layer.

It is necessary to emphasize that the plasma generator's jet is strongly non-uniform. Its external layers interacting with air crossflow are relatively cold (their temperature T~ 500° K) and do not contain the charged plasma. Internal jet layers consist of such a plasma, they do not interact with air flow. The jet gas expands and cools to temperature of T~ 1000° - 2000° K at moving away from the boundary of the blowing in. The jet in this case consists of the gas and does not contain the charged plasma (see. Fig. 4.3.7). So such a plasma stays in the jet near the boundary of the blowing in and it does not interact with the air cross flow. At the same time there is practically full dissociation of nitrogen molecules in the plasma near the region of the jet injection to a flow (see Fig. 4.3.8 for atoms N_N). This could lead to additional heating of this region, due to diffusion of atoms from the plasma and the following recombination of atoms.

In figures one can see that the jet is unstable, its heavy periphery parts strongly slow down by the flow and can mix with air. However the temperature in the mixing zone does not exceed T~1000-2000° K. This temperature range also satisfies conditions of hydrocarbon-air mixtures ignition.

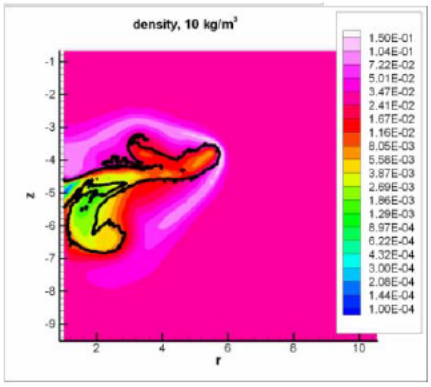

Fig. 4.3.2 Distribution of pressure at plasma jet interaction with the supersonic cross flow at the angle of 135°. Cross flow parameters: T=250 K, pressure 0.2 atm., Mach number M= 2. Nitrogen plasma jet parameters plasma generator power is W~10 kW, plasma forming gas mass f low rate is 2 g/s.

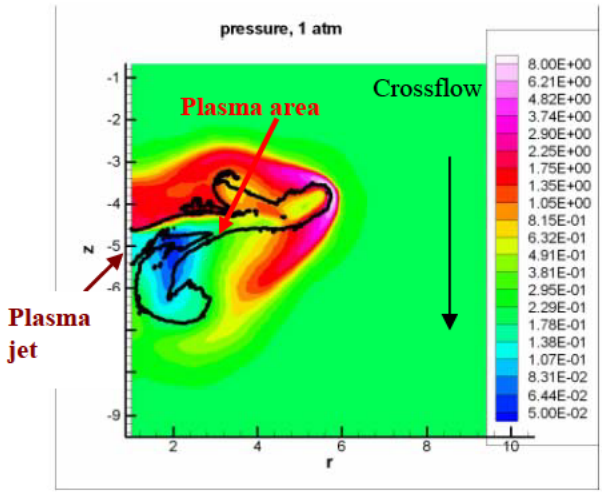

Fig. 4.3.3 Distribution of density at plasma jet interaction with the supersonic cross flow at the angle of 135°. Cross flow parameters: T=250 K, pressure 0.2 atm., Mach number M= 2. Nitrogen plasma jet parameters plasma generator power is W~10 kW, plasma forming gas mass f low rate is 2 g/s.

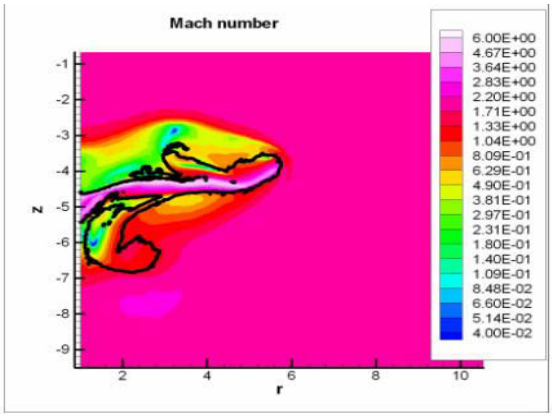

Fig. 4.3.4 Mach number distribution at plasma jet interaction with the supersonic cross flow at the angle of 135°. Cross flow parameters: T=250 K, pressure 0.2 atm., Mach number M= 2. Nitrogen plasma jet parameters plasma generator power is W~10 kW, plasma forming gas mass f low rate is 2 g/s.

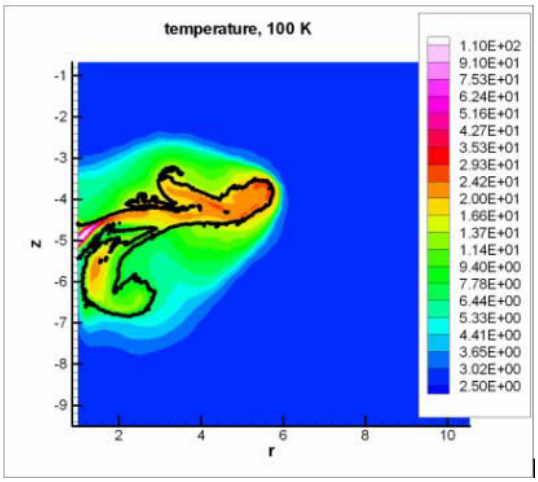

Fig. 4.3..5 Temperature distribution at plasma jet interaction with the supersonic cross flow at the angle of 135°. Cross flow parameters: T=250 K, pressure 0.2 atm., Mach number M= 2. Nitrogen plasma jet parameters plasma generator power is W~10 kW, plasma forming gas mass f low rate is 2 g/s.

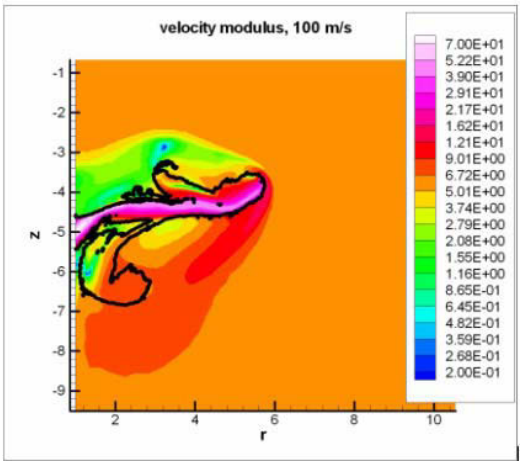

Fig. 4.3.6 Absolute value of velocity distribution at plasma jet interaction with the supersonic cross flow at the angle of 135°. Cross flow parameters: T=250 K, pressure 0.2 atm., Mach number M= 2. Nitrogen plasma jet parameters plasma generator power is W~10 kW, plasma forming gas mass f low rate is 2 g/s.

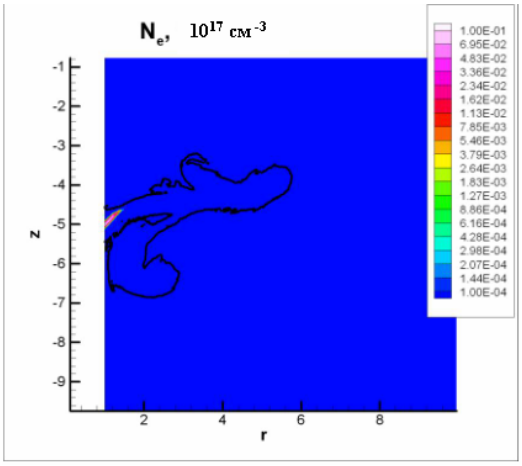

Fig. 4.3.7 Electron concentration distribution at plasma jet interaction with the supersonic cross flow at the angle of 135°. Cross flow parameters: T=250 K, pressure 0.2 atm., Mach number M= 2. Nitrogen plasma jet parameters plasma generator power is W~10 kW, plasma forming gas mass f low rate is 2 g/s.

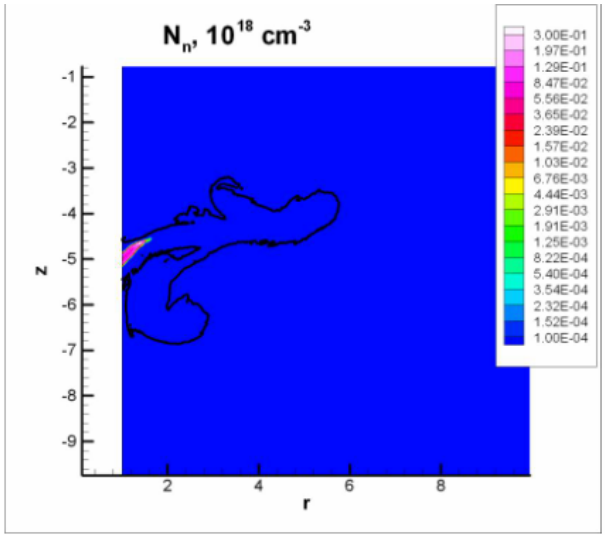

Fig. 4.3..8 Atoms concentration at plasma jet interaction with the supersonic cross flow at the angle of 135°. Cross flow parameters: T=250 K, pressure 0.2 atm., Mach number M= 2. Nitrogen plasma jet parameters plasma generator power is W~10 kW, plasma forming gas mass f low rate is 2 g/s.

4.4. Modeling of propane-air mixture combustion at plasma jent and the cross flow interaction at the angle of 150°

As in our simulations in Chapter 2-3 the gasdynamic equations are coupled with the 2-D Maxwell equations and the plasma dynamics equations, accounting for ohmic heating and radiative plasma cooling. Specific parameters are nitrogen gas mass flow in the generator $m_f = 2$ g/s, power input P=15, 30 kW. Appropriate thermodynamic, optical and transport properties of nitrogen and air plasmas were used in the computations. Propane-air chemistry was the same as in section 4.2. A Lagrange method based on a completely conservative implicit difference scheme with an adaptive triangular unstructured mesh described above was applied. This was effective in modeling the coupling of the internal and external flows inside and outside the counterflow jet and its nozzle. The mesh was concentrated in the region of the combustion by

the adaptive method. Computations of plasma jet injection to the crossflow of propane-air flammable mix have been made at the angle 150 °. Plasma forming gas (nitrogen) mass flow rate was 2 g/s, plasma generator power was 15 kW and 30 kW at the temperature of the incident propane-air stoichiometric mix 1000 K.

In Fig. 4.4.1-6. represented results of computations of gasdynamic and fuel characteristics distributions at the plasma jet interaction with the supersonic propane-air stoichiometric mix flow at the angle 150° for the moment 18 μs. The flow parameters: T=1000 K, Pressure 0.2 atm., the Mach number is M= 2. The jet parameters: the nitrogen jet from the plasma generator, The source power W=15 kW, the mass flow rate 2 g/s (up down in the figures).

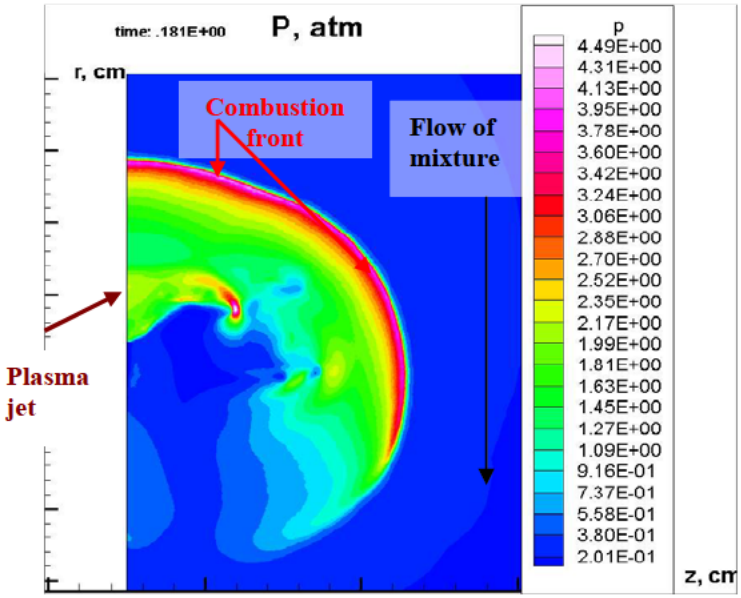

Fig.4.4.1. Pressure distribution at flat plasma jet interaction with the supersonic propane-air crossflow (flow direction is up-down) under the angle of 150° at the time moment 18 μs. Flow parameters: T=1000 K, pressure 0.2 atm., M= 2. Nitrogen plasma jet parameters: putted in power is W=15 kW, plasma forming gas mass flow rate is 2 g/s.

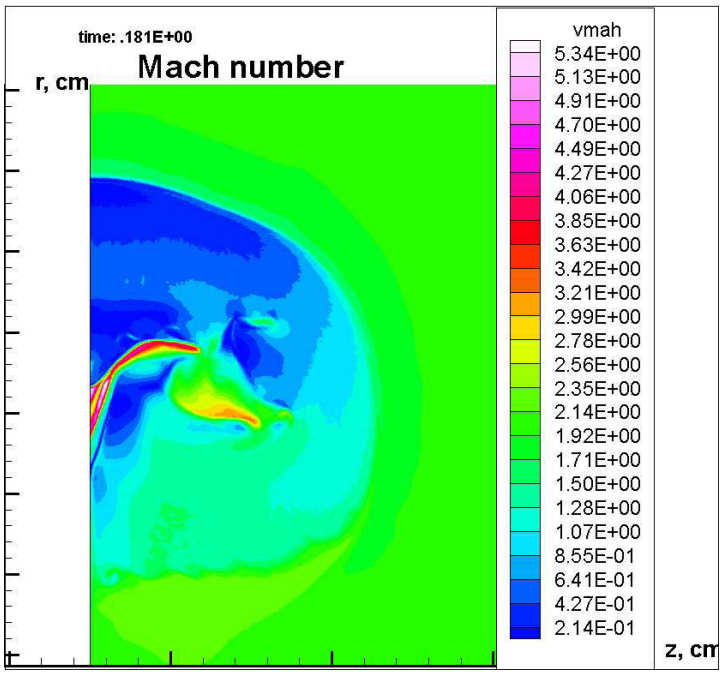

Fig.4.4.2. Mach number distribution at flat plasma jet interaction with the supersonic propane-air crossflow (flow direction is up-down) under the angle of 150° at the time moment 18 μs. Flow parameters: T=1000 K, pressure 0.2 atm., M= 2. Nitrogen plasma jet parameters: putted in power is W=15 kW, plasma forming gas mass flow rate is 2 g/s.

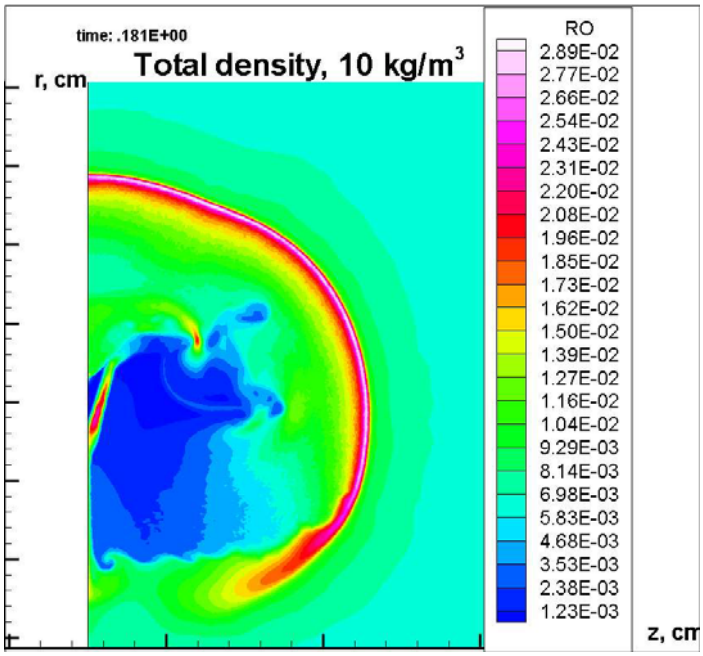

Fig.4.4.3. Total density distribution at flat plasma jet interaction with the supersonic propane-air crossflow (flow direction is up-down) under the angle of 150° at the time moment 18 μs. Flow parameters: T=1000 K, pressure 0.2 atm., M= 2. Nitrogen plasma jet parameters: putted in power is W=15 kW, plasma forming gas mass flow rate is 2 g/s.

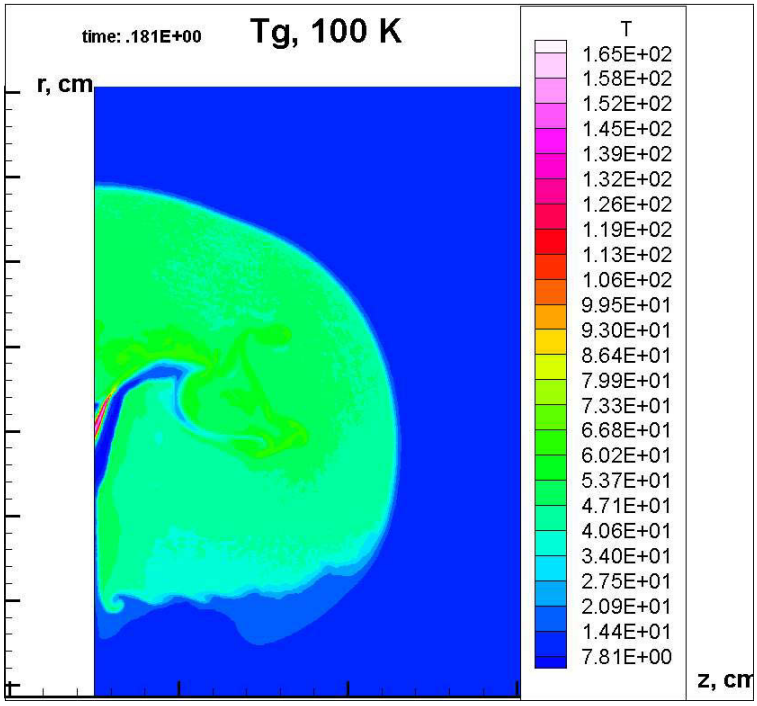

Fig.4.4.4. Temperature distribution at flat plasma jet interaction with the supersonic propane-air crossflow (flow direction is up-down) under the angle of 150° at the time moment 18 μs. Flow parameters: T=1000 K, pressure 0.2 atm., M= 2. Nitrogen plasma jet parameters: putted in power is W=15 kW, plasma forming gas mass flow rate is 2 g/s.

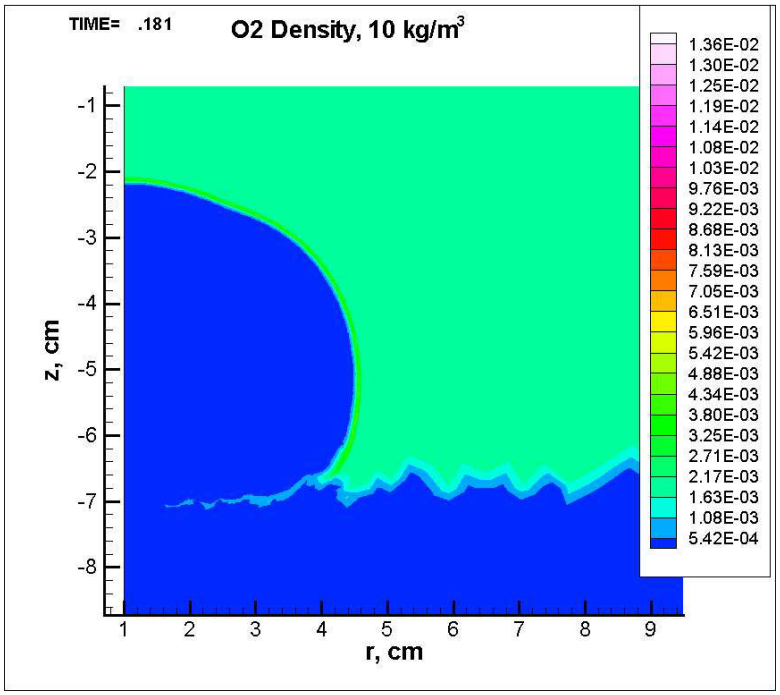

Fig.4.4.5. Oxygen density distribution at flat plasma jet interaction with the supersonic propane-air crossflow (flow direction is up-down) under the angle of 150° at the time moment 18 μs. Flow parameters: T=1000 K, pressure 0.2 atm., M= 2. Nitrogen plasma jet parameters: putted in power is W=15 kW, plasma forming gas mass flow rate is 2 g/s.

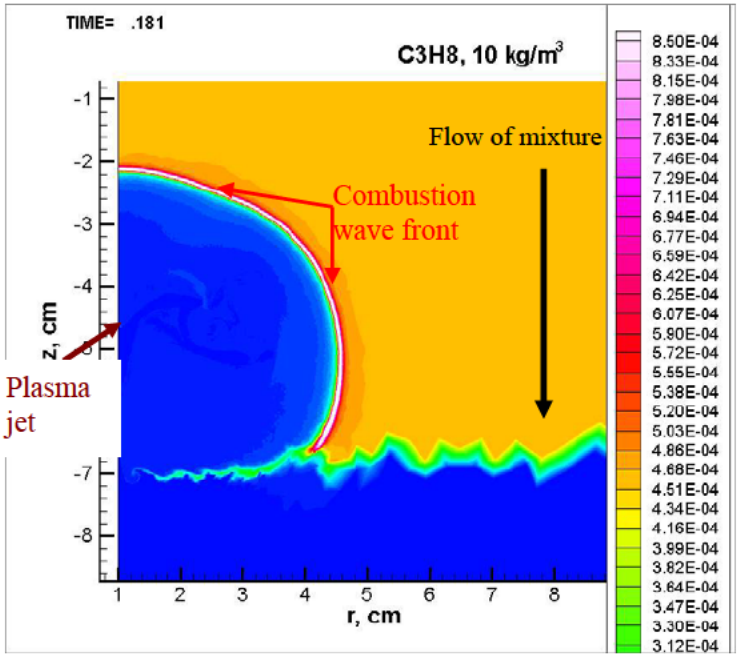

Fig.4.4.6. Propane density distribution at flat plasma jet interaction with the supersonic propane-air crossflow (flow direction is up-down) under the angle of 150° at the time moment 18 μs. Flow parameters: T=1000 K, pressure 0.2 atm., M= 2. Nitrogen plasma jet parameters: putted in power is W=15 kW, plasma forming gas mass flow rate is 2 g/s.

Comparison of Figures 4.4.5-6 and 4.4.4 shows quick propagation of density, pressure and temperature wave in case of the fuel mixture. At that it propagates counter the supersonic flow, and this validates the occurrence of detonation. At the same time considerable increase of density and pressure takes place on the wave front, it leads to acceleration of propane combustion. In the jet area appear regions with low density it indicates appearance of vorticle structures, there takes place the break of the jet also. In the result there appears a large area of the hydrodynamic interaction of the plasma with the crossflow. Results of computations represented in Fig.4.4.5 and 4.4.6 show fast propane burning out and oxygen decrease in the region of high temperature, where it reaches 3000-4000 K. Our calculations show that realization of combustion wave takes place during ~ 8-10 μs.

Computation results show the possibility of propane-air mixture crossflow ignition at its interaction with the nitrogen plasma jet from the plasma generator with power putted into the gas of P = 15 kW at the initial temperature of 1000 K.

The mixture is compressed in the combustion wave front (see red curve on the front in Fig 4.4.6) and it accelerates ignition.

We do not know now any work devoted to ignition of flammable supersonic mixes by plasma jets. So there was no opportunity to compare our results. Determination of the minimum plasma jet power at which the plasma from the jet penetrates the cross flow and still ignites the fuel requires additional investigations. However, we are limited with power P >13 at which

plasma jet is locked by the cross flow. Our results show the possibility of application of high power-low energy plasma jets with the pulse duration of about 10 –100 μs for ignition and combustion applications. They can be used in pulse repetitive mode which decrease the energy losses of plasma jets.

Conclusions to Chapter 4

1. The model of ignition and combustion of the stoichiometric propane-air mixture with a help of the plasma jet from the plasma generator to the incident flow and crossflow of the flammable mix. This model uses one step effective chemical reaction between propane and oxygen molecules. It accounts heating of the medium due to energy released by chemical reactions and by the plasma jet.
2. Lagrange method on a completely conservative implicit difference scheme with an adaptive triangular unstructured grid was used in computations. The total number of knots was 15000-150000. The mesh was concentrated in the region of the combustion by the adaptive method.
3. This method is applied for clarification of initial and boundary conditions at investigation of the plasma jet-flammable mix cross flow interaction (at angles 135, 150º).
4. Computations of plasma jet injection to the incident flow of propane-air flammable mix have been made. Plasma forming gas (nitrogen) mass flow rate was 2 g/s, plasma generator power was 15 kW and 30 kW at the temperature of the incident propane-air stoichiometric mix 250 K and 1000 K.
5. Results of computations demonstrated the ignition possibility of propane-air mixture with a help of plasma generators with the power 15 kW at the incident propane-air stoichiometric mix temperature 1000 K.
6. The realization of fast combustion wave processes at typical times of ~10 microseconds is observed both in cylindrical and flat cases.

References to Chapter 4.

4.1. Combustion Chemistry Ed. W.C. Gardiner, Jr. Springer –Verlag New-York Inc. NY-Berlin-Heidelberg-Tokyo. 1984

4.2. Davidson D.F., Herbon J.T., Horning D.C., Hanson R.K. OH concentration time histories in n-alkane oxidation. Int. J.Chem. Kinet. 2001. V. 33. P.775-783.

4.3. Cadman P., Thomas G.O., Butler P. The auto-ignition of propane at intermediate temperatures and high pressures, PCCP; Physical Chemistry Chemical Physics. 2000. 002. 023 (December 07) P. 5411-5419.

4.4. Horning D.C., Davidson D.F., Hanson R.K. High temperature autoignition of n-alkane/O2/Ar mixtures. J. of Propulsion and Power. 2002. V.18. P. 363-371.

4.5. Koert D, Pitz W.J., Bozelli J.W., Cernansky N.P. Chemical kinetic modeling of high pressure propane oxidation and comparison to experimental results.27-th Symposium (International) on Combustion. The Combustion Institute. Pittsburg. 1999. P.633.

4.6. Brown C.J., Thomas G.O. Experimental Studies of shock induced ignition and transition to detonation in ethylene and propane mixtures- their nature, effects and control. Combustion and flame. 1999. V.117. n.4 (June). P.861-870.
4.7. Zhukov V.L., Sechenov V.A. , A.Yu. Starikovsky. Selfignition of lean propane/air mixture at high pressure. Khimicheskaya Fizika. 2003.Report № 3 on the Project ISTC 2449-p"Plasma-Jet Studies for Plasma Chemical Fuel Activation" for the third quarter. Moscow. 2003.
4.8. Varatharajan B., Williams F.A. Reduced chemistry for ignition and detonation of higher hydrocarbons. AIAA 2002-0611. 40-th AIAA Aerospace sciences Meeting & Exhibit 14-17 January, 2002, Reno Hilton, NV.
4.9. Westbrook, C.K., Dryer, F.L. Simplified Reaction Mechanisms for the Oxidation of Fuels in Flames. Combustion Science and Technology, 1981, Vol.27, pp.31-43
4.10. Katta, V.R., Roquemore, W.M. Simulation of Unsteady Flows in an Axisymmetric Research Combustor Using Detailed-Chemical Kinetics. AIAA/ASME/SAE/ASEE Joint Propulsion Conference & Exhibit, 34th, Cleveland, OH, July 13-15, 1998
4.11. Petrova M.V., Varatharajan B., Williams F.A. Theory of Propane autoignition. AIAA 2004-1325. 40-4t AIAA Aerospase Sciences Meeting & Exhibit. 5-8 January, 2004, Reno, NV.
4.12. Bychkov V.L., Gromov V.G., Ershov A.P., Levin V.A., Chernikov V.A., Shibkov V.M., Surkont O.S. Timofeev I. B. An electrode ignition discharges in supersonic propane-air flows. In: Combustion and Atmospheric pollution. Eds. G.D. Roy, S.M.Frolov, A.M. Starik. Moscow: Torus Press, 2003, 278-282.
4.13. Ershov A.P., Surkont O.S., Timofeev I.B., Chernikov V.A., Shibkov V.M., Ardelyan N.V., Chuvashev S.N., Bychkov V.L., Gromov V.G., Levin V.A. Parameters of electrode ignition discharges in supersonic propane-air flows. 3 –d Workshop Thermochemical and plasma processes in aerodynamics. Saint – Petersburg. 28-31 July. 2003. P.64-73.
4.14. Shetinkov E.S. Physics of gases combustion. Nauka. Moscow. 1965.
4.15. Warnatz J., Maas U., Dibble R.W. Combustion Springer –Verlag New-York Inc. NY-Berlin-Heidelberg-Tokyo. 2001.
4.16. Westbrook C.K., Chase L.L. Chemical Kinetics and Thermochemical data for Combustion Applications. Lawrence Livermore Laboratory. UCID-17833. 1981.

Chapter 5. Combined discharge plasma influence on propane-air mix ignition

5.1 Formulation. Ignition enhancement of fuels with a help of plasma is under detailed investigation of last years. Our works on this subject devoted to an application of plasma jets have shown that there is a strong gasdynamic interaction between the incident flow and the jet plasma which leads to fast heating of the incident flammable mix with creation of a shock in the place of the contact and the following heating of the incident mix to temperatures necessary for ignition. However plasma chemical reactions do not play important role due to slow molecular transport from the plasma zone to the fuel. Analogous situation is observed in some works on heat sources application in supersonic combustion [5.1]. In this case it is reasonable to locate some sort of plasma source to insure plasma chemical influence on the fuel with production of excited species and active radicals. In order such a source could produce active radicals independently of gas flow parameters the time of its interaction has to be smaller than typical gasdynamic times.

There are a number of devices which can produce such an effect, they are X-radiation plates, non-selfmaintained discharges, and ultra-violet radiation sources. Application of X-radiation requires high parameters of radiation sources, which are not realized now and applications of special protection measures. In this work we will consider an application of the non-selfmaintained discharge. In Fig.1 one can see a possible test channel scheme with the application of the non-selfmaintained discharge and plasma jet. The self maintained discharge device is located upstream the step and the plasma jet. The self maintained discharge represents a combination of electron beam and the gas discharge. Where electrons and ions are produced by the beam, and the discharge is realized at voltage lower than the breakdown one. In this case produced excited components will be moved down where they will take part in ignition process.

For analysis of this scheme is necessary: a) to investigate possible parameters of the ignition which can be produced by the flammable mix interaction with excited chemically active species produced by the discharge, b) to formulate necessary parameters for non-selfmaintained discharge. Namely to this research problem this work is devoted, where on the basis of calculations of ignition of modified stoichiometric propane-air mix by oxygen atoms generated by non-selfmaintained discharge in air is considered the question of applicability of this scheme.

5.2. Approach. For solution of the complete problem of ignition enhancement of propane-air stoichimetric mixture it is necessary to solve the problem for definite channel construction with full-scale solutions of gasdynamics and plasma chemistry equations as we did, for example, in [5.2]. Since the present problem has the research character we consider the simplest case of addition of chemically active species to propane air stoichiometric mix in motionless conditions.

In literature [5.3-6] there is an information only about reaction of the atomic oxygen with components of propane (C_3H_8) decomposition, and indication [5.6] on influence of vibrationally excited state of the oxygen molecule , $O_2(v)$. So we consider the ignition of propane-air stoichiometric mix at addition to it of oxygen atoms.

The model of C_3H_8 –air mix kinetics includes detailed chemical mechanism involving 30 species (*C_3H_8 ,O, H, O_2, N_2, H_2, CO, OH, H_2O, HO_2, H_2O_2, HCO, CO_2, CH, CH_2, CH_3, CH_4, C_2H, C_2H_2, C_2H_3, C_2H_4, C_2H_5, C_2H_6, C_3H_5, C_3H_6, i-C_3H_7, n-C_3H_7, CH_2O, CH_2OH, CH_3OH*) and 75 elementary chemical reactions taken in the main from [5.4]. Only rate constants of recombination reactions were used in calculations. If in the reference source it was listed rate constants of dissociation reaction so rate constant of recombination reactions is calculated through equilibrium constant of this reaction and it is approximated by Arrhenius formula. Adiabatic, fully non-catalytic model of gas-wall thermal and chemical interactions was used in all calculations.

We also solved the system of chemical equations of air excited by non-selfmaintained discharge. It includes equations for 13 chemically active components in air, ions O^+, O_2^+, negative ions O^-, O_2^-, O_3^-, atoms O, molecules O_2, O_3, vibrationally and electronically excited states, including $O_2(^1\Delta_g)$ electron and gas temperatures modified in chemical reactions as in [5.2].

5.3 Results of calculations. In Fig. 5.2-3 one can see calculations of propane part and gas temperature variation dependencies at C_3H_8 burning out at atomic oxygen addition to stoichiometric propane-air mix. The calculations were made for initial temperatures of T=1500 and 2000 K at initial atmospheric pressure, atomic oxygen part in the mix δ= 0.0, 0.001, 0.01. Preliminary calculations showed that reasonable temperature range of propane burning out (ignition) in undisturbed conditions with typical times of τ<200 μs corresponds to initial temperatures *T*>1800 K.

The presence of atomic oxygen in the mix significantly influences propane burning out. Calculation shows that appearance of 0.1% of atomic oxygen in the mix leads to ~1.5-2 times greater reduction of propane (ignition) during the same time as in the case of the undisturbed mix. Appearance of 1% of atomic oxygen in the mix leads to ~.5-6 times greater reduction of propane (ignition) during the same time as in the case of the undisturbed mix.

In Fig.5.4 a –b one can see components appearing at addition of atomic oxygen in reacting gas. Main of them are C_3H_6, n-C_3H_7, H_2O. At initial temperature of 1500 K and part of atomic oxygen δ= 0.001 the whole process of molecular transformation takes place during τ_{ch} ~40 μs, and it decreases to τ_{ch} ~20 μs with increasing of δ to δ= 0.01. This time allows to

estimate the plasma area width needed for plasma formation, it is $L_p \sim \tau_p \cdot v_f$ where v_f –is flow velocity, so L_p~*2* cm at v_f~1000 m/s.

These calculations show that if the temperature in the mix is realized by external plasma source in the range of 1800-2500 T, and the dissociation of the oxygen molecules leads to the appearance of 0.01-01% (of the total mix) oxygen atoms then the ignition process will be realized during typical times smaller than the gasdynamic ones (we consider typical length of plasma region created by non-self maintained discharge~0.02 m and M~2, see above).

In Fig. 5.5-7 one can see temporary dependencies of charged, excited and active particles created in the plasma of non-selfmaintained gas discharge excited by the electron beam at the excitation rate of Q~10^{17} cm^{-3} s^{-1} corresponding a) to E-beam power of about ~0,6 W and a)), at the discharge electric field of 10^3 V/cm and b) the discharge electric field of 10^4 V/cm.

In Fig.5.5 one can see charged particles temporary dependencies in such a plasma. Obtained results allow to estimate current density in realized plasma $j \sim e n_e w_{dr}$, where e-electron charge, n_e-electron concentration, w_{dr}- electron drift velocity (for air see [5.7]), obtained results give j~3 A/cm^2 at E=10^3 V/cm, and 600 A/cm^2 at E=10^4 V/cm.

In Fig.5.6-7 one can see neutral and excited states temporary dependencies in the plasmas.

In Fig.5.8 one can see gas and electron temperature temporary dependencies in the plasmas created by non-selfmaintained discharges.

Calculations show that favorable for combustion enhancement conditions are created at Q~10^{17} cm^{-3} s^{-1} and the discharge electric field value of 10^4 V/cm (electric discharge source power~10.0 kW). They correspond to E/N value of about 10^{-15} V·cm^2 , it is near the threshold of molecular oxygen dissociation. High temperature realized at that can cause the ignition.

The calculations also show high number (~10-20%) of vibrationally excited molecular oxygen species and about the same number of single molecular oxygen (O_2d = $O_2(\Delta)$) in both cases. These components can reduce additionally the ignition time and reduce necessary power of applied plasma source.

Having this data it is possible to estimate the power W of the discharge section of 2 ×5×5cm, one can obtain W~15 W at E=10^3 V/cm, and W~30 kW. The last value can be easily decreased to W<10 kW in the pulsed mode of electric field, due to long decay of plasmas at temperature T~2500K [5.8].

Conclusions to Chapter 5.

In the present Report we considered influence of excited species produced by the non-selfmaintained discharge on propane ignition.

Calculation shows that appearance of 0.1% of atomic oxygen in the mix leads to ~1.5-2 times greater reduction of propane (ignition) during the same time as in the case of the undisturbed mix. Appearance of 1% of atomic oxygen in the mix leads to ~5-6 times greater reduction of propane (ignition becomes shorter by ~5-6) during the same time as in the case of the undisturbed mix.

Moderate power self-maintained discharge (≤10.0 kW) can be used for ignition and ignition enhancement of propane-air stoichiometric mix due to generation of atomic oxygen and heating of the mix by the discharge. High amount of vibrationally and electronically excited states can considerably reduce necessary power value. Application of discharges combination: the non -selfmaintained discharge and plasma jet (see Fig.5.1) at low non-selfmaintained discharge power (~20 W) can be perspective for the ignition, since vibrationally and electronically excited oxygen states can significantly enlarge reaction rate constants and can be effective at interaction of incident excited mix with the plasma jet.

More precise values of necessary ignition enhancement power value require detailed solution of non-selfmaintained discharge in air-fuel mix including rates of vibrationally and electronically excited states of molecular oxygen and hydrocarbon molecules reactions and the solution of gasdynamics equations in the definite duct. The solution of the first problem is complicated because of necessary rate constants absence. The solution of the second problem can be realized in approach developed in this Report and can be the subject of further investigations.

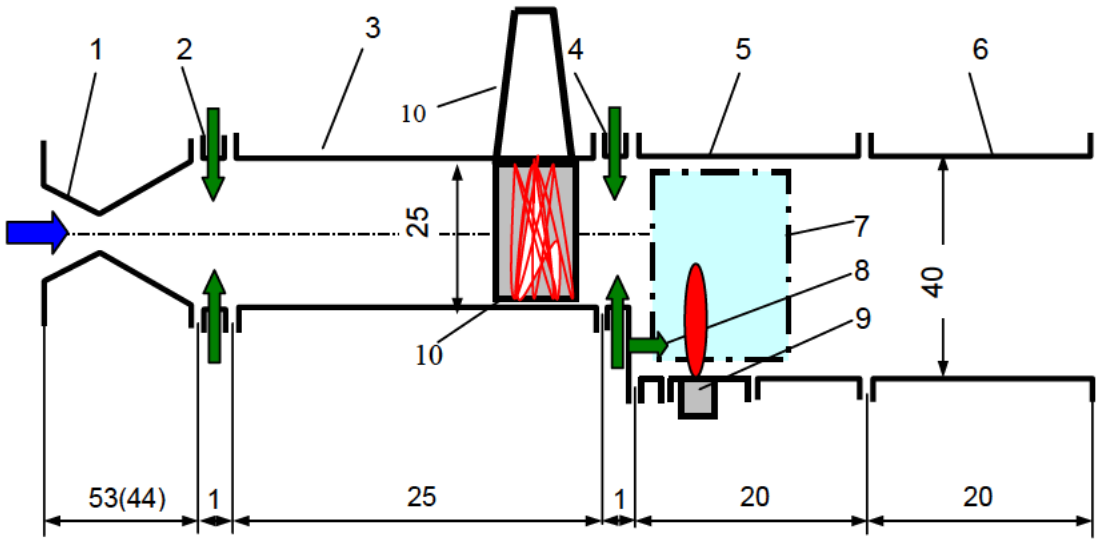

Fig.5.1 Schematics of the channel with combination of discharges

1 – supersonic M=2 nozzle, 2 – collectors of preliminary fuel injection (first injector set), 3 – insulator channel, 4 - collectors of main fuel injection (second injector set), 5 – 1st section of combustor, 6 – 2 nd section of combustor, 7 – quartz window, 8 – third fuel injector set, 9 – plasma jet generator, 10 – non-selfmaintained discharge generator

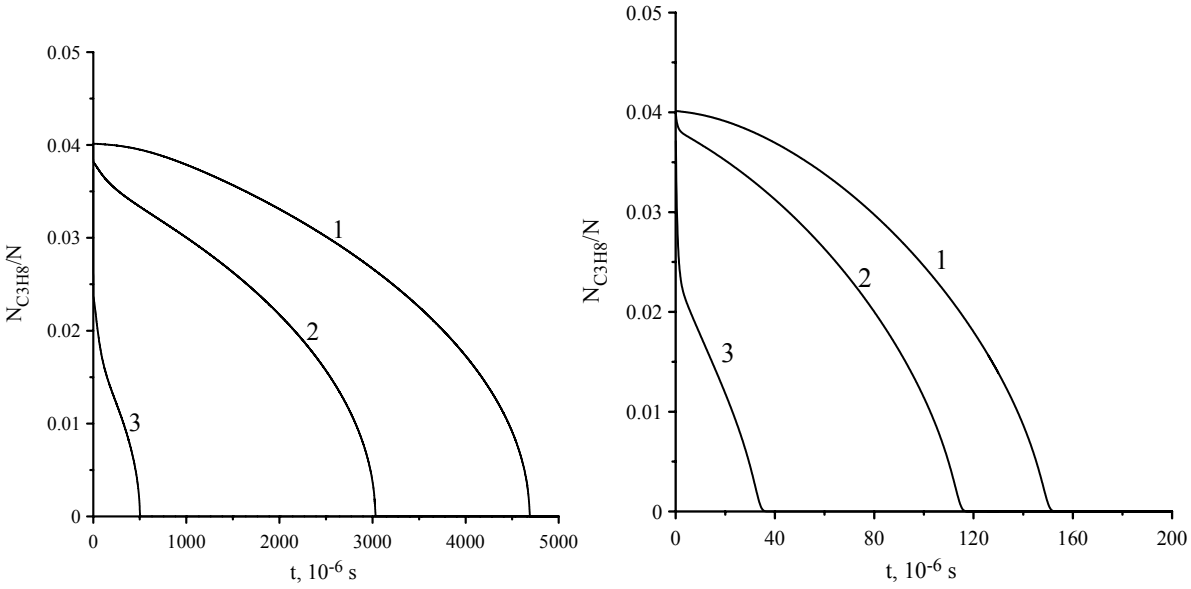

Fig.5.2a **Fig.5.2b**

Fig 5.2. C_3H_8 burning out temperature dependence at atomic oxygen addition to stoichiometric propane-air mix.

a) initial gas temperature T=1500 K, b) initial gas temperature T=2000 K. Part of oxygen 1-0.0, 2-0.001., 3-0.01

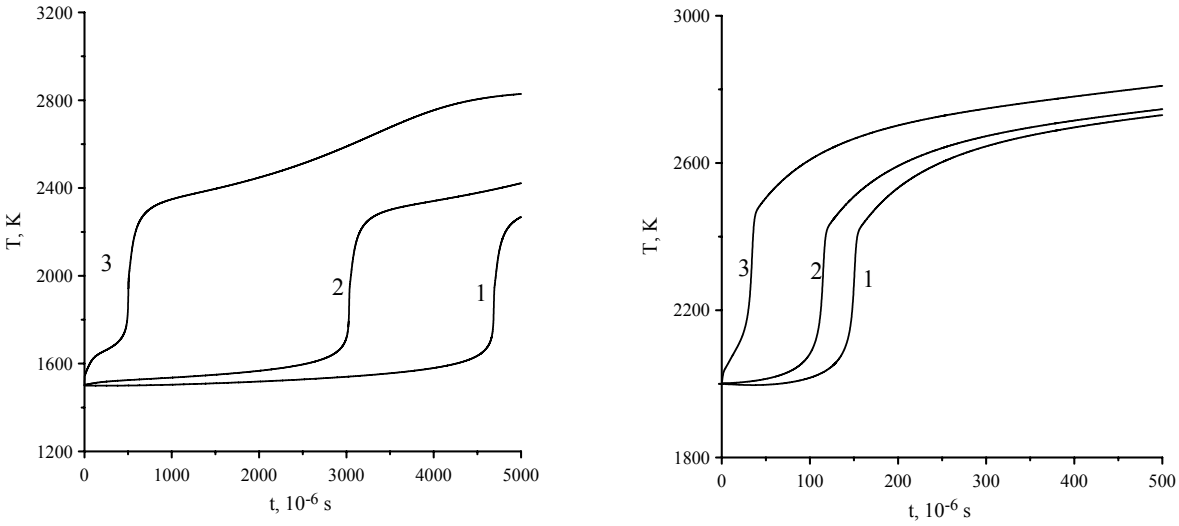

Fig.5.3a **Fig.5.3b**

Fig.5. 3. Temperature variation at C_3H_8 burning out temperature dependence at atomic oxygen addition to stoichiometric propane-air mix.

a) initial gas temperature T=1500 K, b) initial gas temperature T=2000 K. Part of oxygen 1-0.0, 2-0.001., 3-0.01

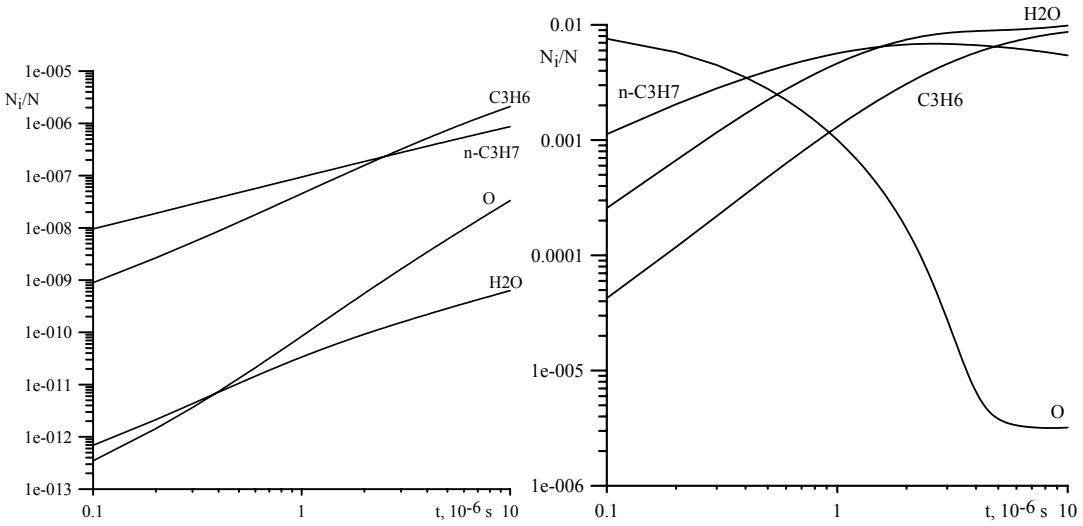

Fig.5.4a **Fig.5.4b**

Fig. 5.4. Temporary generation of active particles appearing due to atomic oxygen, at atomic oxygen addition to stoichiometric propane-air mix. Initial gas temperature T=1500 K

Part of atomic oxygen δ : Fig4a δ=0.0, Fig.4b δ=0.01

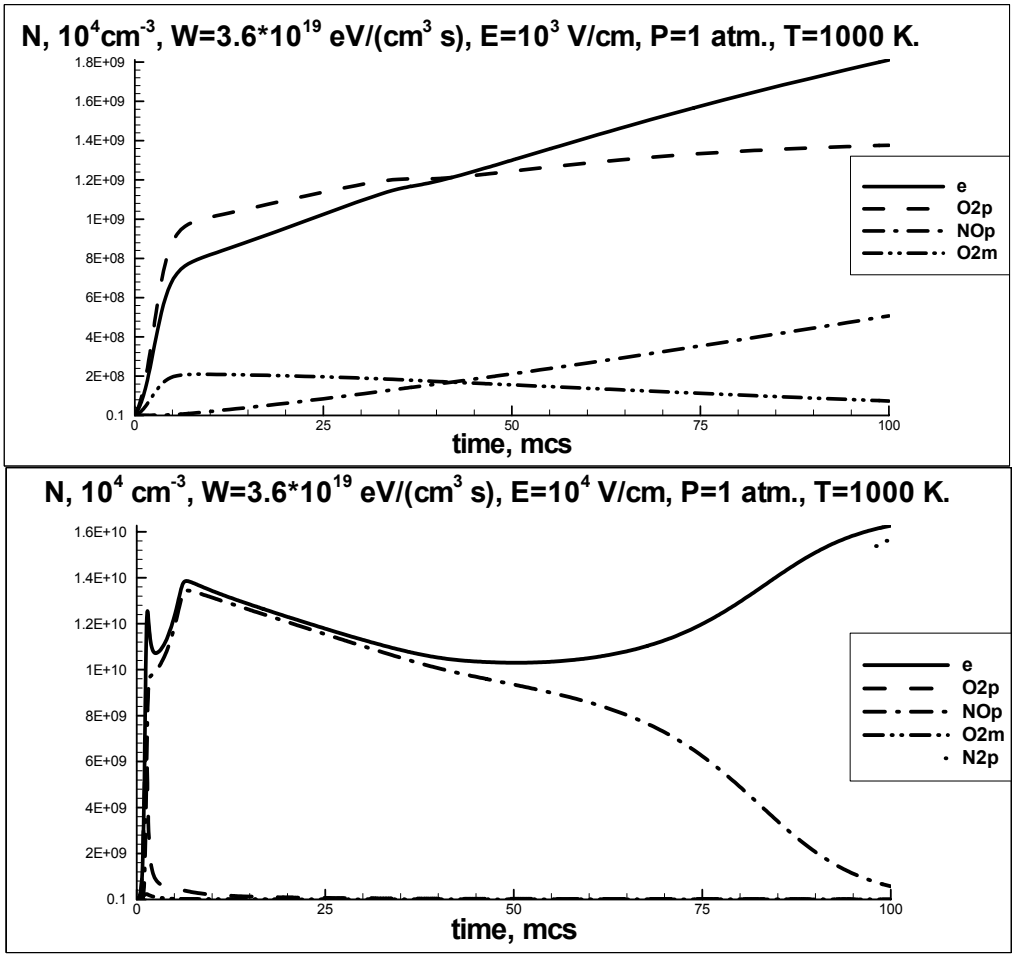

Fig.5.5 Main charged particles temporary dependencies in the plasmas created by non-selfmaintained discharges. Initial gas temperature 1000K, Pressure 1 atm. Upper figure –a) -E-beam source power ~0.6 W, discharge electric field of ~10^3 V/cm; lower figure –b)-E-beam source power ~0.6 W, discharge electric field of ~10^4 V/cm (p-positive ions, m-negative ions) .

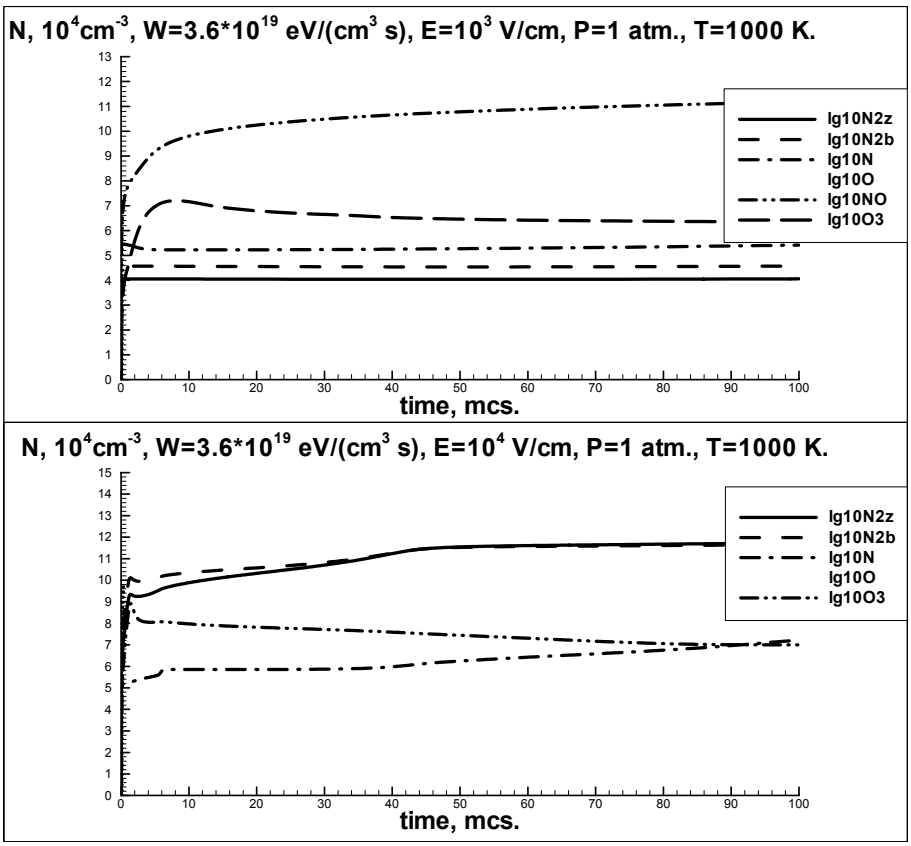

Fig.5. 6 Main neutral and excited states temporary dependencies in the plasmas created by non-selfmaintained discharges. Initial gas temperature 1000K, Pressure 1 atm. Upper figure –a) -E-beam source power ~0.6 W, discharge electric field of ~10^3 V/cm; lower figure –b)-E-beam source power ~0.6 W, discharge electric field of ~10^4 V/cm. (N2z- $N_2(A)$, N2b- $N_2(B)$.

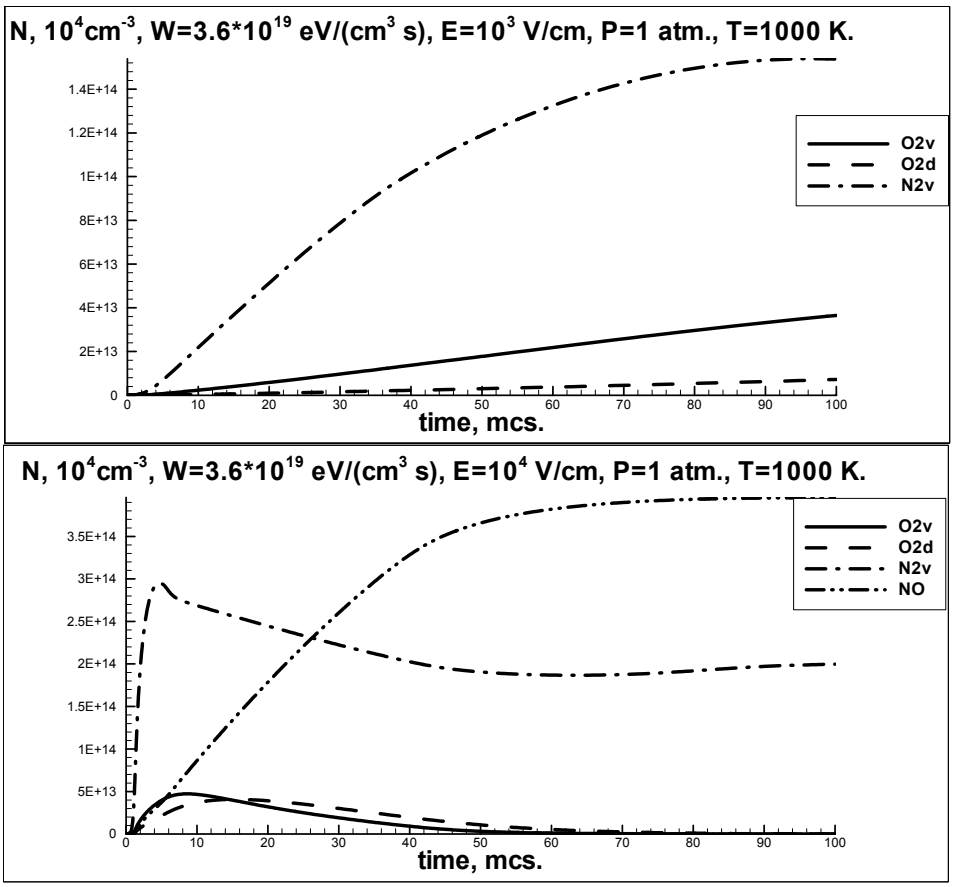

Fig.5.7 Main vibrational and excited states temporary dependencies in the plasmas created by non-selfmaintained discharges. Initial gas temperature 1000K, Pressure 1 atm. Upper figure –a) E-beam source power ~0.6 W, discharge source power~1.0 kW; lower figure –b) E-beam source power ~0.6 W, discharge source ~10 kW. (O2v,N2v- effective 1-st vibrational levels of O_2 and N_2, molecules, O2d – $O_2(\Delta)$).

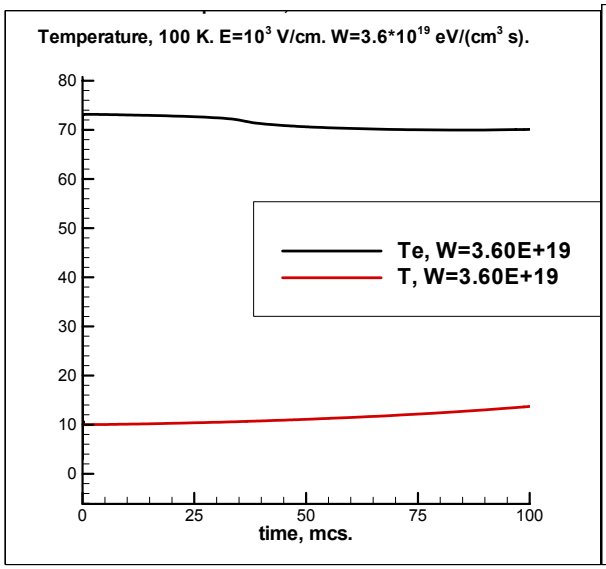

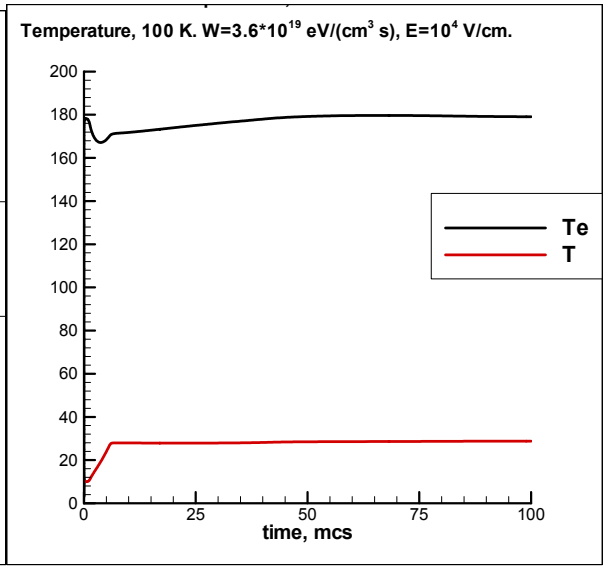

Fig.5.8a **Fig.5.8b**

Fig.5.8 Gas and Electron temperature temporary dependencies in the plasmas created by non-selfmaintained discharges. 5.8a -E-beam source power ~0.6 W, discharge source power~1.0 kW; 5.8b -E-beam source power ~0.6 W, discharge source ~10 kW.

Table 1. Reactions of dissociation –recombination of atomic particles [5.4]

Rate constant form $k_r = AT^n \exp(-E/T)$, $cm^6/(mol^2\,s)$

Reaction					E, K	A	n
O2	⇔	O	+	O	0.	2.9e17	-1.
H2O	⇔	OH	+	H	0.	2.2e22	-2.
H2	⇔	H	+	H	0.	1.8e13	-1.
OH	⇔	O	+	H	0.	1.0e16	0.
CO2	⇔	CO	+	O	2060.	5.9e15	0.
HO2	⇔	H	+	O2	0.	2.3e18	-0.8
HO2	⇔	OH	+	O	0.	1.0e17	0.
H2O2	⇔	OH	+	OH	0.	3.25e22	-2.0
HCO	⇔	CO	+	H	0.	1.1e15	0.
CH4	⇔	CH3	+	H	0.	2.5e11	1.0
CH2O	⇔	HCO	+	H	0.	4.7e15	0.
C2H4	⇔	C2H2	+	H2	0.	1.9e16	0.
C2H5	⇔	C2H4	+	H	0.	6.3e13	0.
C2H6	⇔	CH3	+	CH3	0.	3. 6e13	0.
C3H6	⇔	C2H3	+	CH3	0.	3.5e10	0.
C3H7I	⇔	C2H4	+	CH3	0.	1.0e11	0.
C3H7N	⇔	C2H4	+	CH3	0.	1.6e11	0.
C3H7N	⇔	C3H6	+	H	0.	2.9e14	0.
C3H8	⇔	CH3	+	C2H5	0.	2.0e17	-1.8
C3H8	⇔	C3H7n	+	H	0.	3.6e13	0.
C3H8	⇔	C3H7i	+	H	0.	2.4e13	0.
CH2OH	⇔	CH2O	+	H	0.	1.4e14	0.

Table 2. Rate constants of exchange reactions

Rate constant form $k_r = AT^n \exp(-E/T)$, $cm^6/(mol^2\,s)$

Reaction							A	n	E,K
OH	+	O	=	H	+	O2	2.00e14	0.	8455.
OH	+	H	=	O	+	H2	5.06e04	2.67	3160.
H2O	+	H	=	H2	+	OH	1.00e08	1.60	1661.
O	+	H2O	=	OH	+	OH	1.50e09	1.14	50.
OH	+	OH	=	HO2	+	H	1.50e14	0.0	503.
H2	+	O2	=	HO2	+	H	2.50e13	0.0	348.
H2O	+	O2	=	HO2	+	OH	6.00e13	0.0	0.
H2O	+	O	=	HO2	+	H	3.00e13	0.0	866.
OH	+	O2	=	HO2	+	O	1.80e13	0.0	-204.
H2O2	+	O2	=	HO2	+	HO2	2.50e11	0.0	-624.
H2O	+	OH	=	H2O2	+	H	1.00e13	0.0	1802.
H2O	+	HO2	=	H2O2	+	OH	5.40e12	0.0	503.
CO2	+	H	=	CO	+	OH	4.40e06	1.5	-372.
HCO	+	O	=	CH	+	O2	3.00e13	0.0	0.
HCO	+	CO	=	CO2	+	CH	3.40e12	0.0	348.
CO	+	H2	=	HCO	+	H	2.00e14	0.0	0.
CO	+	H2O	=	HCO	+	OH	1.00e14	0.0	0.
CO	+	HO2	=	HCO	+	O2	3.00e12	0.0	0.
CH	+	H2	=	CH2	+	H	8.40e09	1.5	169.
HCO	+	H2	=	CH2O	+	H	2.50e13	0.0	2008.
HCO	+	OH	=	CH2O	+	O	3.50e13	0.0	2008.
HCO	+	H2O	=	CH2O	+	OH	3.00e13	0.0	604.
CH2	+	H2	=	CH3	+	H	1.80e14	0.0	7574.
CH2O	+	H	=	CH3	+	O	7.00e13	0.0	0.
CH2O	+	OH	=	CH3	+	O2	3.40e11	0.0	4499
CH3	+	H2	=	CH4	+	H	2.20e04	3.0	4399.
CH3	+	OH	=	CH4	+	O	1.20e07	2.1	3835.
CH3	+	H2O	=	CH4	+	OH	1.60e06	2.1	1238.
C2H2	+	H	=	C2H	+	H2	1.10e13	0.0	1443.
CH2	+	CO	=	C2H2	+	O	4.10e08	1.5	854.
C2H	+	H2O	=	C2H2	+	OH	1.10e13	0.0	3522.
C2H2	+	H2	=	C2H3	+	H	3.00e13	0.0	0.
C2H2	+	HO2	=	C2H3	+	O2	5.40e11	0.0	0.
C2H3	+	H2	=	C2H4	+	H	1.50e14	0.0	5133.
C2H3	+	H2O	=	C2H4	+	OH	3.00e13	0.0	1515.
CH3	+	CH3	=	C2H5	+	H	3.00e13	0.0	0.
C2H4	+	HO2	=	C2H5	+	O2	2.00e12	0.0	2513.
C2H5	+	H2	=	C2H6	+	H	5.40e02	3.5	2621.
C2H5	+	OH	=	C2H6	+	O	3.00e07	2.0	2573.
C2H5	+	H2O	=	C2H6	+	OH	6.30e06	2.0	325.
C3H5	+	H2	=	C3H6	+	H	5.00e12	0.0	765.
C3H6	+	HO2	=	C3H7I	+	O2	1.00e12	0.0	2513.
C3H7n	+	H2	=	C3H8	+	H	1.30e14	0.0	4881.
C3H7i	+	H2	=	C3H8	+	H	1.00e14	0.0	4196.
C3H7n	+	OH	=	C3H8	+	O	3.00e13	0.0	2942.
C3H7i	+	OH	=	C3H8	+	O	2.60e13	0.0	2248.
C3H7n	+	H2O	=	C3H8	+	OH	3.70e12	0.0	829.
C3H7i	+	H2O	=	C3H8	+	OH	2.80e12	0.0	433.
CH2O	+	H2	=	CH2OH	+	H	3.00e13	0.0	0.
CH2O	+	HO2	=	CH2OH	+	O2	1.00e13	0.0	3619.
CH2OH	+	H2	=	CH3OH	+	H	4.00e13	0.0	3066.
CH2OH	+	H2O	=	CH3OH	+	OH	1.00e13	0.0	853.
C3H8	+	O2	=	C3H7n	+	HO2	5.50e05	1.5	0.

C3H8	+	O2	=	C3H7i	+	HO2	3.00e09	0.5	0.

Table 3. Reaction rate constants in non selfmaintained air discharge, T in-°K, [5.2].

Number	Reaction	Rate (cm^6/s, cm^3/s) /Cost (eV)	Comments	En. release	Energy defect, eV
1a	$\hat{e} + O_2 \rightarrow O_2^+ + \hat{e} + e$	V_e= 141	Konovalov		
1b	$\hat{e} + O_2(v) \rightarrow O_2^+ + \hat{e} + e$	V_e= 141	Konovalov		
1c	$\hat{e} + O_2(\Delta_{effec}) \rightarrow O_2^+ + \hat{e} + e$	V_e= 141	Konovalov		
1d1	$\hat{e} + N_2 \rightarrow N_2^+ + \hat{e} + e$	V_e= 43.1	Konovalov		
1d2	$\hat{e} + N_2(v) \rightarrow N_2^+ + \hat{e} + e$	V_e= 43.1	Konovalov		
1d3	$\hat{e} + N_2(A^3\Sigma_u^+) \rightarrow N_2^+ + \hat{e} + e$	V_e= 43.1	Konovalov		
1d4	$\hat{e} + N_2(B^3\Pi_g) \rightarrow N_2^+ + \hat{e} + e$	V_e= 43.1	Konovalov		
2a1	$\hat{e} + N_2 \rightarrow N + N + \hat{e}$	V_N =33.6	Konovalov N_2, Rydberg states, with threshold 12.25		
2a2	$\hat{e} + N_2(A^3\Sigma_u^+) \rightarrow N + N + \hat{e}$	V_{N^*} =33.6	Konovalov N_2, Rydberg states, with threshold 12.25		
2a3	$\hat{e} + N_2(B^3\Pi_g) \rightarrow N + N + \hat{e}$	V_{N^*} =33.6	Konovalov N_2, Rydberg , with 12.25 eV threshold		
2a4	$\hat{e} + N_2(v) \rightarrow N + N + \hat{e}$	V_{N^*} =33.6	Konovalov		
3a	$\hat{e} + O_2 \rightarrow O + O + \hat{e}$	V_o =44.4	Konovalov O_2 all from $O_2(A^3\Sigma_u^+$		
3b	$\hat{e} + O_2(v) \rightarrow O + O + \hat{e}$	V_o =44.4	Konovalov O_2 all from $O_2(A^3\Sigma_u^+$		

3c	$\hat{e}+O_2(\Delta_{effective})\rightarrow O+O+\hat{e}$	V_o =44.4	Konovalov O_2 all from $O_2(A^3\Sigma_u^+$		
3d	$\hat{e}+O_2(b)\rightarrow O+O+\hat{e}$	V_o =44.4	Konovalov O_2 all from $O_2(A^3\Sigma_u^+$		
4a1	$\hat{e}+O_2\rightarrow O_2(\Delta_{effective})+\hat{e}$	$V_{O2(\Delta)}$=93.3	Konovalov $O_2(a^1\Delta)$,		
4a2	$\hat{e}+O_2(v)\rightarrow O_2(\Delta_{effective})+\hat{e}$	$V_{O2(\Delta)}$=93.3	Konovalov $O_2(a^1\Delta)$, ,		
4a3	$\hat{e}+O_2\rightarrow O_2(b)+\hat{e}$	$V_{O2(b}$=386	Konovalov $O_2(b^1\Sigma)$,		
4a4	$\hat{e}+O_2(v)\rightarrow O_2(b)+\hat{e}$	$V_{O2(\Delta)}$=386	Konovalov $O_2(b^1\Sigma)$,		
4a5	$\hat{e}+O_2\rightarrow O_2(A)+\hat{e}$	$V_{O2(b}$=170	Konovalov $O_2(A^3\Sigma_u^+)$,		
4a6	$\hat{e}+O_2(v)\rightarrow O_2(A)+\hat{e}$	$V_{O2(\Delta)}$=170	Konovalov $O_2(A^3\Sigma_u^+)$,		
5a1	$e+O_2^+\rightarrow O+O$	$2\cdot10^{-7}\cdot(300/T_e)^{0.7}$	Smirnov	gas	+7.1
5a2	$O+O\rightarrow O_2^++e$	$1.18\cdot10^{-21}\cdot(T)^{2.7}$ exp(-80600/T)	Gupta	gas	-7.1
5b1	$O+M\rightarrow O^++M+e$	$2.0\cdot10^{-20}\cdot(T)^{1.5}\cdot$exp(-158000/T)	Zamyshlyaev M=N_2, O_2, N, O, NO	gas	-16
5b2	$O^++M+e\rightarrow O+M$	$6\ 10^{-27}\cdot(300/T_e)^{1.5}$	Kossyi M=N_2, O_2, N, O, NO	gas	+16
5c1	$O+e\rightarrow O^++e+e$	$2.0\cdot10^{-20}\cdot(T)^{1.5}\cdot$exp(-158000/T)	Zamyshlyaev Maikapar	gas	-16
5c2	$O^++e+e\rightarrow O+e$	$9.05\cdot10^{-20}\cdot(300/T_e)^{4.5}$	Smirnov	gas	+16

6a1	$e + NO^+ \rightarrow N + O$	$3.7\cdot10^{-7}\cdot(300/T_e)^{0.65}$	Park	gas	+2.75
6a2	$N + O \rightarrow e + NO^+$	$1.5\cdot10^{-15}\cdot(T)\cdot\exp(-32\,000/T)$	Park	gas	-2.75
6b1	$e + N_2^+ \rightarrow N + N$	$2.8\cdot10^{-7}\cdot(300/T_e)^{0.5}$	smirnov	gas	+5.85
6b2	$N + N \rightarrow e + N_2^+$	$2.4\cdot10^{-13}\cdot(T)^{0.5}\cdot\exp(-67\,300/T)$	Zamyshlyaev	gas	-5.85
6c1	$N + M \rightarrow N^+ + M + e$	$2.0\cdot10^{-20}\cdot(T)^{1.5}\cdot\exp(-158000/T)$	$M=N_2, O_2, N, O, NO$ Zamyshlyaev	gas	-14.53
6c2	$N^+ + M + e \rightarrow N + M$	$6\ 10^{-27}\cdot(300/T_e)^{1.5}$	Kossyi	gas	+14.53
6d1	$N + e \rightarrow N^+ + e + e$	$2.0\cdot10^{-20}\cdot(T)^{1.5}\cdot\exp(-158000/T)$	Zamyshlyaev	gas	-14.53
6d2	$N^+ + e + e \rightarrow N + e$	$9.05\cdot10^{-20}\cdot(300/T_e)^{4.5}$	Smirnov	gas	+14.53
6f1	$N_2 + M \rightarrow N_2^+ + M + e$	$2.0\cdot10^{-20}\cdot(T)^{1.5}\cdot\exp(-158000/T)$	$M=N_2, O_2, N, O, NO$ Zamyshlyaev	gas	-15.6
6f2	$N_2^+ + M + e \rightarrow N_2 + M$	$6\ 10^{-27}\cdot(300/T_e)^{1.5}$	$M=N_2, O_2, N, O, NO$ Kossyi	gas	+15.6
6g1	$N_2 + e \rightarrow N_2^+ + e + e$	$2.0\cdot10^{-20}\cdot(T)^{1.5}\cdot\exp(-158000/T)$	Zamyshlyaev	gas	-15.6
6g2	$N_2^+ + e + e \rightarrow N_2 + e$	$9.05\cdot10^{-20}\cdot(300/T_e)^{4.5}$	Smirnov	gas	+15.6
7a	$e + O_2 + O_2 \rightarrow O_2^- + O_2$	$K_{att} = 1.7\cdot10^{-31}\cdot \sum_{j=1}^{8} \frac{\alpha_j \cdot f(\varepsilon_j)}{1 + b_j \cdot (N_{O_2}, cm^{-3})}, m^6/s$	Alexandrov	gas	-0.43
7b	$O_2^- + O_2 \rightarrow O_2 + e + O_2$	$8.\ 10^{-10}\cdot\exp(-6035/T)$	Mnatsakanyan, Naidis	gas	+0.43
8	$O_2(\Delta) + O_2^- \rightarrow e + O_2 + O_2$	$2.\ 10^{-10}$	kossyi	gas	+0.55
9	$O_2^+ + NO \rightarrow NO^+ + O_2$	$4.4\ 10^{-10}$	kossyi	gas	+2.95
10	$O + O_2 + O_2 \rightarrow O_3 + O_2$	$8.6\ 10^{-31}\cdot T^{-1.25}$	kossyi	gas	+1.04
11	$O + O_2 + N_2 \rightarrow O_3 + N_2$	$5.6\ 10^{-29}\cdot T^{-2.}$	kossyi	gas	+1.04
12a	$O_2(a^1\Delta) + O_3 \rightarrow O + O_2 + O_2$	$9.7\cdot10^{-13}\ \exp(-1564/T)$	kossyi	gas	-0.06
12b	$O_2(a^1\Delta) + N \rightarrow NO + O$	$2.0\ 10^{-14}\ \exp(-600/T)$	Kossyi	gas	+1.88

12c	$O_2(a^1\Delta) + N_2 \rightarrow N_2 + O_2$	3.0 10^{-21}	Kossyi	gas	+0.98
12d	$O_2(a^1\Delta) + O_2 \rightarrow O_2 + O_2$	2.2 10^{-18} $(T/300)^{0.8}$	Kossyi	gas	+0.98
12f	$O_2(a^1\Delta) + O \rightarrow O_2 + O$	7.0 10^{-16}	Kossyi	gas	+0.98
12g	$O_2(a^1\Delta) + NO \rightarrow O_2 + NO$	2.5 10^{-11}	Kossyi	gas	+0.98
13a1	$N_2 + O_2 \rightarrow N + N + O_2$	$5.0 \cdot 10^{-8} \cdot \exp(-113200/T) \cdot [1 - \exp(-3354/T)]$	Krinonosova	gas	-9.76
13a2	$N + N + O_2 \rightarrow N_2 + O_2$	$8.27\ 10^{-34} \cdot \exp(500/T)$, T=100-600 K, $1.9\ 10^{-33}$, T=600-6300 K,	Krinonosova	gas	+9.76
13b1	$N_2 + N_2 \rightarrow N + N + N_2$	$5.0 \cdot 10^{-8} \cdot \exp(-113200/T) \cdot [1 - \exp(-3354/T)]$	Krinonosova	gas	-9.76
13b2	$N + N + N_2 \rightarrow N_2 + N_2$	$8.27\ 10^{-34} \cdot \exp(500/T)$, T=100-600 K, $1.9\ 10^{-33}$, T=600-6300 K,	Krinonosova	gas	+9.76
13c1	$N_2 + NO \rightarrow N + N + NO$	$5.0 \cdot 10^{-8} \cdot \exp(-113200/T) \cdot [1 - \exp(-3354/T)]$	Krinonosova	gas	-9.76
13c2	$N + N + NO \rightarrow N_2 + NO$	$5.0\ 10^{-33} \cdot \exp(500/T)$, T=100-600 K, $1.14\ 10^{-32}$, T=600-6300 K,	Krinonosova	gas	+9.76
13d1	$N_2 + O \rightarrow N + N + O$	$1.1 \cdot 10^{-7} \cdot \exp(-113200/T) \cdot [1 - \exp(-3354/T)]$	Krinonosova	gas	-9.76
13d2	$N + N + O \rightarrow N_2 + O$	$5.0\ 10^{-33} \cdot \exp(500/T)$, T=100-600 K, $1.14\ 10^{-32}$, T=600-6300 K,	Krinonosova	gas	+9.76
13e1	$N_2 + N \rightarrow N + N + N$	$1.8 \cdot 10^{-8} \cdot \exp(-113200/T) \cdot [1 - \exp(-3354/T)]$, 300-6000 K, $1.4 \cdot 10^{-2} \cdot T^{-2.5} \cdot \exp(-$	Krinonosova	gas	-9.76

		113200/T), 6000-20000 K,			
13e2	$N + N + N \rightarrow N_2 + N$	$1.8 \cdot 10^{-8} \cdot \exp(-113200/T) \cdot [1 - \exp(-3354/T)]$, 300-6000 K, $1.4 \cdot 10^{-2} \cdot T^{-2.5} \cdot \exp(-113200/T)$, 6000-20000 K	Krinonosova	gas	+9.76
13f1	$N_2 + O \rightarrow N + NO$	$1.3\ 10^{-10} \cdot \exp(-38000/T)$	Krinonosova	gas	-3.3
13f2	$N + NO \rightarrow N_2 + O$	$1.05 \cdot 10^{-12} \cdot (T)^{½}$, 200-4000 K	Krinonosova	gas	+3.3
14	$N + O + M \rightarrow NO + M$	$1.8\ 10^{-31} \cdot T^{-0.5}$	Krivonosova	gas	+9.25
15	$O_2^- + O + O_2 \rightarrow e + O_3 + O_2$	$3.0\ 10^{-30}$	Smirnov	gas	+0.61
15a	$O_2^- + O \rightarrow e + O_3$	$1.5\ 10^{-10}$	Kossyi	gas	+0.61
16	$O_2^- + O \rightarrow O_2 + O^-$	$3.3\ 10^{-10}$	kossyi	gas	+1.03
17	$O_2^- + O_3 \rightarrow O_3^- + O_2$	$4.\ 10^{-10}$	Kossyi	gas	+1.57
18	$O^- + O_2(\Delta) \rightarrow e + O_3$	$3.\ 10^{-10}$	Smirnov	gas	+0.5
18a	$O^- + O_2 + O_2 \rightarrow O_3^- + O_2$	$1.1\ 10^{-30}$ (300/T)	Kossyi	gas	+0.54
18b	$O^- + O_2 \rightarrow O_2^- + O$	$8.8\ 10^{-13}\ T^{1/2} \exp(-111837/T)$	Naidis	gas	-1.02
18c	$O^- + O_2 + N_2 \rightarrow O_3^- + N_2$	$1.1\ 10^{-30}$ (300/T)	Kossyi	gas	+0.54
18d	$O^- + O_2(\Delta) \rightarrow O_2^- + O$	$1.\ 10^{-10}$	Kossyi	gas	+2.01
19	$O_3^- + O_2 \rightarrow e + O_3 + O_2$	$2.3\ 10^{-11}$	Samoilovich	gas	-2
19a	$O_3^- + O \rightarrow O_2^- + O_2$	$3.2\ 10^{-10}$	Kossyi	gas	+0.56
20	$O_2^- + O_2^+ \rightarrow O_2 + O_2$	$4.2\ 10^{-7}\ (300/T)^{0.5}$	Smirnov	gas	+11.77
21	$O_2^- + O_2^+ + M \rightarrow O_2 + O_2 + M$	$0.5 \cdot 10^{-25}\ (300/T)^{1.5}$		gas	+11.77
21a	$O_2^- + O_2^+ + O_2 \rightarrow O_2 + O_2 + O + O$	$0.5 \cdot 10^{-25}\ (300/T)^{1.5}$		gas	+6.67

22	$O_2^- + O_2^+ \rightarrow O_2 + O + O$	$1 \cdot 10^{-7}(300/T)^{0.5}$		gas	+6.67
23	$O^- + O_2^+ + M \rightarrow O + O_2 + M$	$1.0 \cdot 10^{-25}\ (300/T)^{1.5}$		gas	+10.74
24	$O_3^- + O_2^+ \rightarrow O_3 + O_2$	$2\ 10^{-7}\ (300/T)^{0.5}$		gas	+10.2
25	$O_3^- + O_2^+ + M \rightarrow O_3 + O_2 + M$	$1.0 \cdot 10^{-25}\ (300/T)^{1.5}$		gas	+10.2
26	$O_3^- + O_2^+ \rightarrow O + O + O_3$	$2\ 10^{-7}\ (300/T)^{0.5}$		gas	+5.1
27	$O_3^- + O_2^+ + M \rightarrow O_3 + O + O + M$	$1.0 \cdot 10^{-25}\ (300/T)^{1.5}$		gas	+5.1
27b	$O + O_3 \rightarrow O_2 + O_2(\Delta)$	$2.0 \cdot 10^{-11}$ exp(-2275/T)	Baulch	gas	+3.08
28	$O^- + NO^+ \rightarrow NO + O$	$5 \cdot 10^{-7}(300/T)^{0.5}$		gas	+7.79
29	$O^- + NO^+ + M \rightarrow O + NO + M$	$1.0 \cdot 10^{-25}\ (300/T)^{1.5}$		gas	+7.79
30	$O_2^- + NO^+ \rightarrow NO + O_2$	$3 \cdot 10^{-7}(300/T)^{0.5}$		gas	+8.82
31	$O_2^- + NO^+ + M \rightarrow O_2 + NO + M$	$1.0 \cdot 10^{-25}\ (300/T)^{1.5}$		gas	+8.82
32	$O_3^- + NO^+ \rightarrow O_3 + NO$	$2 \cdot 10^{-7}(300/T)^{0.5}$		gas	+7. 25
33	$O_3^- + NO^+ + M \rightarrow O_3 + NO + M$	$1.0 \cdot 10^{-25}\ (300/T)^{1.5}$		gas	+7. 25
34a	$e + e + O_2^+ \rightarrow O_2 + e$	$9.05 \cdot 10^{-20} \cdot (300/T_e)^{4.5}$		gas	+12.1
34b	$e + e + N_2^+ \rightarrow N_2 + e$	$9.05 \cdot 10^{-20} \cdot (300/T_e)^{4.5}$		gas	+15.6
35	$e + e + NO^+ \rightarrow NO + e$	$9.1 \cdot 10^{-20} \cdot (300/T_e)^{4.5}$		gas	+9.25
36	$e+O_2 \rightarrow O^- + O$	Reaction is approximated in [2]	under E-field action below $E/N=10^{-15}$ $V \cdot cm^2$ $Te=8.617 \cdot 10^{-5} * T$; T, K.	elect	-1.47
36a	$O^- + O \rightarrow e + O_2$	$5.0 \cdot 10^{-10}$	kossyi	gas	+1.47
37	$e+O_2(a\Delta) \rightarrow O^- + O$	Reaction constant is approximated	under E-field action below $E/N=10^{-15}$ $V \cdot cm^2$	elect	-2.45

			Te=8.617·10^{-5}*T; T, K.		
38	$e+O_2\ (v=1) \rightarrow O^- + O$	Reaction constant is approximated	under E-field action below Te=8.617·10^{-5}*T; T, K.	elect	-1.28
39a	$e+O_2 \rightarrow O_2\ (a\Delta)+e$	Reaction constant is approximated	below E/N=10^{-15} V·cm^2	elect	-0.98
39aa	$e+O_2(a\Delta) \rightarrow O_2 + e$	Reaction constant is approximated		elect	+0.98
39b	$e+O_2(v) \rightarrow O_2\ (a\Delta)+e$	K_{39}		elect	
40a	$e+O_2 \rightarrow O + O + e$	Reaction constant is approximated	under E-field action below E/N=10^{-15} V·cm^2 Te=8.617·10^{-5}*T; T, K.	elect	-5.11
40b	$e+O_2(v) \rightarrow O + O + e$	K_{40}		elect	-4.9
40c	$e+O_2(\Delta) \rightarrow O + O + e$	K_{40}		elect	-4.12
41	$e+N_2 \rightarrow N_2(v) + e$	Reaction constant is approximated	below E/N= 10^{-15} V·cm^2 Te=8.617·10^{-5}*T; T, K.	elect	-.292
41a	$e+N_2(v) \rightarrow N_2 + e$	Reaction constant is approximated		elect	+0.292
42	$e+O_2 \rightarrow O_2(v) + e$	Reaction constant is approximated	below E/N=10^{-15} V·cm^2 Te=8.617·10^{-5}*T; T, K.	elect	-0.196
42a	$e+O_2(v) \rightarrow O_2 + e$	Reaction constant is approximated		elect	+0.196
43	$N_2(v) + M \rightarrow N_2 + M$	$7\cdot10^{-10}\cdot\exp(-141/(T, K)^{1/3})$	(M-molec)	gas	+0.293
44	$N_2(v) + O \rightarrow N_2 + O$	$5\cdot10^{-12}\cdot\exp(-128/(T, K)^{1/2})$		gas	+0.293
45	$O_2(v) + O_2 \rightarrow O_2 + O_2$	$1.41\cdot10^{-12}\cdot$ $\exp(-90/(T, K)^{1/3})$, T≤500,		gas	+0.196

		m^3/s $1.31 \cdot 10^{-12}$ $\exp(-126/(T, K)^{1/3})$, m^3/s T>500			
46	$\hat{e} + N_2 \rightarrow N_2(v) + \hat{e}$	V_e= 14.5	Konovalov (normalized on pure N2 in air)		
47	$\hat{e} + O_2 \rightarrow O_2(v) + \hat{e}$	V_e=3.19 eV	(normalized on pure O2 in air)		
48a	$e + O_2 \rightarrow O_2^+ + 2e$	K_{48}	$5 \cdot 10^{-16}$ <E/N <$2 \cdot 10^{-15}$ V·cm^2	elec	-12.1
48b	$e + O_2(v) \rightarrow O_2^+ + 2e$	K_{48}		elec	-11.9
48c	$e + O_2(\Delta_{effec}) \rightarrow O_2^+ + 2e$	K_{48}		elec	-11.1
48d	$e + N_2 \rightarrow N_2^+ + 2e$	K_{48}		elec	-15.6
48e	$e + N_2(v) \rightarrow N_2^+ + 2e$	K_{48}		elec	-15.3
48f	$e + N_2(A^3\Sigma_u^+) \rightarrow N_2^+ + 2e$	K_{48}		elec	-9.43
48g	$e + N_2(B^3\Pi_g) \rightarrow N_2^+ + 2e$	K_{48}		elec	-8.25
49a	$\hat{e} + N_2 \rightarrow N_2(A^3\Sigma_u^+) + \hat{e}$	V_N^* =258.0 eV	Konovalov (normalized on pure N2 in air) Threshold E=6.17 eV		
49b	$\hat{e} + N_2 \rightarrow N_2(B^3\Pi_g) + \hat{e}$	V_N^* =249.0 eV	Konovalov (normalized on pure N2 in air) Threshold E=7.35 eV		
50a	$e + N_2 \rightarrow N_2(A^3\Sigma_u^+) + e$	Reaction constant is approximated	$3 \cdot 10^{-16}$ <E/N <E/N=$2 \cdot 10^{-15}$ V·cm^2	elec	-6.17
50aa	$e + N_2(A^3\Sigma_u^+) \rightarrow e + N_2$	Reaction constant is approximated		elec	6.17
50b	$e + N_2 \rightarrow N_2(B^3\Pi_g) + e$	Reaction constant is approximated	$3 \cdot 10^{-16}$ <E/N <E/N=$2 \cdot 10^{-15}$ V·cm^2	elec	-7.35

50bb	$e + N_2(B^3\Pi_g) \rightarrow N_2 + e$	Reaction constant is approximated		elec	7.35
51	$N_2(A^3\Sigma_u^+) + N_2(A^3\Sigma_u^+) \rightarrow N_2(X^1\Sigma_g^+) + N_2(B^3\Pi_g)$	$2.6 \cdot 10^{-10}$	Kossyi	gas	+4.99
52	$N_2(A^3\Sigma_u^+) + N_2(A^3\Sigma_u^+) \rightarrow N_2(X^1\Sigma_g^+) + N_2(B^3\Pi_g)$	$1.1 \cdot 10^{-9}$	$N_2(X^1\Sigma_g^+)$ considered as N_2	gas	+4.99
53a	$N_2(A^3\Sigma_u^+) + N_2(X^1\Sigma_g^+, v) \rightarrow N_2(X^1\Sigma_g^+, w) + N_2(B^3\Pi_g)$	$3.0 \cdot 10^{-10}$	$N_2(X^1\Sigma_g^+, v$ considered as N_2	gas	-0.9
53b	$N_2(A^3\Sigma_u^+) + O_2 \rightarrow N_2 + O + O$	$2.54 \cdot 10^{-12}$	Baulch Kossyi	gas	+1.07
53c1	$N_2(B^3\Pi_g) + N_2 \rightarrow N_2(A^3\Sigma_u^+) + N_2$	$5.0 \cdot 10^{-11}$	Kossyi	gas	+1.18
53c2	$N_2(B^3\Pi_g) \rightarrow N_2(A^3\Sigma_u^+) + h\nu$	$1.5 \cdot 10^5$ s^{-1}	Kossyi	gas	+1.18
53c3	$N_2(B^3\Pi_g) + NO \rightarrow N_2(A^3\Sigma_u^+) + NO$	$2.4 \cdot 10^{-10}$	Kossyi	gas	+1.18
53c4	$N_2(B^3\Pi_g) + O_2 \rightarrow N_2 + O + O$	$3.0 \cdot 10^{-10}$	Kossyi	gas	+2.25
54a	$N_2^+ + O_2 \rightarrow O_2^+ + N_2$	$K_{54}=2.86 \cdot 10^{-10}$ cm^3/s	Charge exchange N_2^+ ion averaged over N_2^+ and N_4^+ it appears in $N_2^+ + 2N_2 \rightarrow$ and $N_4^+ + O_2 \rightarrow$	gas	+3.4
54b	$N_2^+ + O_2(v) \rightarrow O_2^+ + N_2$	$K_{54}=2.86 \cdot 10^{-10}$ cm^3/s		gas	+3.4
54c	$N_2^+ + O_2(\Delta_{effec}) \rightarrow O_2^+ + N_2$	$K_{54}=2.86 \cdot 10^{-10}$ cm^3/s		gas	+2.4
55a1	$O_2 + O_2 \rightarrow O + O + O_2$	$3.7 \cdot 10^{-8} \cdot \exp(-59380/T) \cdot$	Krinonosova	gas	-5.1

		[1- exp(-2240/T)] , T=300-4000; 16.0· $(T)^{-2..5}$exp(-59380/T) T=4000-20000;			
55a2	$O + O + O_2 \rightarrow O_2 + O_2$	2.45 10^{-31}· $(T)^{-0.63}$ T=300-4000;	Krinonosova	gas	+5.1
55b1	$O_2 + N \rightarrow O + O + N$	9.3·10^{-9}· exp(-59380/T) · [1- exp(-2240/T)] , T=3000-7000;	Krinonosova	gas	-5.1
55b2	$O + O + N \rightarrow O_2 + N$	6.3 10^{-32}· $(T)^{-0.63}$ T=300-4000;	Krinonosova	gas	+5.1
55b3	$O_2 + N \rightarrow O + NO$	1.0· 10^{-14} · T·exp(-3150/T)	Krinonosova	gas	-1.4
55c1	$O_2 + NO \rightarrow O + O + NO$	9.3·10^{-9}· exp(-59380/T) · [1- exp(-2240/T)] T=300-4000; 4.0· $(T)^{-2..5}$exp(-59380/T) T=4000-20000;	Krinonosova	gas	-5.1
55c2	$O + O + NO \rightarrow O_2 + NO$	6.3 10^{-32}· $(T)^{-0.63}$ T=300-4000;	Krinonosova	gas	+5.1
55d1	$O_2 + O \rightarrow O + O + O$	1.3·10^{-7}· exp(-59380/T) · [1- exp(-2240/T)] T=300-4000; 5.8 10^{-2} $(T)^{-2..5}$exp(- 59380/T) T=4000-20000;	Krinonosova	gas	-5.1
55d2	$O + O + O \rightarrow O_2 + O$	8.8 10^{-31}· $(T)^{-0.63}$ T=300-4000;	Krinonosova	gas	+5.1
55e1	$O_2 + N_2 \rightarrow O + O + N_2$	9.3·10^{-9}· exp(-59380/T) · [1- exp(-2240/T)]	Krinonosova	gas	-5.1
55e2	$O + O + N_2 \rightarrow O_2 + N_2$	2.76 10^{-34}· exp(720/T)	Krinonosova	gas	+5.1

56a1	$NO + O_2 \rightarrow N + O + O_2$	$8.7\ 10^{-9}$ $\cdot \exp(-76\ 000/T)$	Krinonosova	gas	-6.5
56a2	$N + O + O_2 \rightarrow NO + O_2$	$2.8\ 10^{-28} \cdot (T)^{-0..5}$	Zamyshlyaev	gas	+6.5
56b1	$NO + N_2 \rightarrow N + O + N_2$	$8.7\ 10^{-9}$ $\cdot \exp(-76\ 000/T)$	Krinonosova	gas	-6.5
56b2	$N + O + N_2 \rightarrow NO + N_2$	$1.8\ 10^{-31} \cdot (T)^{-0..5}$	Krinonosova Sovpadaet s 14	gas	+6.5
56c1	$NO + O \rightarrow N + O + O$	$1.7\ 10^{-7}$ $\cdot \exp(-76\ 000/T)$	Krinonosova	gas	-6.5
56c2	$N + O + O \rightarrow NO + O$	$5.6\ 10^{-27} \cdot (T)^{-0..5}$	Zamyshlyaev	gas	+6.5
56c3	$NO + O \rightarrow N + O_2$	$2.5\ 10^{-15} \cdot (T)$ $\cdot \exp(-19\ 500/T)$	Krinonosova	gas	+1.4
56d1	$NO + N \rightarrow N + O + N$	$1.3\ 10^{-2}$ $\cdot (T)^{-1..5} \exp(-75530/T)$	Zamyshlyaev	gas	-6.5
56d2	$N + O + N \rightarrow NO + N$	$5.6\ 10^{-27} \cdot (T)^{-0..5}$	Zamyshlyaev	gas	+6.5
56d3	$NO + N \rightarrow O + N_2$	$1.05\ 10^{-12}$ $\cdot (T)^{0..5}$ **T=200-4000 K**	Krinonosova	gas	+3.26
56e1	$NO + NO \rightarrow N + O + NO$	$1.7\ 10^{-7}$ $\cdot \exp(-76\ 000/T)$	Krinonosova	gas	-6.5
56e2	$N + O + NO \rightarrow NO + NO$	$5.6\ 10^{-27} \cdot (T)^{-0..5}$	Zamyshlyaev	gas	+6.5
58	$N + NO \rightarrow N_2 + O$	$1.0\ 10^{-12} \cdot (T)^{0..5}$	Krinonosova	gas	+3.28
62	$N + O_2 \rightarrow NO + O$	$4.1\ 10^{-12} \cdot \exp(-3200/T)$	Baulch	gas	+1.4
63	$N + O_3 \rightarrow NO + O_2$	$5.5\ 10^{-12}$	Baulch	gas	-3.3
64	$N_2(A^3\Sigma_u^+) + O \rightarrow N_2 + O$	$2.1\ 10^{-11}$	Kossyi	gas	+6.17
65	$N_2(A^3\Sigma_u^+) + O \rightarrow NO + N$	$7.0\ 10^{-12}$	Kossyi	gas	+2.91
66	$N_2 + O_2 \rightarrow O + N_2O$	$2.5\ 10^{-10} \cdot \exp(-50391/T)$	krivonosova	gas	-3.9
67	$O^- + NO \rightarrow e + NO_2$	$2.6\ 10^{-10}$	Kossyi	gas	+1.64
68	$O_2(b) + O_3 \rightarrow O + O_2 + O_2$	$1.8 \cdot 10^{-11}$	kossyi	gas	+0. 6
69	$O_2(b) + N_2 \rightarrow N_2 + O_2(a^1\Delta)$	$4.9\ 10^{-15} \cdot \exp(-253/T)$	Kossyi	gas	+0.66

71	$O_2(b)+O_2 \rightarrow O_2+O_2(a^1\Delta)$	$4.3\ 10^{-22}\cdot T^{2.4}\ \exp(-241/T)$	Kossyi	gas	+0.66
72	$O_2(b)+O \rightarrow O_2(a^1\Delta)+O$	$8.0\ 10^{-14}$	Kossyi	gas	+0.66
73	$O_2(b)+NO \rightarrow O_2(a^1\Delta)+NO$	$4.0\ 10^{-14}$	Kossyi	gas	+0.66
74	$O_2(A)+O_2 \rightarrow O_2(b)+O_2(b)$	$2.9\ 10^{-13}$	Kossyi	gas	+1.22
75	$O_2(A)+O \rightarrow O_2(b)+O(D)$	$9.0\ 10^{-12}$	Kossyi	gas	+0.89
76	$O_2(A)+N_2 \rightarrow N_2+O_2(b)$	$3.0\ 10^{-13}$.	Kossyi	gas	+2.86

References to chapter 5.

5.1. Baev V.K., Golovichev V.I., Tretyakov P.K. et.al. Combustion in a supersonic flow. Nauka. Novosibirsk. 1984.

5.2. Ardelyan N., Bychkov V., Kosmachevskii K., Chuvashev S., Malmuth N. Modeling of Plasmas in Electron Beams and Plasma Jets . AIAA 2001-3101 Proc. 32-nd AIAA Plasmadynamics and Lasers Conference and 4 th Weakly Ionized gases Workshop 11-14 June 2001, Anaheim, CA.

5.3. Westbrook, C.K., Dryer, F.L. Simplified Reaction Mechanisms for the Oxidation of Fuels in Flames. Combustion Science and Technology, 1981, Vol.27, pp.31-43

5.4. Katta, V.R., Roquemore, W.M. Simulation of Unsteady Flows in an Axisymmetric Research Combustor Using Detailed-Chemical Kinetics. AIAA/ASME/SAE/ASEE Joint Propulsion Conference & Exhibit, 34th, Cleveland, OH, July 13-15, 1998.

5.5. Warnatz, J., Maas, U., Dibble, R.W. *Combustion. Physical and Chemical Fundamentals, Modeling and Simulations, Experiments, Pollutant Formation.* Springer, 2001

5.6. Zhukov V.N., Sechenov V.A., Khorunzhenko V.I., A.Yu.Starikovskii Hydrogcarbon-air mixture ignition kinetics. 3 –d Workshop Thermochemical and plasma processes in aerodynamics. Saint – Petersburg. 28-31 July. 2003. P.296.

5.7. Bychkov V.L., Grachev L.P., Esakov I.I.,Deriugin A.A., Zabrodin A .V., Klimov A.I., Kochetov I.V., Lutskii A.E., Lutskaya T.Yu., Napartovich A.P., Khodataev K.V., Cherkashin V.A. Computational-experimental studies of the flow around the blunt body at presence of the longitudinal gas discharge. Preprint IPM by M.V. Keldysh RAS, No 27, 1997.

5.8. Bychkov V.L., Kuranov A.L., Yurovski V.A. Non equilibrium high pressure beam plasma in hot air. Materials of the YIII All Union Conference "Physics of Low Temperature Plasma".1991. Minsk. Pt.2.P.47-48.

Chapter 6. Stationary and pulsed plasma jets for ignition

6.1. Technical starting of the plasma generator with the divergent conical nozzle

In accordance with the technical task and the calendar plan of works technical starting of the plasma generator with the divergent conical nozzle has been realized. (Main elements of the plasma generator construction were considered in the Report [1]).

Nitrogen and argon were used plasma forming gases. Modes of the plasma generator work have been studied, its Ampere-Volt characteristics, distributions of plasma jet parameters have been studied with respect to the sort of the gas and its flow rate. The gas flow rate varied in the range 1 – 1,5 g/s. Strong erosion of the electrode surface arises at gas flow rates smaller than 1 g/s. Main series of the experiments was carried out at gas flow rate of 1,25 g/s. This corresponds to nitrogen flow rate of ~ 75 liter/minute and argon flow rate of ~ 40 liter/minute.

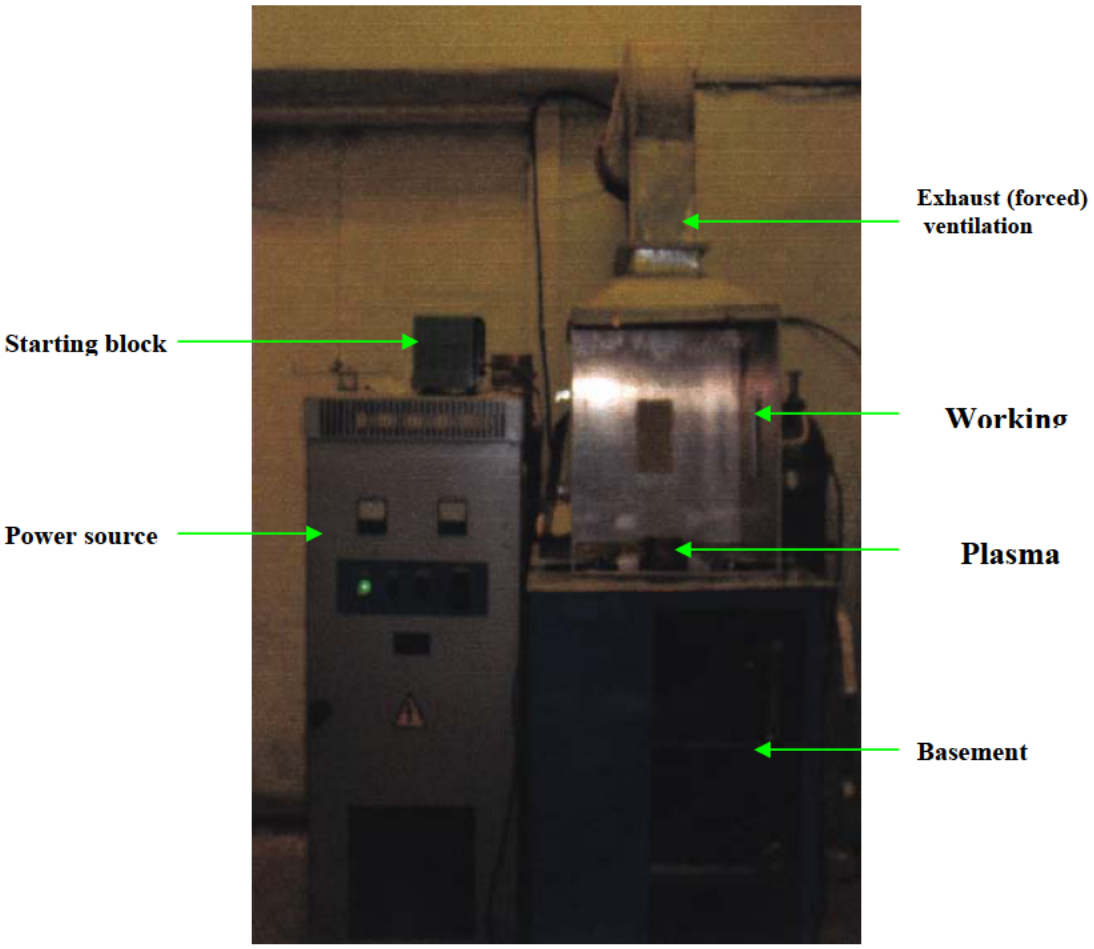

Fig.1

In Fig.6.1 one can see a photo of the set up. Main elements of the set up are the follows:

1. Power source with power ≤ 15 kW;

2. Starting block, it forms an ignition pulse at amplitude of ~ 5 kV, duration of an ignition pulse is about of 100 μs;
3. Basement, in which placed systems of water cooling, current stabilizing, gas delivery and consumption;
4. Working chamber with the plasma generator (the photo is made without of protecting glass – a filter)
5. System of forced ventilation.

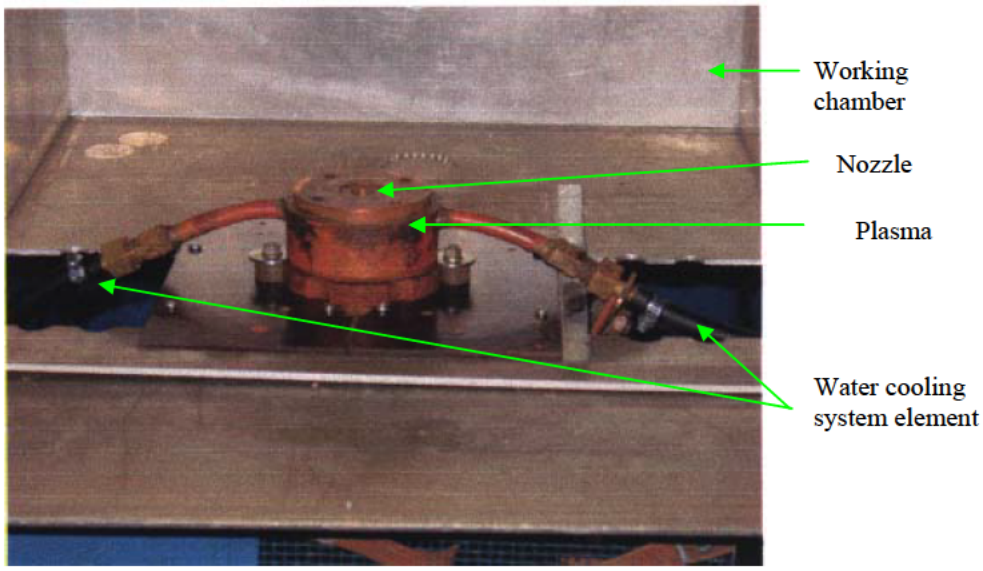

The plasma generator appearance in Fig.6.2 ; chamber is represented in Fig.6.2.

In Fig. 6.3 – Fig. 6.5 one can see photos of the plasma jet at different values of the inputted power (Fig. 6.3 – 3 kW; Fig. 6.4 – 4,5 kW; Fig. 6.5– 6,5 kW)

Fig. 6.3

Fig.6.4

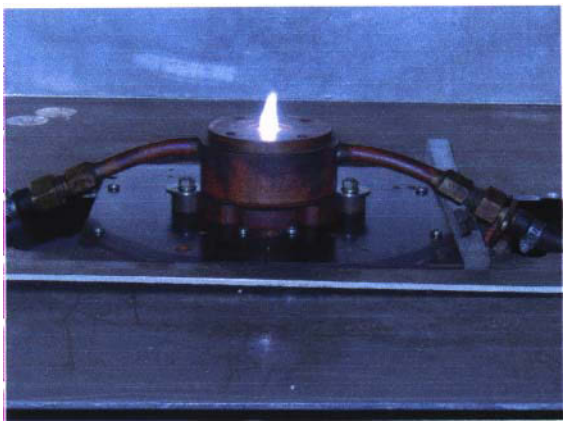

Fig.6.5

First two photos were made with the application of dense neutral light filter. Non symmetrical picture of the jet luminescence can be described by large vortex component (see part 2 of the Report about the vortices in the channel) of the velocity. (Remember that in the present plasma generator design the tangential swirling is used for the flow stabilizing and for the gasdynamic protection of electrodes. At that the vortical velocity component V_r equals to the axial component of the flow velocity V_a, and the angle between them is $\alpha \approx 45°$).

6.2. Determination of the gas temperature in the discharge created by the plasma generator with divergent conical nozzle

Information about the gas temperature T_g is important for an analysis of plasma processes. The most simple situation in case of molecular plasma corresponds to local thermodynamic equilibrium when $T_g = T_V = T_R$, here T_V and T_R – are the vibrational and rotational temperatures, respectively. T_V and T_R – are the parameters determining vibrational and rotational level populations in the Boltzmann function characterizing molecular distribution function. Both T_V and T_R can be obtained from radiation spectra of the plasma.

T_g in non-equilibrium plasmas also can be determined on a basis of T_R measurements [2]. Plasma radiation spectra give information on rotation temperatures T^*_R of molecules in excited electronic states. T^*_R dependence of the spectral components I_{lk}, belonging to the rotational structure of spectral lines corresponds to the transition from the 1-st and the k-th states is described by the formulae

$$(k_B /B^*)\ln(I_{lk}/i\ \nu^4_{ik}) = C - j(j+1)/T^*_R,$$

here k_B is the Boltzmann constant, j – full molecular angular momentum, i – quantum mechanical intensity coefficient, n_{lk} – radiation frequency of the quantum, C - constant One

can determine T^*_R from the graph of the function $(k_B /B^*)\ln(I_{lk}/i\ \nu^4_{ik})$ through j(j+1) and measurement of its slope tg α:

$$T^*_R = 1/\mathrm{tg}\ \alpha.$$

The probability of rotational energy changing is negligibly small for a stable molecule, and rotational distribution functions over the excited and ground states of molecules are identical, $T_R = T^*_R$. Intense exchange of translational and rotational energies at collisions leads to equality of T_g and T_R of molecules in the ground electronic state. But there are some features in real conditions, which have to be accounted. If molecules take part in plasma chemical reactions then some part of their activation energy can transfer to the rotational energy, this leads to the distortion of the initial rotational distribution function, $T_R \neq T^*_R$ in this case. This is typical for chemically active radicals. Another source of errors is connected with the fact that one determines not T_R from spectra but B^*/T_R, here B* is the rotational constant of the upper state at the radiation transition. The rotational energy distribution can stay the same at excitation of this state by the electron collision but it corresponds to the temperature

$$T_R = T_g\ B^*/B^o,$$

here B^o is the rotational constant for the ground state. So it is necessary to choose stable molecules with $B^* \approx B^o$ for determining of T_g.

If one uses the second positive nitrogen system then in this case one can suppose ν^4_{lk} to be constant (the corresponding error is ~ 0,5 %, and it can be neglected), B* = 1,826; so the formulae for T_R has the following form in this case:

$$0{,}89\ \ln(I_{lk}/i) = \mathrm{Const} - j(j+1)/T_R.$$

A set up for spectral measurements of plasma parameters is represented in Fig.8.1.6. The discharge radiation was focused to the inlet slot of the spectrograph STE –1 with a help of quartz lens (1) with the focal distance f = 50 cm with scaling down 1 : 2. The device dispersion was~ 0,35 nm/mm in the range of waves 300 - 400 nm. The discharge image was oriented along the inlet spectrograph hole for obtaining of spatially resolved radiation spectrum .

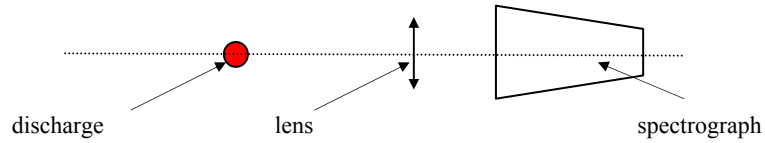

Fig. 6.6. A scheme of radiation spectra detection.

For example in Fig.8.1.7 is represented the discharge radiation spectrum in the range of wavelengths λ = 360 - 400 nm for a discharge with electric inputting power 3 kW. In this case the electrode erosion was rather weak. It is probable that CN molecules in present experiments are generated at recombination of nitrogen and carbon atoms. Atomic carbon is the product of interaction of the plasma with the inter electrode partitions that contain organic elements.

At low inputting power it is possible to detect the gas temperature (nitrogen in this case) on a basis of non resolved CN bands with the threshold wavelengths 3883 A^o and 3871 A^o [3]. These methods are based on: 1) ratio of radiation integrals of two bands; 2) ratio of the threshold intensities of these bands; 3) rotation transition intensities distribution of the band (0;0) with the quantum wavelength 3883 A^o.

The spectrum changes at increasing of the inputted power: intense lines of copper and manganese appear. The temperature in this case can be determined on a base of relative intensities of chosen line pairs.

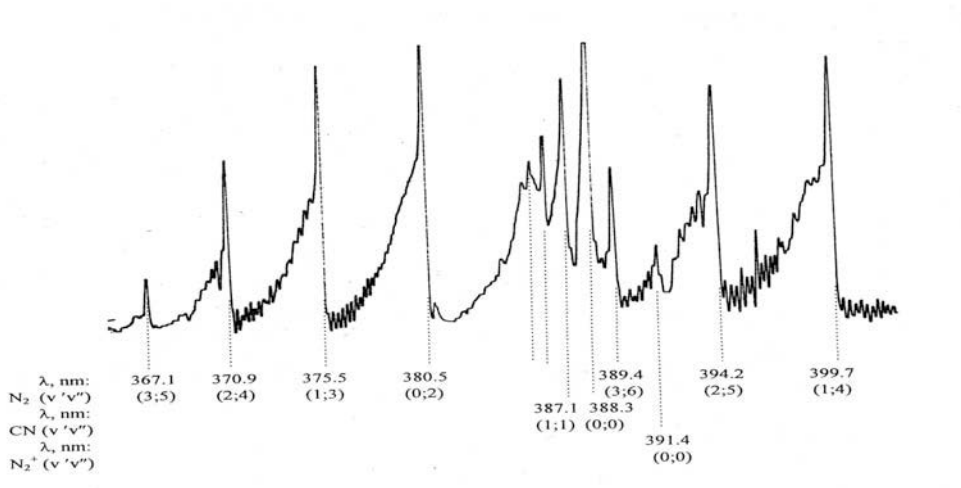

Fig.6.7. Nitrogen plasma jet radiation spectrum at the inletting power 3 kW.

Analysis of radiation spectra has shown that the gas temperature of the plasma jets in the investigated range of inputted power in the plasma relaxation region (behind the nozzle cut) lies in the range T_g = (3500 - 6600°) K. Its longitudinal dependence is not monotonous. Axial

temperature distributions show that the gas temperature rises with the current rise and it decreases down the flow (see Fig.6.8).

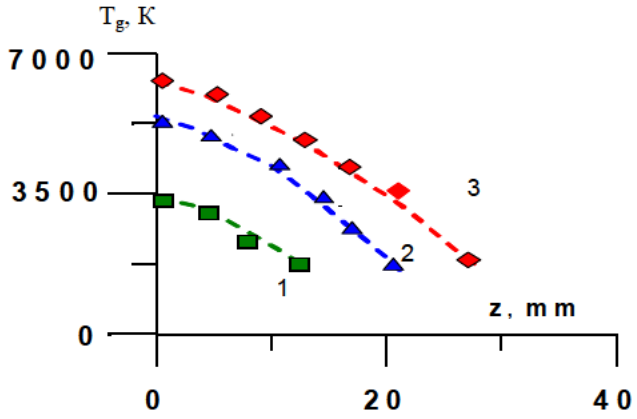

Fig.6.8. Longitudinal distribution of the gas temperature of the nitrogen jet: Inputted power 1 –3 kW; 2 – 4,5 kW, 3- 6,5 kW.

Spatial distribution of electron concentration can be obtained with good accuracy by the Saha equation (see [4]) at known gas temperature distribution. In such a way the electron concentration near the nozzle cut is several units 10^{16} cm^{-3} in the case of the inputted power 6,5 kW and it is in agreement with results of our calculations.

6.3. Results of experiments carried out with the plasma generator with divergent conical nozzle

In accordance with the technical task and the calendar plan of works investigations of main parameters of the plasma flowing out of the stationary plasma generator with the divergent conical nozzle have been made.

Modes of the plasma generator operation in the wide range of the initial conditions have been studied.

The mass flow rate of a gas was varied in the range 0,7 – 2 g/s, the power characteristics were varied in the range 3 – 7 kW.

It was shown that the gas temperature at the outlet from the nozzle changes in the range from 3500 K to 6000 K at changing of the inputted power in the range from 3 to 6,5 kW.

The typical values of the electron density lie in the range $7 \cdot 10^{15}$ - $5 \cdot 10^{16}$ cm^{-3} as it was obtained by the scanning electric probe transversally to the axis in the mode of the continuous medium.

It was shown that the strong erosion of the electrode surface takes place at the mass flow rates smaller than 1 g/s even at low values of the inputted power (P< 4 kW), it leads to their rapid destruction.

The detailed analysis of the planned experiments conditions (7-10 quarters) on the stationary supersonic gaseous and plasma jets shows that:

1. developed and put into the exploitation powerful stationary plasma generator is highly effective plasma source, which stably works at high values of the power put in (up to 10 kW) and at high mass flow rates of the plasma forming gas (in particular nitrogen and argon). It can be successfully applied for the plasma chemical activation of the high speed (supersonic) flows of the air-fuel mixture in the large scaled stationary engine devices, which transversal sizes are no less than 20 – 30 cm. Namely this type of the plasma generator can be recommended for the applications in the set ups of these devices;

2. At the application of the engine model with the typical size of 2-3 cm (developed and manufactured in MSU) and working in the quasi-stationary mode (the duration of the working cycle is ~2-3 s) the using of such stationary high temperature source is unlikely advisable since:

a) the high thermal loads can lead to the rapid destruction of the supersonic channel walls;

в) it will substantially change the gasdynamic structure of the main supersonic flow due to large additional injection of the plasma forming gas;

c) it will lead to the uncontrolled experimental conditions over the initial conditions (rapid uncontrolled pressure increase in the receiver)

d) it is connected with large difficulties at the synchronizing of the main supersonic tract work , the plasma source and the delivery device of the plasma forming gas (rather long time, about of 10 – 20 s, is required for the plasma generator to reach the stable mode of the operation).

6.4. Small sized quasi stationary plasma generator

In connection with conclusions of #8.1.1. the small sized quasi stationary plasma generator has been developed by us and put to the manufacturing. The nozzle geometry corresponds to those of the main already developed construction. The typical parameters of this plasma generator are:

a. Sizes – the external diameter is 16 mm, the length is 80 mm;
b. the voltage pulse duration – 5 - 6 ms;
c. – 280 V;
d. the discharge current maximum value 120 A;
e. the discharge current pulse form is the bell type

The plasma generator general scheme is represented in Fig.6.9 .

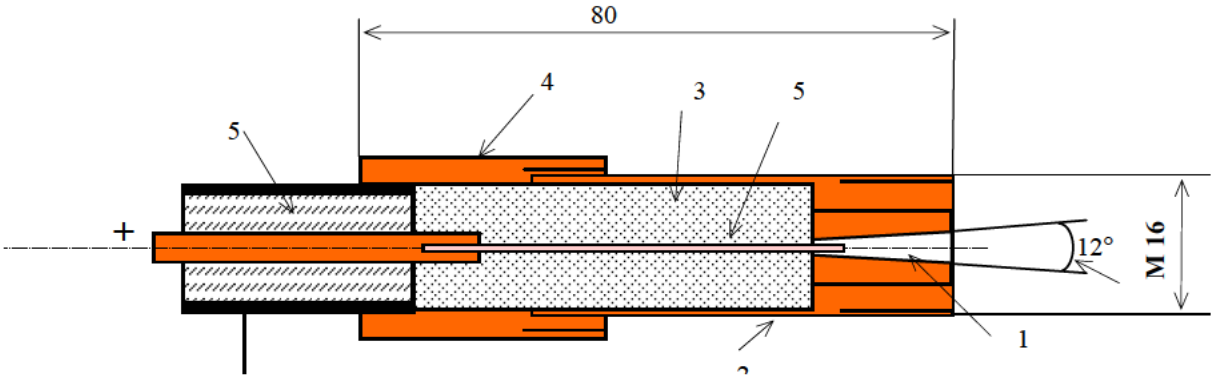

Fig.6.9 – the nozzle, 2 – the body, 3 – the dielectric, 4 – the joint, 5 – the central electrode, 5- the coaxial cable.

The plasma generator represents the cylindrical axially symmetric construction. Its main elements are made of copper (the nozzle, the body, the mounting joint for the plasma generator connection with the coaxial cable). The central (axial) electrode is made of the tungsten. The organic glass or the heat proof ceramics are used for the dielectric. The thread M16 is foreseen in the front part of the plasma generator nozzle. It is required for the adjoining of the plasma generator to the supersonic tract or to the intermediate receiver chamber.

The plasma generator is placed in the direct vicinity to the supersonic flow on the twisting device, which allows to investigate the interaction of the high speed gaseous and plasma flows directed at different angles.

He plasma generator is connected with the power source with the outlet voltage of ≈ 300 V. The voltage pulse duration can be varied in the range from 1 to 10 ms. The energy stored in the capacity storage is about of 145 J, and it corresponds to the power put of 145 kW to the load at the pulse duration of ≈ 1 ms.

The generator starting is realized by the voltage high voltage pulse with the amplitude of 30 kV. The possibility of the low voltage synchronizer pulse application, which comes from the starting scheme, allows to start the plasma generator in any time period with respect to the general pneumovalve starting the supersonic channel.

6.5. Plasma parameter measurements of small sized quasistationary plasma generator

For generation of quasi-stationary plasma jets the small sized energy storage with total capacity of C =3200 μF has been applied. The design of the energy storage controlling block allowed to work at different fixed values of the stored energy, namely, 50, 100 and 200 J. The operating voltage was ~ 300 V. The current pulse duration was 2, 12 and 14 ms. The maximum discharge current value was 150 A, the current pulse form was the bell type.

The general plasma generator design was discussed in details in the previous part. The plasma generator represented the cylindrical axisymmetrical construction, its main parts were made of copper (the nozzle, the body, fixing joint for connection of the plasma generator and the coaxial cable). The central axial electrode is made tungsten. Organic glass was used as the dielectric material. Starting of the scheme and detection devices was realized by synchronizing-pulse coming from the generator G5-15.

Investigation of the plasma injecting to air was undertook at the invariable plasma generator working chamber geometry. Only imputed energy to the discharge was varied. Spectra detection was realized by the spectrograph STE -1.

Schlieren method was applied for plasma flow character (laminar or turbulent) determination. Shadow pictures were obtained with a help of the super high-speed photo recorder.

In Fig.6.10 one can see the integral photo of the plasma jet in the motionless air at the pressure of 1 atm. This plasma jet has almost right cylindrical form, it is surrounded by weakly luminescent low temperature “coat” (but the area directly adjoining the jet, where the plasma temperature is the highest). The plasma boundaries are not disturbed, the flow is close to the laminar one. Investigations of the jet dynamics have shown that the plasma flowing out from the injector nozzle takes place with considerable delay time (about of 800 – 900 μs) with respect to the current pulse beginning. The discharge was developing inside the plasma generator working chamber during this time period.

Fig. 6.10. Plasma jet

The plasma flow character was investigated with a help of the shadow method. In Fig.6.11 one can see fragments of the frame-accurate shadow image corresponding to the initial (a, b – rising of the discharge current) and the final (about 5 ms) phases of the process. They were obtained at the stored energy value of 50 J.

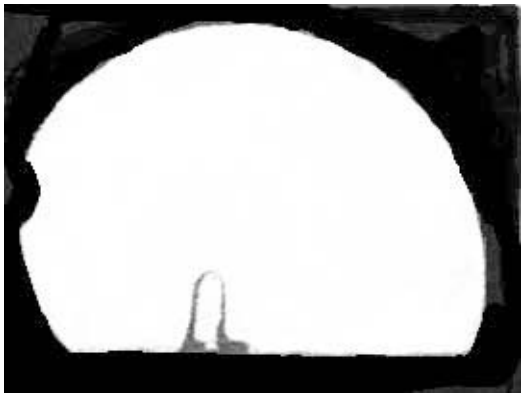

a

b

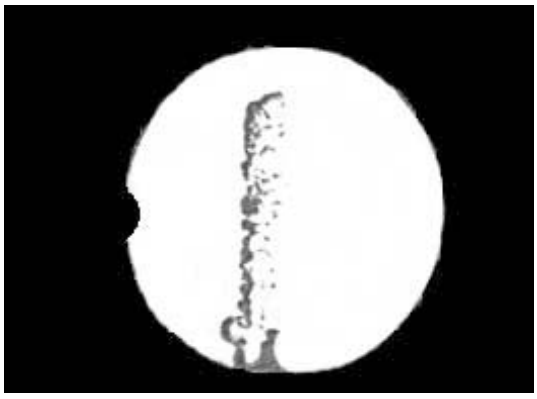

c

Fig.6.11. Fragments of the jet shadow image

One can see that the flow is the laminar at the initial stage of the process. The noticeable turbulization of the plasma surrounding "coat" is observed in the end of the energy put pulse.

Plasma parameters diagnostics was carried out by the optical methods over the jet radiation spectrum. It proved out to be that with respect to the power input there were the lines of CN and carbon C_2 in different ratios, the continuous spectrum detected from regions near the plasma generator nozzle, lines of the H_α, H_β, H_γ, copper, sodium, carbon, etc. The hydrogen lines H_α, H_β, H_γ were strongly spread, at that the spreading value depended on the spatial coordinate (in the longitudinal and the transversal directions) of the jet.

The plasma temperature was measured either over the lines of CN with the quantum wavelength λ = 383,3 nm (the line 0;0) or over copper lines with the wavelength λ = 510,55 nm, 515,32 nm and 521,82 nm.

The sample of the spectrum image of the line (0;0) is represented in Fig. 6.12.

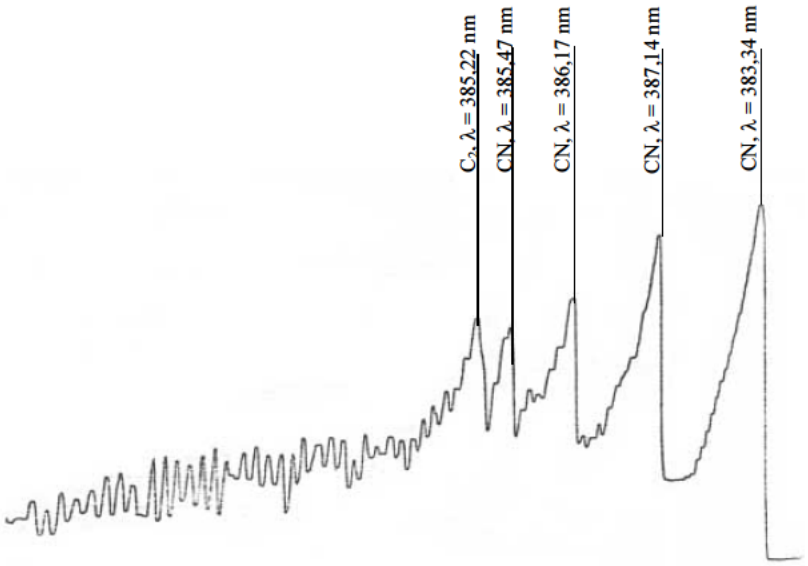

Fig.6.12

The electron concentrations were determined by Stark spreading of the hydrogen line H_α and by the electric probe method.

In Fig.6.13 and 6.14 one can see the dependencies of the maximum values of the plasma temperature and the electron concentrations near the plasma generator nozzle cut with respect to the energy stored in the power storage. One can see that the plasma temperature rises from ~ 4 kK to ~ 6,5 kK in the investigated ranges of the stored energy, at the same time the electron concentration rises from ~ $2 \cdot 10^{17}$ cm^{-3} to $5{,}5 \cdot 10^{17}$ cm^{-3} at the energy W variation from 50 J to 200 J.

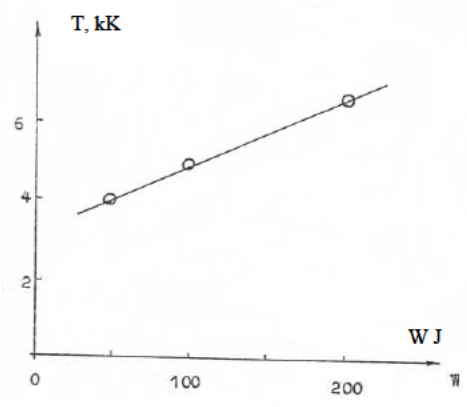

Fig. 6.13

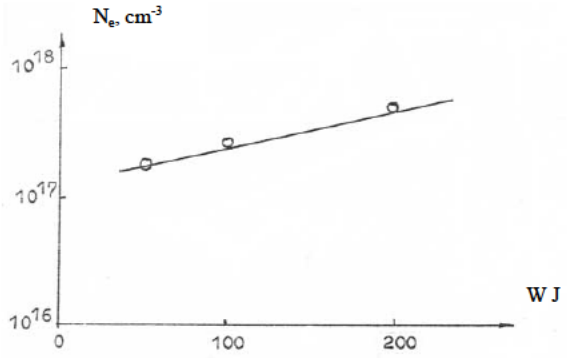

Fig..6.14

.6.15

for two values of energy stored in the power storage: 100 J (the curve 2) and 200 J (the curve 1). One can understand from the represented data that the temperature monotonously decreases with increase of the distance from the plasma generator cut, and at a distance of about 10 cm it is ~3 kK for100 J and it is 5,5 kK at 200 J.

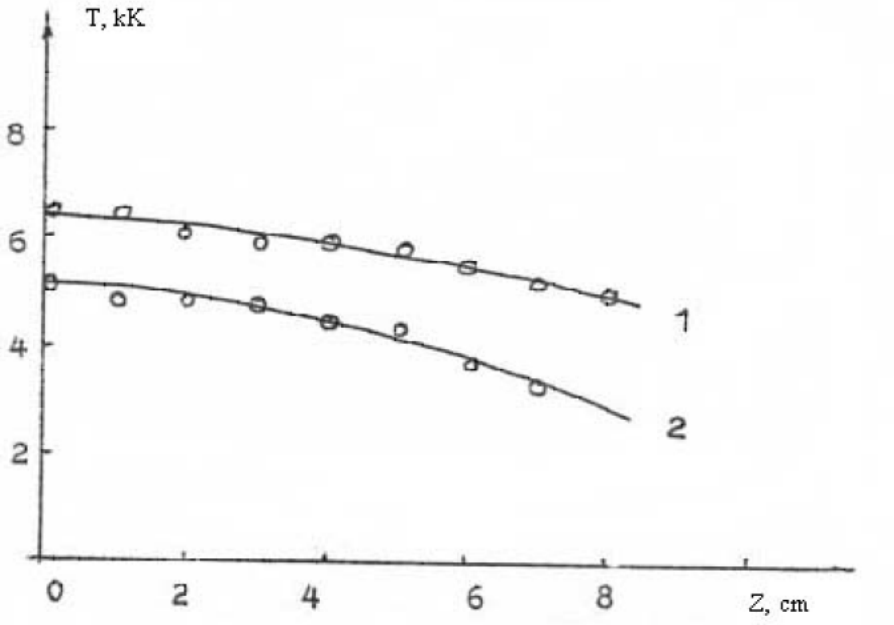

Fig.6.15

The Stark spreading of the hydrogen lines is much greater than the spreading due to other factors at the electron concentration $N_e \geq 10^{14}$ cm^{-3}. Spreading of spectral lines in conditions of our experiments can take place due to the Doppler effect (~ 0,01 nm), external Stark effect (~ 0,01 nm), spectrograph instrumental function (~ 0,01 nm), but the spreading of the line H_α detected in the experiments varied from 0,1 to 3,5 nm. The choice of the line H_α for the electron concentration determination was conditioned by the following: the accuracy of the line spreading

theoretical calculations is sufficiently high (~ 10%) and the given line corresponds to the transition between considerably low-lying levels. So it is easily excited in plasmas even the hydrogen is present as small admixture. In Fig.6.16 one can see the axial distribution of the electron density N_e for two values of energy stored in the power storage: 100 J (the curve 2) and 200 J (the curve 1).

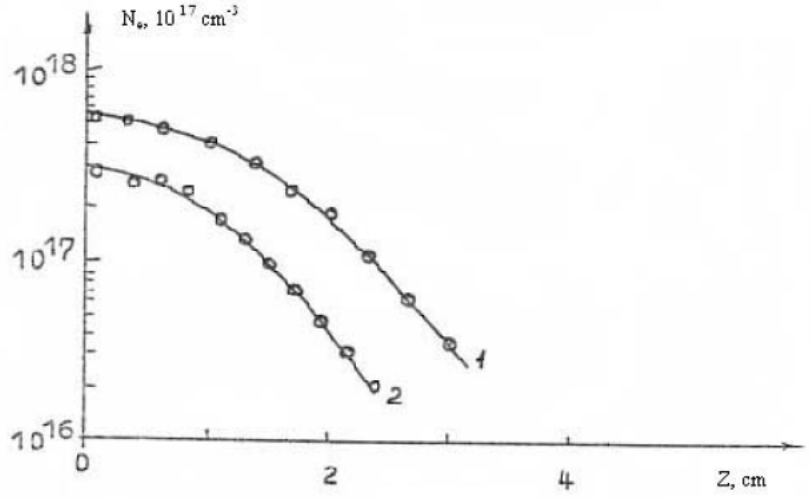

Fig.6.16

One can see that the electron concentration at distances in the range~1 cm decreases comparably slowly, and then, starting from distances about 1- 1,5 cm it decreases practically linearly. If one considers that at larger distances ~5 – 10 cm it decreases linearly with the longitudinal coordinate then he obtains the electron concentration ~ 10^{13} cm^{-3} at the distance of 10 cm. This was confirmed by results of the probe measurements.

From the analyses of the experimental data one can make the following conclusions:

The developed and applied generator of the quasi-stationary plasma jets reproduces main plasma characteristics of the powerful plasma generator with the expendable power up to 15 kW.

The spatial extension of the plasma jet of the quasi-stationary plasma generator reaches 10 cm.

Conclusions to chapter 6

Analysis of the powerful plasma generator application possibilities for the investigation of the plasma and gas crossflows have been made on a basis of the obtained results.

It was established that such an experiment can be undertaken at the large sized supersonic devices with the cross section no less than 20 cm.

It was shown that the developed plasma generator is the highly effective plasma source stably working at high energy put in and large mass flow rates of the plasma forming gas. It most probably can be successfully applied at the plasma chemical activation of the high speed (supersonic) flows of the fuel-air mixtures.

For the realization of the experiment in the small sized devices it is advisable to use the small sized quasi stationary plasma generators with the external controlled starting. Such plasma source has been developed and manufactured.

The range of plasma parameters of the quasi-stationary plasma generator allows to assert that this type of the plasma source is of use for ignition of the fuel supersonic flows both in the region of the flow stabilization and in the region of the main fuel flow.

This plasma source has applicable mass and weight characteristics.

This plasma source will be applied for an ignition of hydrocarbon fuels in the supersonic direct-flow channel developed designed and manufactured in MSU.

References to chapter 6

1. Report № 4 on the Project ISTC 2449-p “Plasma-Jet Studies for Plasma Chemical Fuel Activation” for the third quarter. Moscow. 2003.
2. Zarin A.S., Kuzovnikov A.A., Shibkov V.M.. Svobodno Lokalizovannyi SVCh Razrad v Vozduhe (Freely Localized Microwave Discharge in Air). Moscow: Oil & Gas.1996. 204 p. (In Russian).
3. Ershov A.P., Imad I., Timofeev I.B., Chuvashev S.N., Shibkov V.M.. High-Speed Plasma Jets in the Air. 2, Parameters of a Pulsed Plasma Jet Injected into the Atmosphere by a Cumulative Plasmatron. //Teplofizika Vysokih Temperatur (High Temperature). 1993. V.31. № 4. P. 531-534 (In Russian).
4. Report № 2 on the Project ISTC 2449-p “Plasma-Jet Studies for Plasma Chemical Fuel Activation” for the third quarter. Moscow. 2002.

General conclusions

Applicability of plasma generators with divergent plasma nozzles for ignition of the supersonic incident flammable mixture flow has been demonstrated.

Two embodiments of a stationary plasma generator with a vortical flow stabilizing and diverging plasma channel have been realized. Our theory and experiments show that they insure high mass flow rate, high efficiency of working gas heating and smallness of heat losses into water-cooled anode surface. The first plasma generator is a large device for application to complex chemically aggressive media. The second plasma generator is a compact apparatus. It can be applied for creation of a quasi-plane jet in a real scramjet, using a row of such plasma generators. Analysis of radiation spectra of the first generator plasma jet showed that the gas temperature investigated range of inputted power in the plasma relaxation region (behind the nozzle entrance) lies in the range T_g = (3500 - 6600°) K sufficient for ignition of hydrocarbon fuels.

Lagrange method on a completely conservative implicit difference scheme with an adaptive triangular unstructured grid was used in computations. The total number of knots was 15000-150000. The mesh was concentrated in the region of the combustion by the adaptive method.

This method is applied for clarification of initial and boundary conditions at investigation of the plasma jet-flammable mix cross flow interaction (at angles 135, 150º).

Computations of plasma jet injection to the incident flow of propane-air flammable mix have been made. Plasma forming gas (nitrogen) mass flow rate was 2 g/s, plasma generator power was 15 kW and 30 kW at the temperature of the incident propane-air stoichiometric Our calculations show deep penetration of plasma jet into the incident freestream and crossflows of air and flammable mixture. The model of ignition and combustion of the stoichiometric propane-air mix with a help of the plasma jet from the plasma generator to the incident flow of the flammable mix has been developed. It uses one step effective chemical reaction between propane and oxygen molecules.

Results of computations demonstrated the ignition possibility of propane-air mix with a help of plasma generators with the power 15 kW at the incident propane-air stoichiometric mix temperature 1000 K. Realizatuion of combustion wave towards the supersonic flow both in cylindrical and flat cases was observed in computed variants at typical times of ten microseconds. The mixture is compressed on the combustion front and it in turn accelerates ignition.

As showed our previous computations concentrations of atoms in plasma are very high. This can additionally increase the fuel activation in the incident flow.

Present investigations show the principle possibility of supersonic channel creation with geometry of chamfered wall without a step, as it is shown in Fig. C1. The corresponding calculations are necessary for choice of optimal parameters of plasma generator and supersonic channel.

Calculations show that "high power and low energy" generators can be applied for combustion in supersonic conditions.

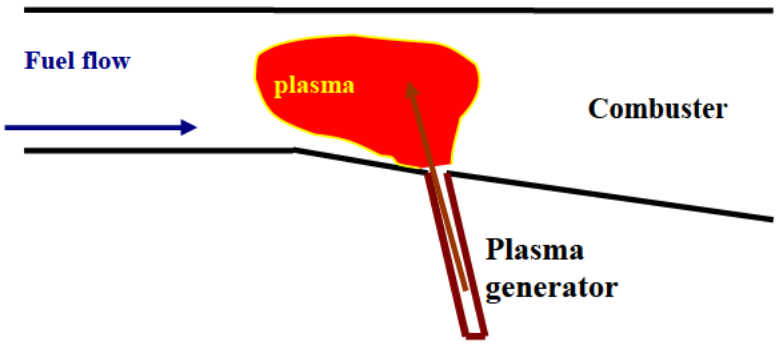

Fig.C.1.

Undertaken investigations show that appearance of 0.1% of atomic oxygen in the mix leads to ~1.5-2 times greater reduction of propane (ignition) during the same time as in the case of the undisturbed mix. Appearance of 1% of atomic oxygen in the mix leads to ~5-6 times greater reduction of propane (ignition becomes shorter by ~5-6) during the same time as in the case of the undisturbed mix.

Moderate power self-maintained discharge (≤10.0 kW) can be used for ignition and ignition enhancement of propane-air stoichiometric mix due to generation of atomic oxygen and heating of the mix by the discharge. High amount of vibrationally and electronically excited states can considerably reduce necessary power value. Application of discharges combination: the non -selfmaintained discharge and plasma jet (see C.2) at low non-selfmaintained discharge power (~20 W) can be perspective for the ignition, since vibrationally and electronically excited oxygen states can significantly enlarge reaction rate constants and can be effective at interaction of incident excited mix with the plasma jet.

More precise values of necessary ignition enhancement power value require detailed solution of non-selfmaintained discharge in air-fuel mix including rates of vibrationally and electronically excited states of molecular oxygen and hydrocarbon molecules reactions and the solution of gasdynamics equations in the definite duct. The solution of the first problem is complicated because of necessary rate constants absence. The solution of the second problem

can be realized in approach developed in this Report and can be the subject of further investigations.

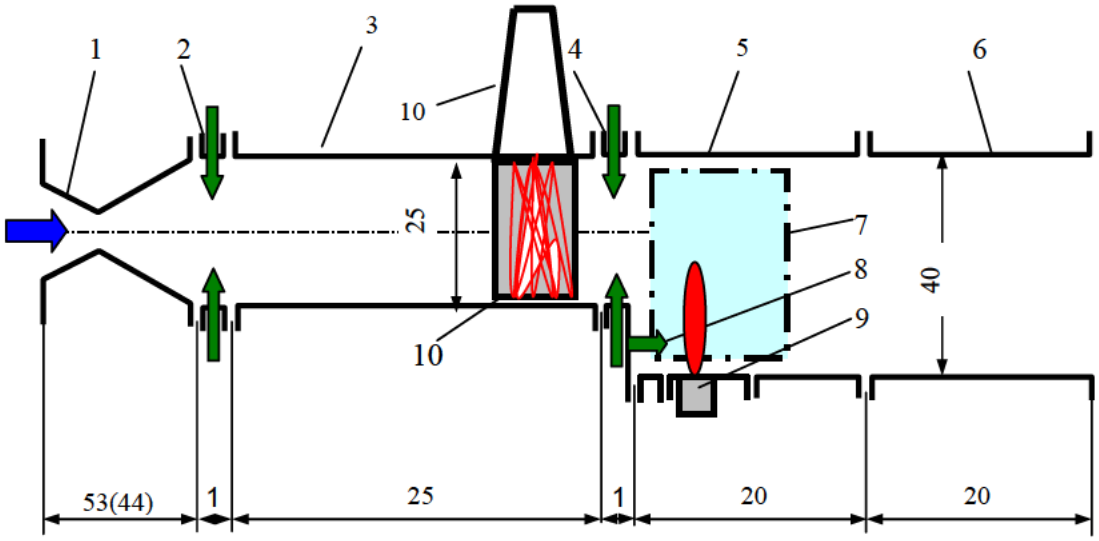

Fig.C2 Schematics of the channel with combination of discharges

1 – supersonic M=2 nozzle, 2 – collectors of preliminary fuel injection (first injector set), 3 – insulator channel, 4 - collectors of main fuel injection (second injector set), 5 – 1st section of combustor, 6 – 2 nd section of combustor, 7 – quartz window, 8 – third fuel injector set, 9 – plasma jet generator, 10 – non-selfmaintained discharge generator

List of publications

1. Ardelyan N., Bychkov V., Kosmachevskii K., Chuvashev S., Malmuth N. Modeling of Plasmas in Electron Beams and Plasma Jets . AIAA 2001-3101 Proc. 32-nd AIAA Plasmadynamics and Lasers Conference and 4 th Weakly Ionized gases Workshop 11-14 June 2001, Anaheim, CA.(15 P).
2. Ardelyan N., Bychkov V., Kosmachevskii K., Solodovnikov N., Timofeev I., Malmuth N. Modeling of Plasma Jet Interaction with Cross Flows for Propulsion Enhancement. AIAA 2003-1191 Proc. 41-st AIAA Aerospace Science Meeting and Exhibit 6-9 January 2003, Reno, Nevada.(10 P).
3. Ershov A., Ardelyan N., Bychkov V., Chernikov V., Shibkov V., Surkont O. Mechanisms of transversal electric discharge sustansion in supersonic air and propane-air flows. AIAA 2003-0872 Proc. 41-st AIAA Aerospace Science Meeting and Exhibit 6-9 January 2003, Reno, Nevada.(10 P).
4. Ardelyan N., Bychkov V., Kosmachevskii K., Solodovnikov N., Timofeev I.. Interaction of supersonic gas flow and a plasma jet. Abstracts of 30 Zvenigorod Conf. on plasma physics and controlled fusion 2003 (24-28 February 2003). P.219.
5. Ardelyan N.V., Bychkov V.L., Solodovnikov N.A., Timofeev I.B. Computations of electric arc plasma generator for influencing on supersonic gas flow. 5 –th International workshop on Magnetoplasma aerodynamics in aerocosmic applications. Abstracts of reports. Moscow 7-10 April 2003 IVTAN RAS. P.105-107.
6. Bychkov V.L., Gromov V.G., Ershov A.P., Levin V.A., Chernikov V.A., Shibkov V.M., Surkont O.S. Timofeev I. B. An electrode ignition discharges in supersonic propane-air flows. In: Combustion and Atmospheric pollution. Eds. G.D. Roy, S.M.Frolov, A.M. Starik. Moscow: Torus Press, 2003, 278-282.
7. Ershov A.P., Surkont O.S., Timofeev I.B., Chernikov V.A., Shibkov V.M., Ardelyan N.V., Chuvashev S.N., Bychkov V.L., Gromov V.G., Levin V.A. Parameters of electrode ignition discharges in supersonic propane-air flows. 3 –d Workshop Thermochemical and plasma processes in aerodynamics. Saint – Petersburg. 28-31 July. 2003. P.64-73.
8. Ardelyan N.V., Bychkov V.L., Kosmachevskii. K.V., Timofeev I.B. Stationary electric arc generator for influencing on supersonic gas flow. 3 –d Workshop Thermochemical and plasma processes in aerodynamics. Saint – Petersburg. 28-31 July. 2003. P.320-328.
9. Ardelyan N.V., Bychkov V.L., Gordeev O.A., Klimov A.I. Combined non-self-maintained in air for generating of chemically active particles. Thermochemical and plasma processes in aerodynamics. Saint – Petersburg. 28-31 July. 2003. P.337-344.
10. Ardelyan N.V., Bychkov V.L., Ershov A.P., Kalinin A.V., Surkont O.S., Timofeev I.B., Chuvashev S.N. Investigations of high speed plasma flows for plasma aerodynamics. Collection of works of 6–th International symposium on radiation plasmadynamics. Moscow 2003. P. 47-52.
11. Ardelyan N.V., Bychkov V.L., Kosmachevskii. K.V., Solodovnikov N.A., Timofeev I.B. Interaction of supersonic gas and plasma flows. Collection of works of 6–th International symposium on radiation plasmadynamics. Moscow 2003. P. 65-70.
12. Ardelyan N., Bychkov V., Kosmachevskii K., Timofeev I., and Malmuth N. Plasma jet generators with divergent nozzles for aerodynamic applications. AIAA-2004-0179 Proc. 42-nd AIAA Aerospace Science Meeting and Exhibit 5-8 January 2004, Reno, Nevada.(10 P).
13. Ardelyan N.V., Bychkov V.L., Kosmachevskii K.V., Timofeev I.B. Stationary electric arc plasma generator with conical nozzle for inpact on a supersonic flow. Abstracts of 31-st Zvenigorod Conf. on plasma physics and controlled fusion 2004 (16-20 February 2004). P.242.
14. Ardelyan N.V., Bychkov V.L., Kosmachevskii. K.V., Timofeev I.B. Investigations of plasma jets applicability in aerodynamics. 4 –d Workshop Thermochemical and plasma processes in aerodynamics. Saint – Petersburg. 12-14 July. 2004. P.20 (10 pages).
15. Aleksandrov A.F., Bychkov V.L., Timofeev I.B. Plasma aerodynamic experiments. Materials Intern Symp. «Energy Conversion Fundamentals». 21-25 June. 2004. Istanbul.Turkey. 24 pages.
16. Aleksandrov A.F., Bychkov V.L., Chernikov V.A., Ershov A.P., Shibkov V.M., Timofeev I.B. Plasma aerodynamics investigations in MSU physical department (Review of investigations). AIAA-2005-1433 Proc. 43-d AIAA Aerospace Science Meeting and Exhibit 10-13 January 2005, Reno, Nevada.(4 P).
17. Ardelyan N., Bychkov V., Kosmachevskii K., Timofeev I., and Malmuth N. Ignition of a propane-air stoichiometric mixture by a plasma jet generator with a divergent nozzle. AIAA-2005-990 Proc. 43-d AIAA Aerospace Science Meeting and Exhibit 10-13 January 2005, Reno, Nevada.(7 P).